REPUBLIC OF IRAQ
MINISTRY OF HIGHER EDUCATION
AND SCIENTIFIC RESEARCH
UNIVERSITY OF BABYLON

Design and Analysis of a Healthcare Monitoring System Based on Visible Light Communication (VLC)

A Thesis

Submitted to the Department of Electrical Engineering /

College of Engineering / University of Babylon in Partial Fulfillment of the Requirements for the Degree of Doctor of Philosophy

in Engineering / Electrical Engineering / Electronics and Communication

By

Mayasah Razzaq Abdali Mohammed

Supervised by

Prof. Dr. Ibrahim Abdullah Murdas

August 2022

وَفَوْقَ كُلِّ ذِي عِلْمٍ عَلِيمٌ

صدق الله العظيم

سورة يوسف

الآية: ٧٦

Supervisor Certification

I certify that the thesis entitled " **Design and Analysis of a Healthcare Monitoring System Based on Visible Light Communication (VLC)** " was prepard by **Mayasah Razzaq Abdali** under my supervision at the Department of Electrical Engineering, Collage of Engineering, University of Babylon, as a partial fulfillment of requirements for the degree of Doctor of Philosophy in Electronic and Communication Engineering.

Signature:

Name: **Prof. Dr. Ibrahim Abdullah Murdas**

(Supervisor)

Date: / 8 / 2022

In view of the above recommendation, I am forward this thesis for discussion by the examination committee.

Signature:

Name: **Assist. Prof. Dr. Shamam Fadhil Alwash**

(Head of Electrical Engineering Dept)

Date**:** / 8 / 2022

Examining Committee Certificate

We certify that we have read this thesis entitled " **Design and Analysis of a Healthcare Monitoring System Based on Visible Light Communication (VLC)**" and, as examination committee examined the student **Mayasah Razzaq Abdali** in its contents and that in our opinion it meets the standard of a thesis for the degree of Doctor of Philosophy in Electronics and Communications Engineering.

Signature:
Name: **Prof. Dr. Sinan M. Abdul-Sattar**
(Member)
Date: / 8 / 2022

Signature:
Name: **Prof. Dr. Saad S. Hasson**
(Member)
Date: / 8 / 2022

Signature:
Name: **Prof. Dr. Yousif I. Mohammed**
(Member)
Date: / 8 / 2022

Signature:
Name: **Prof. Dr. Haider J. Abd-Nassar**
(Member)
Date: / 8 / 2022

Signature:
Name: **Prof. Dr. Laith Ali Abdul-raheem**
(Chairman)
Date: / 8 / 2022

Signature:
Name: **Prof. Dr. Ibrahim A. Murdas**
(Supervisor)
Date: / 8 / 2022

Signature:
Name: **Asst. Prof. Dr. Shamam Fadhil Alwash**
(Head of Electrical Engineering Dept.)
Date: / 8 / 2022

Signature:
Name: **Prof. Dr. Hatem Hadi Obeid**
(Dean of College of Engineering)
Date: / 8 / 2022

Dedication

To my "MOTHER", the cause of my success…

To the spirit of my "FATHER"....

To my biggest supporter in my PhD journey "HUSBAND"

To my small heart AHMED and SAMA

To my sisters ….

To all my beloved family….

I dedicate this work

Mayasah

Acknowledgement

First of all, my deepest gratitude goes to Allah, the Compassionate, the Most Merciful, and the Lord of all creations.

Then, I would like to acknowledge the enthusiastic supervision, guidance, and encouragement of my supervisor Prof. Dr. Ibrahim Abdullah Murdas during this work.

My appreciation and thanks extends to the Department of Electrical Engineering, University of Babylon for providing me the facilities needed.

Words remain incapable of expressing my gratitude and obligation to my mother, husband and family, who always bestow me of unbounded love and support throughout my PhD study.

Abstract

Visible light communication (VLC) is a form of optical wireless communication (OWC) that has arisen in recent years. Instead of using radio spectrum to transmit data wirelessly, it employs the visible light spectrum via illumination of light-emitting diode (LED) bulbs. However, even though VLC can address some of the RF communication problems in certain situations, its capabilities for Internet-of-Things (IoT) applications are yet to be realized.

The many benefits of VLC have been taken in healthcare monitoring systems, especially the elderly segment of hospitalized people. The thesis examined two applications of VLC technology: the first is the smart healthcare monitoring system using Li-Fi technology (which is a practical application of VLC) based IoT. The second is Indoor Positioning System (IPS) for monitoring the patient's position using VLC technology.

In the first system, the temperature and heartbeat rate of the patient are transmitted via Li-Fi technology, then to the central station. This data is uploaded to the ThingSpeak platform cloud via python code so that the doctor could view it anywhere. This system is also provided through sending email notifications in abnormal cases. The system was designed and implemented with all steps, including selecting components and operating programming. The used software and platforms included Arduino Integrated Development Environment (IDE) to get sensor data, Thingspeak IoT platform as graphical user interface for the doctor, Python Language for uploading these data to Thingspeak, and If-this-then-that (IFTTT) application for the alert purpose. The results were divided into two parts. The first part was related to the Li-Fi technology. The system tested multiple distances, different channel status, and ambient noise. The second part was the

results of the IoT, where the results were presented on the ThinkSpeak platform and notification by email in critical cases. The system was successfully tested on Imam Al-Sadiq Hospital– Babylon city patients. The obtained results are approved and satisfactory.

As for the second system, it depends on positioning the patient inside the hospital using VLC technology. The designed system is based on a new hybrid algorithm. It has different steps. Firstly, the combination method divides the entire anchors into different groups. Secondly, a weighted least squares (WLS) positioning approach is employed to compute the patient position by each group. Then, anchor selection (AS) is used to select the group having the best positioning accuracy using the derived mean square error (MSE) metric. Finally, the selected group is chosen to relocate the patient using its estimated position as an initial point for the maximum likelihood (ML) positioning approach. The simulation results show that the proposed algorithm outperforms the WLS and conventional ML approaches. It is also found that increasing the number of LEDs in the ceiling leads to improve the accuracy of the system. Simulation is done with the help of MATLAB 2019A.

Contents

Subject	**Page No.**
Abstract	I
Contents	III
List of Figures	VI
List of Tables	IX
List of Abbreviations	X
List of Symbols	XIII
Chapter One: Introduction	
1.1 Introduction	1
1.2 Smart Healthcare Monitoring using Li-Fi based IoT	2
1.3 Indoor Positioning System Using VLC	4
1.4 Problem Statement	5
1.5 Literature Survey	6
1.5.1 Smart Healthcare Monitoring Using Li-Fi based IOT Review	6
1.5.2 IPS using VLC Review	9
1.6 Thesis Objectives	11
1.7 Outline Of The Thesis	12
Chapter Two: Theoretical Part: Visible Light Communication (VLC), Indoor Positioning System (IPS) and Internet of Things(IoT)	
2.1 VLC Communication	14
2.1.1 Light Sources	17
2.1.2 Light Detectors	20
2.1.3 Modulations Scheme	22

2.2 Light Propagation Model	24
2.2.1 LOS Mathematical Modelling	24
2.2.2 NLOS Mathematical Modelling	25
2.3 Noise Model	27
2.3.1 Dark Current Noise	27
2.3.2 Shot Noise	27
2.3.3 Thermal Noise	27
2.4 VLC Applications	28
2.4.1 Light Fidelity (Li-Fi)	28
2.4.2 Indoor Positioning System (IPS) using VLC	31
2.5 Trilateration in 3D using RSS	35
2.6 Separation Received Signals	37
2.6.1 Optical Orthogonal Code (OOC)	37
2.6.2 Code reuse strategy	39
2.7 Position Estimation	40
2.7.1 Weighed Least Square Estimator	40
2.7.2 Maximum Likelihood (ML) Estimator	42
2.8 Anchor selection	44
2.9 Internet of Things (IoT)	46
2.9.1 IoT Definitions	48
2.9.2 IoT Architecture	49
2.9.3 Thingspeak Platform	51
Chapter Three: Proposal Designs for Healthcare Monitoring System	
3.1 Proposed Smart Healthcare Monitoring System using Li-Fi technology based IoT Description	53
3.2 System Building and Implementation	70
3.3 Proposed Indoor Positioning System using VLC technology Description	89

3.3.1 System Block Diagram	72
3.3.2 System Parameters	75
Chapter Four: Practical and Simulation Results with Discussion	
4.1 Performance of smart healthcare monitoring system using Li-Fi technology based IoT	78
4.1.1 Li-Fi Result	96
4.1.2 IoT Result	91
4.2 Performance of the Proposed IPS using VLC technology	95
4.3 Comparative Analysis of the Results	102
Chapter Five: Conclusions and the Future Work	
5.1 Conclusions	105
5.2 Future Work	106
References	108
Appendix A: Hardware Specifications	A-1
Appendix B: Creating IFTTT Notifications	B-1

List of Figures

No. of Figure	Name	Page
(1-1)	The electromagnetic spectrum's visible light range	2
(1-2)	Statistics of IoT connected devices installed	3
(2-1)	Block Diagram of VLC System	15
(2-2)	Link configurations (a) Direct-LOS (b) Non-direct LOS and (c) Non-LOS by the first reflection (d) Tracked	17
(2-3)	Forward bias condition operation in the LED	18
(2-4)	Human eye's response based on the 1978 CIE data	19
(2-5)	PIN photodiode diagram	21
(2-6)	OOK signal OOK signal in which S1(t) stands for binary one and S0(t) stands for binary zero. (a) NRZ scheme (b) RZ scheme (γ = 0.5)	24
(2-7)	LOS link modelling	25
(2-8)	NLOS link modelling	26
(2-19)	Positioning techniques for VLC systems	32
(2-10)	ToA-Measurement	32
(2-11)	AoA-Measurement	33
(2-12)	IPS based VLC	35
(2-13)	Trilateration method	36
(2-14)	Example of RSS detection	39
(2-15)	The code reuse strategy	40
(2-16)	Position estimation using the MLE algorithm	44
(2-17)	A's and C's concept in IoT	47
(2-18)	IoT architecture A) Three Layer architecture. B) Five Layer architecture.	51
(3-1)	Proposed System Block Diagram	54
(3-2)	Transmitter Section	56
(3-3)	MLX90614 IR Temperature Sensor	57
(3-4)	Interfacing between the MLX90614 temperature sensor and Arduino-Uno	58
(3-5)	DFRobot heart rate sensor	59
(3-6)	Interfacing between DFRobot heart rate sensor and Arduino-Uno	60
(3-7)	BC547 Transistor	60
(3-8)	Receiver Section	62
(3-9)	LM258 Op-Amplifier Pinout diagram	63
(3-10)	Flow chart of the Transmitter Code and Receiver Code.	65
(3-11)	Creating channel on ThingSpeak	66

(3-12)	Creating Fields.	67
(3-13)	ThingSpeak Channel	67
(3-14)	Generation of Channel ID and API Key	68
(3-15)	Python Code	68
(3-16)	Steps for building the Patient Health Monitoring System.	70
(3-17)	Implemented Proposed System	71
(3-18)	Block diagram of the created system	74
(3-19)	Experimental activities inside the room and corridor (a) Scenario1, (b) Scenario2	76
(4-1)	Distance vs. Received power for direct LOS under low ambient noise	79
(4-2)	Received power vs. OSNR for direct LOS under low ambient noise	79
(4-3)	Received power vs. ESNR for direct LOS under low ambient noise	80
(4-4)	Distance vs. Received power for direct LOS under high ambient noise	80
(4-5)	Received power vs. OSNR for direct LOS under high ambient noise	81
(4-6)	Received power vs. ESNR for direct LOS under high noise	81
(4-7)	Angle vs. Received power for non- direct LOS under low ambient noise	83
(4-8)	Received power vs. OSNR for non-direct LOS under low ambient noise	83
(4-9)	Received power vs. OSNR for non-direct LOS under low ambient noise	84
(4-10)	Angle vs. Received power for non-direct LOS under high ambient noise	84
(4-11)	Received power vs. OSNR for non-direct LOS under high ambient noise	85
(4-12)	Received power vs. ESNR for non-direct LOS under high ambient noise	85
(4-13)	Received power vs. distance for NLOS under low ambient noise	87
(4-14)	Received power vs. OSNR for NLOS under low ambient noise	87
(4-15)	Received power vs. ESNR for NLOS under low ambient noise	88
(4-16)	Received power vs. distance for NLOS under high ambient noise	88
(4-17)	Received power vs. OSNR for NLOS under high ambient noise	89
(4-18)	Received power vs. ESNR for NLOS under high ambient noise	89
(4-19)	Intensive care of Al-Emam Al-Sadiq Hospital	91
(4-20)	Data Flow in Python	92
(4-21)	Channel view in ThingSpeak website	92
(4-22)	Channel view in ThingView Mobile Application	93
(4-23)	Alert Email with different cases (a) High Heartrate (b)Low Heartrate	94

	(c) High Temperature (d) Low Temperature	
(4-24)	Real and estimated paths in m for scenarios 1 and 2, respectively	100
(4-25)	Empirical disrupted function of MSE for the Proposed, WLS, and ML indoor positioning approaches for scenarios 1 and 2, respectively	101
(B-1)	IFTTT	B-1
(B-2)	Log in IFTTT	B-1
(B-3)	Creating Applet	B-2
(B-4)	Applet Services	B-2
(B-5)	Choosing Webhoks service as a trigger	B-3
(B-6)	Inserting Event Name	B-3
(B-7)	Finishing of creating the trigger	B-4
(B-8)	Adding an action	B-4
(B-9)	Choosing Email service as an action	B-5
(B-10)	Completing an action Fields	B-5
(B-11)	Adding Email and finishing the applet	B-6
(B-12)	Pressing Connect	B-7
(B-13)	Getting URL	B-7
(B-14)	Configuration of ThingHttp	B-8
(B-15)	Creating field for Threshold values	B-8
(B-16)	Setting Threshold value for Body Temperature	B-9

List of Tables

No. of Table	Name	page
(2-1)	Li-Fi and Wi-Fi comparison	30
(3-1)	MLX90614 Pinout Configuration	58
(3-2)	Simulation Parameters for proposed System	77
(4-1)	Direct-LOS link measurements under low ambient noise	82
(4-2)	Direct-LOS link measurements under high ambient noise	82
(4-3)	Non-direct LOS link measurements under low ambient noise	86
(4-4)	Non-direct LOS link measurements under high ambient noise	86
(4-5)	NLOS link measurements under low ambient noise	90
(4-6)	NLOS link measurements under high ambient noise	90
(4-7)	Types of propagation channels for every group of LED	95
(4-8)	MSE for WLS method for different positions of the target in $\boldsymbol{m2}$ (Scenario1)	96
(4-9)	MSE for WLS method for different positions of the target in $\boldsymbol{m2}$ (Scenario2)	97
(4-10)	MSE for the proposed system compared to ML and WLS algorithms in $\boldsymbol{m2}$(Scenario1)	98
(4-11)	MSE for the proposed system compared to ML and WLS algorithms in $\boldsymbol{m2}$ (Scenario2)	98
(4-12)	A comparison study related to Li-Fi's previous works.	103
(4-13)	A comparison study related to IPS's previous works.	104

List of Abbreviation

Abbreviation	Definition
AES	Advances Encryption Standard
APDs	Avalanche Photodiodes
AOA	Angle of Arrival
API	Application Programming Interface
AWGN	Additive White Gaussian Noise
C	Capacitance
CPU	Central Processing Unit
DMT	Discrete Multi-tone
ESNR	Electrical Signal to Noise Ratio
ECG	Electrocardiography
EEG	Electroencephalography
FOV	Field of Vision
FSM	Finite State Machine
3G	Third Generation
4G	Fourth Generation
5G	Fifth Generation
Gbps	Giga bit per second
GPS	Global Positioning System
HTTP	Hypertext Transfer Protocol
ID	Identification
IFTTT	IF This Then That
IP	Internet Protocol
IPS	Indoor Positioning System
IR	Infrared
IoT	Internet of Things
IM/DD	Intensity-Modulation with Direct Detection
LAN	Local Area Network
LED	Light Emitting Diode
Li-Fi	Light Fidelity
LOS	Line of Sight
L-PAM	L-ary Pulse Position Modulation
LS	Least Square
LTE	Long Term Evolution
M2M	Machine to Machine
Mbps	Mega bit per second

ML	Maximum Likelihood
M-PAM	M-ary Pulse Amplitude Modulation
MSE	Mean Square Error
NRZ	Non-Return to Zero
NLOS	Non-line of Sight
OWC	Optical Wireless Communication
OOK	On/Off Keying
OOC	Optical Orthogonal Codes
OSNR	Optical Signal to Noise Ratio
PAM	Pulse Amplitude Modulation
PC	Personal Computer
PD	Photodiode
PHY	Physical
PIC	Peripheral Interface Controller
PIN	PN Junction with Isolation Region
PPG	Photo Platysma Graphy
PN	Positive type with Negative type
PSD	Power Spectral Density
QPSK	Quadrature Phase Shift Keying
R	Resistance
Rb	Bit Rate
RF	Radio Frequency
RFID	Radio Frequency Identification
RGD	Red Green Blue
RSP	Ray Surface Positioning
RSS	Received Signal Strength
RZ	Return-to-Zero
SDOs	Standard Development Organizations
SNR	Signal to Noise Ratio
TDOA	Time Difference of Arrival
THz	Terra Hertz
TOA	Time of Arrival
VLC	Visible Light Communication
WBSNs	Wireless Biomedical Sensor Networks
Wi-Fi	Wireless-Fidelity
Wi-Max	Worldwide Interoperability for Microwave Access
WLAN	Wireless Local Area Network
WLS	Weight Least Square

List of Symbols

Symbol	Definition
η_{power}	Power Efficiency
Φ_{flux}	Luminous Flux
$V(\lambda)$	Normalization factor based on the eye response
$P_{optical}(\lambda)$	LED light's power spectrum
η_{lu}	Luminous Efficiency
$H(j\omega)$	Low pass transfer function
ω	Optical frequency
f_c	3 dB frequency
I_p	Photocurrent
P_p	Incident optical power
q	Electronic charge
η_i	Quantum efficiency
h	Planck constant
hv	Photon energy
R_{PD}	Photodetector responsivity
λ	Light wavelength
R_f	Reflectivity at diode entry
α	Absorption Coefficient
η_B	Bandwidth Efficiency
R_b	Bit rate
γ	Duty Cycle
η_p	Power Efficiency
E_{pulse}	Pulse energy
E_b	Energy per bit
T_b	Bit duration
$\emptyset_{OOK}(t)$	OOK signal
σ^2_{shot}	Total variance of shot noise
I_{bg}	Photocurrent from background radiation
I_2, I_3	Noise Bandwidth factors
B_n	Equivalent noise bandwidth
R_L	Load Resistance
$\sigma^2_{Thermal}$	Total variance of thermal noise
k	Boltzmann's constant
C_f	Fixed capacitance of photodetector per unit area
T_K	Absolute temperature

Go	Open loop gain
Γ	FET channel noise factor
gm	FET transconductance
I_3	FET channel noise factor
σ^2	Total noise variance
$P_{r-total}$	Total received optical power
P_t	Transmitted power by LED
H_{LOS}	LOS channel gain
H_{NLOS}	NLOS channel gain
$R_{LOS}(\theta_1)$	Transmitter radiant intensity for the LOS scenario
θ_1	Irradiance light angle
ψ_1	Incident light angle
A_{PD}	Photodetector effective area
$T_s(\psi)$	Optical gain of the concentrator
$g(\psi)$	Gain of an optical filter
d_i	Distance between *i'th* transmitter and the receiver
m	Lambertian emission
$\theta_{1/2}$	Semi-angle at half luminance of the LED
μ	Coefficient based on Fresnel reflection
$R_{NLOS}(\theta_{2ij})$	Transmitter radiant intensity for the NLOS scenario
i	Transmitter *i'th index*
ρ	Reflectance factor
dA_{wall}	Reflective area of the small region
α	Angle of incidence from multipath
β	Radiance angle to a reflective point from multipath
σ^2_{shot}	Total variance of shot noise
I_{bg}	Photocurrent from background radiation
I_2, I_3	Noise Bandwidth factors
B_n	Equivalent noise bandwidth
R_L	Load Resistance
$\sigma^2_{Thermal}$	Total variance of thermal noise
k	Boltzmann's constant
C_f	Fixed capacitance of photodetector per unit area
T_K	Absolute temperature
Go	Open loop gain
Γ	FET channel noise factor
gm	FET transconductance
I_3	FET channel noise factor
d	Distance

C	Speed of light
t	Transmission time
t_{Diff}	Time difference
n	Code length
K	weight
λ_a	Autocorrelation constraints
λ_c	Cross-correlation constraints
C_{max}	Maximum number of codewords
P	Actual position
L_i	LEDs position
d_i	Estimated distance
r_i	Actual distance
e	Distance Error
$\hat{P}$	Estimated position
W	Weight Matrix
$P(X\|\theta)$	Joint probability density function
$P(x_n\|\theta)$	Conditional probability
$MSE(\hat{T})$	Derived MSE

Chapter One

General Introduction

Chapter One

General Introduction

1.1 Introduction

An Optical Wireless Communication (OWC) system has become increasingly significant in recent years to meet the demands of information and wireless communication technologies. One growing interest in OWC is Visible Light Communication (VLC) that uses Light Emitting Diodes (LED) for both illumination and data communication purposes. This interest is explained by the increase popularity of solid-state lighting, longer lifetime of high-brightness LEDs compared to other sources of artificial light, high bandwidth, data security, low power consumption and fast switching[1]. VLC exploits the visible light spectrum, represented in figure (1-1), considered as a solution for RF spectrum scarcity. The visible light spectrum offers an unregulated/licence-free spectrum ranging from 380 to 800 THz, approximately 1300 times higher than the RF regulated spectrum (20 kHz - 300 GHz) [2]. In addition, it does not interfere with the existing RF-based systems and there are no health regulations to restrict the transmission power. VLC provides higher security than RF communication systems since it is harder to pick up the signal from outside the immediate surroundings, such as a room[3] [4].

One of the realistic implementations of VLC that uses wireless transmission is Light Fidelity (Li-Fi)[5]. Harald Haas coined the word in 2011[6]. This technology uses Light Emit Diode (LED) lights to send data with a high speed as compared to Wireless Fidelity (Wi-Fi). In addition to Li-Fi, VLC can offer highly efficient indoor positioning with accuracy at a centimeter level.

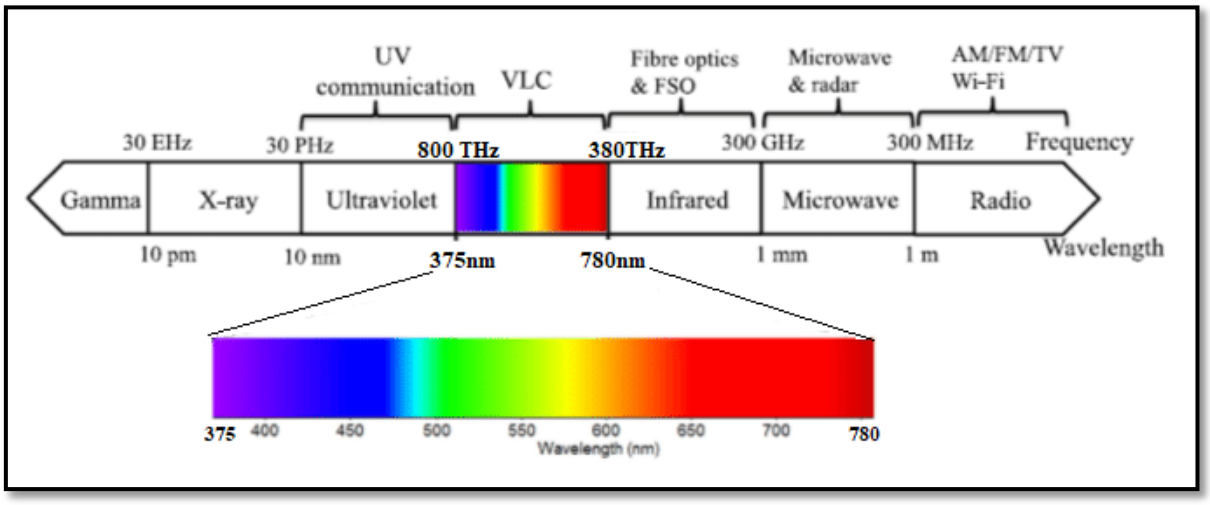

Figure(1-1): The electromagnetic spectrum's visible light range[2].

Healthcare monitoring is an urgent social problem. With the increase of the elderly population, the demand for elder healthcare has been increased. Statistics show that between 2012 to 2050, the elders' population will increase considerably [7]. In this thesis, we will submit the system for remote monitoring of elderly people who need continuous monitoring in the hospital. This system consists of two parts. The first one presents a smart healthcare monitoring system using Li-Fi technology-based Internet of Things (IoT). The second part relates to monitoring the position of elderly people using VLC technology. In the following sections, we demonstrate an introduction to the two aspects mentioned above.

1.2 Smart Healthcare Monitoring using Li-Fi based IoT

Embedding smartness to everyday objects and connecting them to the internet, also termed as the Internet of Things (IoT) paradigm, is becoming a reality. The overall number of connected objects has rapidly increased over the last decade, and this tendency is predicted to continue in the future, as shown in figure (1-2).

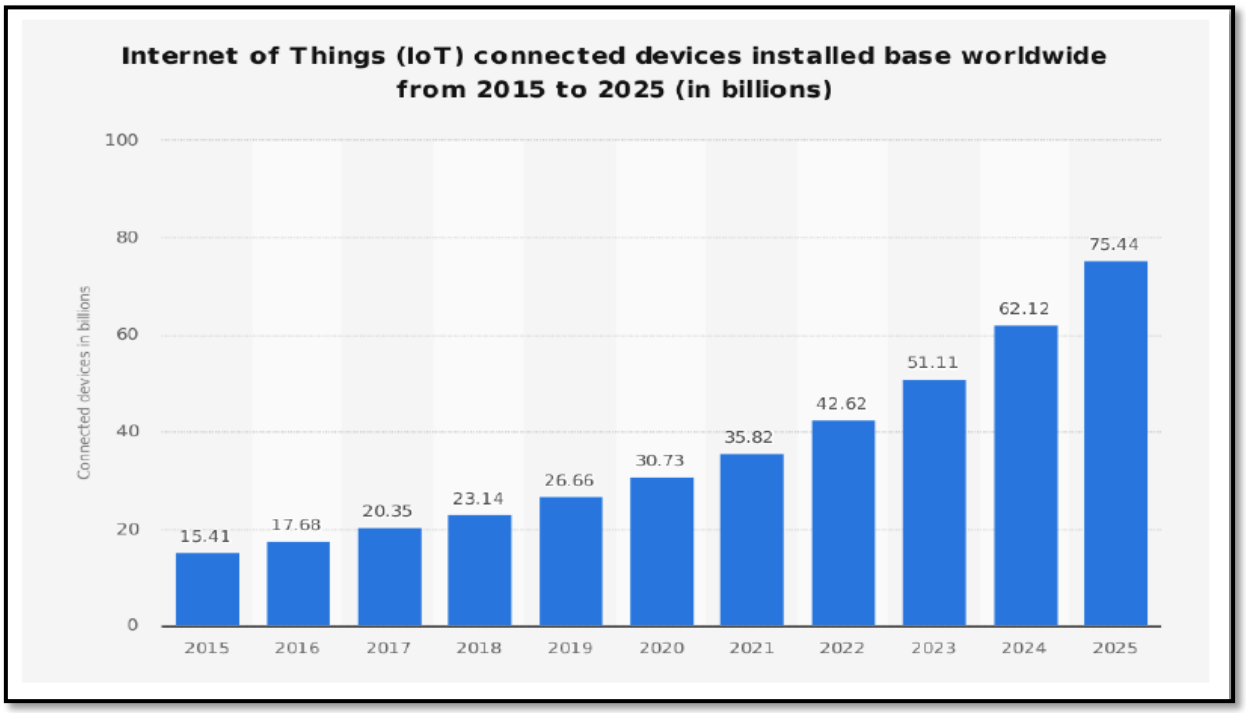

Figure (1-2): Statistics of IoT connected devices installed[8].

However, in addition to its advantages, this paradigm also poses considerable obstacles, particularly in communication. More connections per unit area, higher aggregate bandwidth, widespread coverage, renewable energy supplies, and heightened security will be required for pervasive IoT. A powerful IoT communication option that can overcome these obstacles is Li-Fi. A fundamental benefit of using the visible spectrum for IoT communications is that a lighting infrastructure made up of LED luminaires is widely utilized and will offer illumination to indoor locations where IoT communication is frequently required [9]. The difficulty of high-density IoT nodes can be addressed by converting densely distributed illumination points into IoT access points, enabling short-range connectivity with low energy usage for power-constrained nodes. In addition, compared to other factors such as temperature difference, movement, or RF, light is a good source for energy harvesting. Its higher-efficiency energy harvesting technology (solar cells) results in compact and less-expensive solutions [10].

The usage of Li-Fi for IoT has been a recent study area. Most early studies, for example, [11] and [12], focused on the energy-harvesting element of Li-Fi for IoT nodes or the hybrid operation of Li-Fi with RF. It will also provide us with numerous options to make our lives easier, one of which is a critical opportunity in the healthcare services that affect all of us, including the elderly. As a result, Li-Fi-based IoT is a new reality that has drastically altered our daily lives. It's also a way to revolutionize modern health care entirely.

1.3 Indoor Positioning System (IPS) Using VLC technology

Newly, different favourable applications based on VLC have been developed, and, in particular, indoor positioning services via VLC have been known as very appealing applications[13]. Traditional techniques for indoor positioning rely on radio frequency (RF) like Wi-Fi, infrared, and lasers. Among these techniques, it is well known that RF-based systems have lower costs and are preferable in coverage [14]. However, the accuracy of these systems is the main issue because of the multipath fading effect. Moreover, an indoor positioning system (IPS) based RF cannot be employed in areas sensitive to electromagnetic waves due to the radiation risk for health and interference between these waves. VLC signals are more resistant to multipath propagation losses than RF signals, thus making the positioning systems-based VLC more reliable and predictable.

In the recent development towards IPSs, the VLC based IPS has always been the dominant approach. Many researchers worldwide are working a lot in this field, but many research problems have already been solved quickly. However, many open issues are still significantly less investigated and need a profound test [15]. One of them is that using the same frequency band by the adjacent light cell will instigate the inter-cell interference problem. Additionally, the accuracy of the IPS based VLC is highly dependent on the multipath reflection.

Moreover, minimization of calculating time, the basic procedure to estimate the scene of an object, requires specific general steps, which include data collection, running positioning algorithms, and other ways to lower the positioning error, which costs time. Other research challenges include energy efficiency, receiver design, and mobility. The need to insert a new mathematical model of VLC based IPS is notable and compulsive because of different open and realistic issues that need to be addressed. An important slice benefiting from the indoor positioning system using VLC is elderly people who live in a hospital environment. Thus, in this work, we assign the proposed approach to monitoring the position of elderly people.

1.4 Problem Statement

1. The healthcare systems is developed for the preservation of human life. The traditional designs are complex, expensive, and high power consumption.
2. The concept of designing and implementing smart healthcare systems that use Li-Fi based on IoT is a relatively new field that warrants further investigation.
3. Doctors waste time to meet their patients. So, these systems must send out alerts in the event that a patient's vital signs change dramatically.

Also, the Indoor positioning systems using VLC have the following limitations:

1. A least square (LS) method to estimate the position was used in most papers with a large error, and no alternative was suggested to improve the accuracy.
2. Most researches based for analyzing LOS links only.
3. Using general Mean Square Error (MSE) to evaluate the accuracy which require for an actual position.

1.5 Literature Review

The literature review is divided into the following subsections:

1.5.1 Smart Healthcare Monitoring Using Li-Fi based IOT Review

H. Hass, in 2011, presented an illustration of Li-Fi at the TED Global conference held in Edinburgh. He showed the implementation and benefit of Li-Fi over Wi-Fi. This research led several researchers to work with this technology[6].

S. Kale et al. , in 2013, used Li-Fi technology to monitor the health of patients and provide doctors with real-time information on their condition. Central Processing Unit (CPU) simultaneously records data of the patient. This information can be accessed via the internet while consulting with the patient[16].

D. R. Dhatchayeny et al., in 2015, proposed a novel scheme for transmission of electroencephalography (EEG) biomedical signal using a VLC link. The data transmission is performed in LOS condition at distance 50cm using on-off-keying (OOK) modulation by utilizing all three components, red, green, and blue, of RGB LED. The experimental results show excellent reliability and accuracy of the proposed scheme[17].

S. Sudha et al., in 2016, using the Li-Fi concept, presented a patient monitoring system. The sensors in this model, such as temperature, glucose, heartbeat, and respiration, indicate its specific purposes. These sensors collect information from the body and the outputs are fed into a PIC16F877A microcontroller, which processes them. The microcontroller outcome is fed to the Li-Fi module which transmits the data in the form of light and the receiver end collects this data and then displays the graph for the different parameters using the Personal computers (PC) [18].

J. Patel et al., in 2017, proposed the concept that makes the use of Li-Fi technology, IoT, and sensor networks to make patient monitoring easier for doctors**.** The system uses temperature, pressure, and heartbeat sensors to collect

patients' data and send the data to the controller unit. The controller receives the data, processes it, and then sends it to IoT via a Li-Fi module. The doctor uses his laptop to access a webpage and look up information about his patients [19].

L. I. Abraham. ,in 2018, proposed a Li-Fi-based IoT architecture. A key component of this design is the use of Li-Fi to gather data from various environments. The data generated by Li-Fi was analyzed and processed to make intelligent decisions in order to improve services in numerous industries[20].

J. D. Bokefode et al., in 2018, shown the strategy which permits exchanging gathered IoT information over the cloud safely utilizing Li-Fi innovation. IoT devices are deployed to sense the environment and to collect the various data, and these are connected to the PIC16F877A .The data is then transmitted as light through the Li-Fi module. The light is recognized on the recipient side of the PD. After amplification, this data is transferred to secure system, then transferred on the Microsoft Azure cloud[21].

B. Anitha et al., in 2019, designed smart health care monitoring using Li-Fi technology and Wireless Biomedical Sensor Networks (WBSNs). The node of each WBSN poised of health care sensors and patient's health information are transmitted and received using Li-Fi technology. The breathing rate, pulse rate, body temperature, and other patients' body parameters are monitored using WBSNs and Li-Fi-based patient monitoring systems[22].

E. Ifada et all., in 2019, designed a Li-Fi Data Transmission system to send data (text) with 9600bps bitrate from a PC to another PC using off-the-shelf electronic components. The Data Transmission system constructed when tested showed satisfactory performances. The Li-Fi data transmission system built was very cheap, satisfying the project's major aim – incorporating a Li-Fi medium using off-the-shelf electronic components and devices[23].

J. Pradhan et al., in 2020, designed and implemented a Li-Fi system under ambient noise from different illumination sources (conventional fluorescent light, incandescent lamps, and sunlight). Photo-detectors are exposed to these sources degrading the overall performance of the link. Also, different modulation techniques are implemented to evaluate the link in the presence of ambient noise. Quadratic phase shift keying (QPSK) modulation is superior in performance to other modulation techniques [24].

W. Hashmi et al., in 2021 analyzed and compared the use of photovoltaic cell and PIN diode in the implemented Li-Fi system. The analysis can be deduced that photovoltaic cells provide better NLOS reception of signals than PIN photodiodes. PIN photodiodes have a better tolerance to inter-symbol interference than photovoltaic cells. PIN photodiodes can also operate at a baud rate of 34.8 Kbps compared to a baud rate of 2.4 Kbps provided by the photovoltaic cell[25].

Y. N. Mohammedtawfiq et al., in 2021, introduced a real-time patient monitoring system using Li-Fi technology. This method offers a realistic approach to using four different kinds of sensors installed on a single system. At present, four vital signs are calculated to determine the early warning score: pulse, oxygen in the blood, airflow, body temperature, and electrocardiography (ECG)[26].

V. M. Sangani et al., in 2022, proposed patients' monitoring system based on the Li-Fi technology with heart-rate and ECG sensors. System is designed on the low power embedded boards. It is efficient enough in the emergency case, receiver system can send the feedback to transmitter section. Transmitter system get the notification about emergency in form of buzzer and LED[27].

1.5.2 IPS using VLC Review

M. Aminikashani et al., in 2015, proposed a novel orthogonal frequency division multiplexing (OFDM) VLC system that can be utilized for indoor positioning based on received signal strength (RSS). The proposed system is compared with those that used a single carrier modulation scheme, i.e., OOK modulation. For OFDM modulation, the average root mean square error (RMSE) is 0.26m, whereas for OOK is 1.01m. They show that the OFDM positioning system performs better than the conventional one[28].

W. Gu et al., in 2015, investigated multipath reflections in an indoor visible light positioning system for a typical room. A transmitter and receiver's distance can be calculated using RSS data. There are positioning errors of 0.042m when multipath is ignored and 0.806 m when it is included in the calculations[29].

F. Mousa et al, in 2018 discussed a two-dimensional indoor positioning system based on LED ceiling lamps using RSS. The trilateration method was used to simulate the effects of the received optical power distortions from three transmitters. Using this positioning algorithm and a LOS system, an average error of 5 centimeters can be predicted for each user. In the LOS and NLOS link, however, the error average is approximately 8 cm[30].

E. Lam et al., in 2019, built and demonstrated Ray Surface Positioning (RSP) using low-cost commodity components in a test of a $4\,m \times 4\,m \times 1\,m$ volume. The results offered position estimate errors of less than $30\ cm$ for 95 % of the test volume. The authors used the least square (LS) method to find a target position in this work[31].

G. Shi et al., in 2019, derived the analytical expressions of distance measurement error and the upper bound of a localization error using the LS method based on the RSS technique. In addition, both LOS link and NLOS link are taken into account in a noisy VLC channel. This method of calculating the received power results in

an average localization error of 0.5 m throughout the room. Localization performance is poor at the walls, while the best performance at the center is obtained. This experiment, on the other hand, is carried out with extremely low reflectivity ($\rho = 0.01$) in order to achieve a high localization accuracy of 8mm[32].

S. Li et al., in 2019 , designed RSS-based positioning method for VLC in the presence of orientation uncertainty. The received signal strength is expressed in terms of this orientation uncertainty, which is modelled using the concept of Lie algebra. A position is estimate using maximum likelihood estimation. The positioning error is 0.5m with considering receiver orientation[33].

D. Mai et al., **in 2020,** proposed an entire design of VLC-based large-scale indoor positioning systems, including physical (PHY) and link-layer solutions. The authors used a triangulation method based on an RSS technique for user positioning taking into account the impact of receiver orientation. Each LED's position was separated at the receiver by encoding a unique location identification (ID) with Optical Orthogonal Codes (OOC). Simulation results show that the location error did not exceed 0.5m[34].

M. S. Lima Junior et al., in 2020, proposed and implemented a real-time IPS based on VLC using RSS. It is composed of nine LED-based VLC transmitters installed in the ceiling of an indoor environment, each transmitting different ID codes detected by a photodiode-based mobile correlator receiver. The receiver can measure the distance between itself and the transmitters and use this information to estimate its position in the environment. The average errors in two-dimensional (2D) and three-dimensional (3D) errors were below 25cm and 35cm, respectively, at any point in the test room[35].

B. Pamukti. et al., in 2020, designed a VLC-based positioning system using the RSS method in a closed room with a size of $5 \times 5 \times 3\ m^3$and several numbers of

LEDs. The first scenario uses 4 LEDs, the second scenario uses 6 LEDs and the third scenario uses 8 LEDs. The simulation result shows that the increasing number of LEDs reduces the positioning error and increases the accuracy[36].

A. Chaabna et al., in 2021, studied the impact of ambient light on position accuracy for an IPS based on VLC using the trilateration technique. The study explores both cases considering the effects of wall reflection, and cases neglecting them. The achieved average positioning error is 2.8 cm [37].

X. Meng et al., in 2022, proposed a 3D IPS based on VLC system using an improved whale optimization algorithm (IWOA) to reduce the error caused by the PD rotation. Simulation results show that the average error of 3D positioning is 2.14 cm with no PD rotation. When PD was considered with a rotation angle, the average error of 3D positioning was 27.14 cm when ignoring angle estimation while it was 7.85 cm when the estimation of angle was considered. The positioning error with the PD rotation angle is effectively reduced by the proposed algorithm[38].

1.6 Thesis Objectives

The main objectives of this thesis are:

- To build a smart Healthcare System using Li-Fi technology-based ThingSpeak IoT platform prototype that overcomes the problems in the traditional healthcare system with features including: low-cost, low power consumption, easy to use, and high accuracy.
- Evaluation and validation the performance of the proposed Li-Fi system through different propagation links and ambient noise.
- Making notifications of abnormal cases through sending emails to doctors using IF This Then That (IFTTT) application to add smartness to that system.

- To develop the positioning techniques for elderly people using the VLC system through LOS, NLOS links, and noise.
- Evaluate the IPS using derived MSE, which does not require an actual position.

1.7 Outline Of the Thesis

The thesis is organized in the following way:

C**hapter one** presents an introduction to the VLC technology. Then, a brief introduction to some of its applications, including smart healthcare monitoring systems using Li-Fi technology-based IoT and IPS using the VLC technology. Also, this chapter includes the problem statement of the thesis, related literature survey, aims, and thesis organization.

C**hapter two** describes the theoretical principles for the VLC system including: block diagram and propagation links configuration with its components. The mathematical model of the VLC channel (LOS and NLOS) and noise is given. After that, a VLC applications is shown. IPS using VLC is given, including separation received signals using OCC, trilateration using RSS, position estimation (WLS and ML), anchor selection, and derived MSE. Finally, this chapter presents the IoT concept, definitions, architecture, and ThingSpeak platform.

Chapter three presents the description of the proposed healthcare monitoring system using Li-Fi technology-based IoT design and its implementation. In addition, the description of IPS design using VLC will be given.

C**hapter four** presents lab results of the proposed smart healthcare system using Li-Fi technology based IoT performance analysis under various circumstances.

Then IoT part results with IFTTT notifications are given. Also, the performance of the proposed IPS, including results and discussion, is presented.

C**hapter five** presents the conclusion of the lab and simulation experiments results and suggestions for future work that can improve the performance of the whole systems.

Chapter Two

Theoretical Part: Visible Light Communication (VLC), Indoor Positioning System (IPS), and Internet of Things(IoT)

Chapter Two

Theoretical Part: Visible Light Communication (VLC), Indoor Positioning System (IPS) and Internet of Things(IoT)

2.1 VLC Communication

In 2004, Toshihiko Komine proposed VLC as a newly emerging area in OWC using white LEDs[39]. The VLC technology serves two purposes: indoor lighting and wireless data connectivity [40]. It's suitable for both indoor and short-range networks. As a result, optical wireless technology could complement or possibly replace current wireless communication networks like Wi-Fi and Wi-Max. Despite the method's ability to get an extremely a lot of data rates, the narrow modulation bandwidth of white LEDs is a restricting factor. Intensity modulation with direct detection (IM/DD) is a promising communication approach for developing low-cost VLC systems. Figure (2-1) shows a block schematic of a typical VLC system[41].

The transmitter component of VLC uses a light source, whereas the reception section uses a light detector. The transmitter is an electro-optical device for transforming the electrical signal into optical one. When an optical signal is received, the photodiode converts it to an electrical signal. The Li-Fi channel transmits the transmitter's light intensity-modulated beam. In the receiver section, an optical receiver collects the incoming light signal, which is subsequently processed to obtain the originally provided data[41].

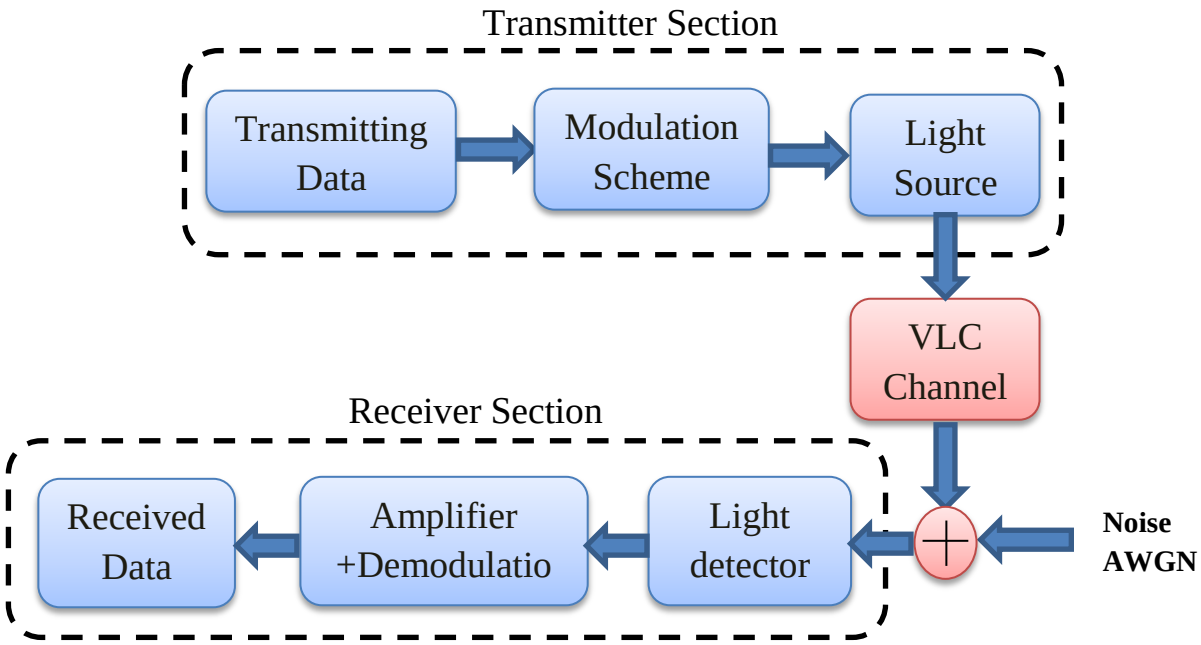

Figure (2-1): Block Diagram of Li-Fi System[41].

The optical path is affected by some factors, including the size of the room, ceiling, walls, and objects' reflectivity. Furthermore, the optical path is influenced by the transmitter and receiver's position and direction, making it more challenging to estimate and compute this loss. As a consequence, an optical link can be configured in several different ways. As shown in figure (2-2), link configurations are commonly classified into four categories.

- Firstly, the directed Line-of-Sight (LOS) link is often used in point-to-point communication links. The links feature a small field of vision (FOV) and slight optical path loss. As a result, it has the highest SNR and in the least transmit power, resulting in the greatest data rates. In addition, this structure has no multipath-induced ISI. Because of its tiny coverage area, its utility for indoor applications may be limited. The directed LOS link requires transmitter-to-receiver alignment; this link topology cannot be employed in mobile applications, as shown in figure (2-2) (a)[42].
- Secondly, the Non-directed LOS is typically used for indoor applications. This link configuration is considered the most flexible

configuration. A broad beam of light transmitter and a large FOV receiver are used together. Surface-scattered signals can be employed to expand the coverage area. Because of its resistance to shadowing and blocking, this connection architecture is ideal for point-to-multipoint broadcast applications. To communicate, the transmitter does not have to be perfectly aligned with the receiver[42].

However, when dealing with significant data rates, this kind of link might suffer from multi - path distortion and high path loss, which severely impacts the system's performance. Furthermore, because of the broad light beam of the transmitters, inter-cell interference occurs when several sources are grouped in a limited region, as illustrated in figure (2-2)(b)[42].

- Thirdly, Non-Line-of-Sight (NLOS) has numerous sub-configurations depending on the number of reflecting sites. It is known as a directed NLOS or first reflection, if it has one, as illustrated in figure (2-2)(c). It's also referred as a diffuse system, and it's utilized to solve issues like blocking and shadowing[42].
- The final arrangement is the tracked link which happens when both the transmitter and receiver are equipped with mechanically steerable optics, as depicted in figure (2-2)(d). This link, however, is both costly and complicated[42]. All link type except the tracked link will be studied in this thesis.

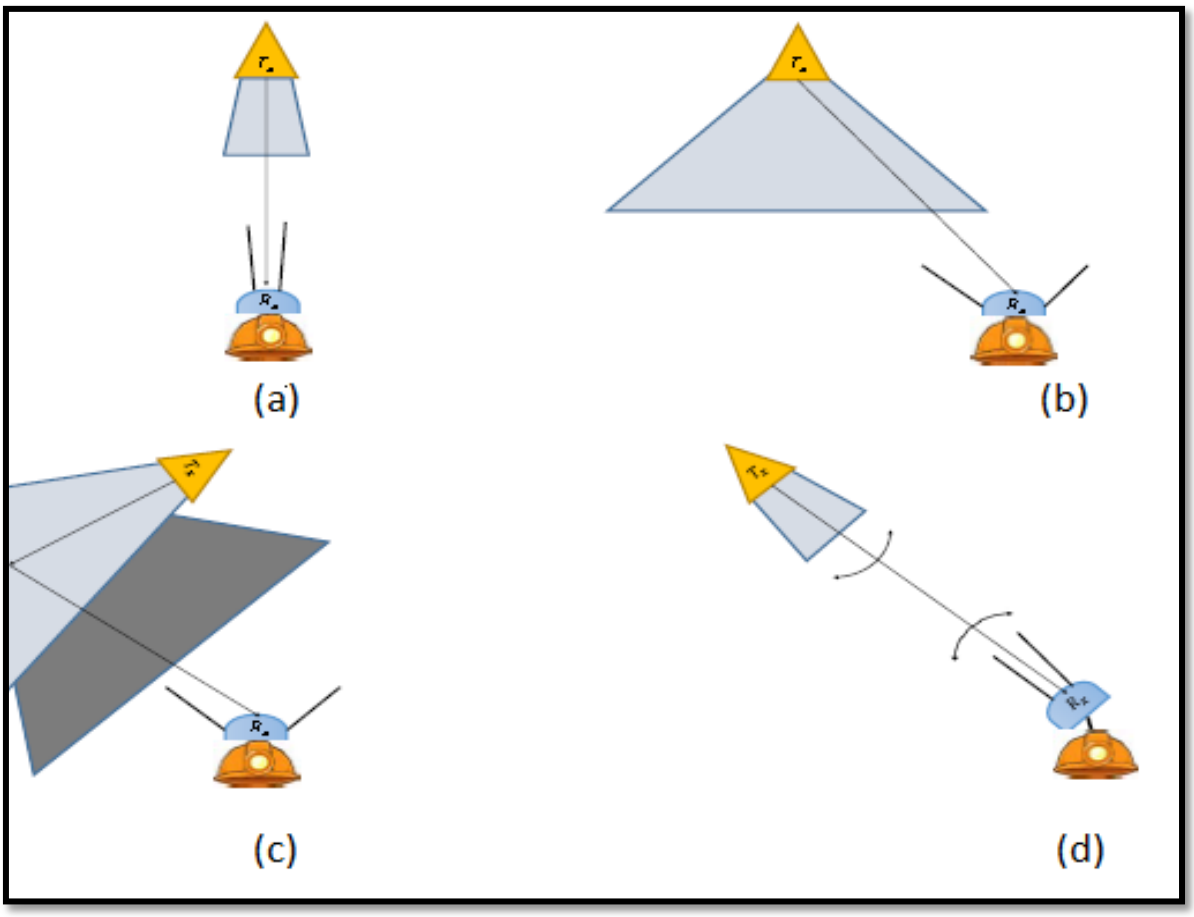

Figure(2-2): Link configurations (a) Direct-LOS (b) Non-direct LOS and (c) Non-LOS by the first reflection (d) Tracked[42].

2.1.1 Light Sources

The most frequent used lighting components in VLC system are lighting emitting diodes (LED). LEDs are solid-state devices emit incoherent light when they are subject to an electronic excitation [43]. This excitation is performed by introducing a forward bias voltage across the p-n junction as shown in figure(2-3). LEDs lights may be made to emit light in a variety of wavelengths (colors) ranging from the visible to the infrared (IR) region of the electromagnetic spectrum[1]. The LED's peak wavelength (color) depends mostly on the band-gap energy of the semiconductor material (E_g) used in the p-n junction.

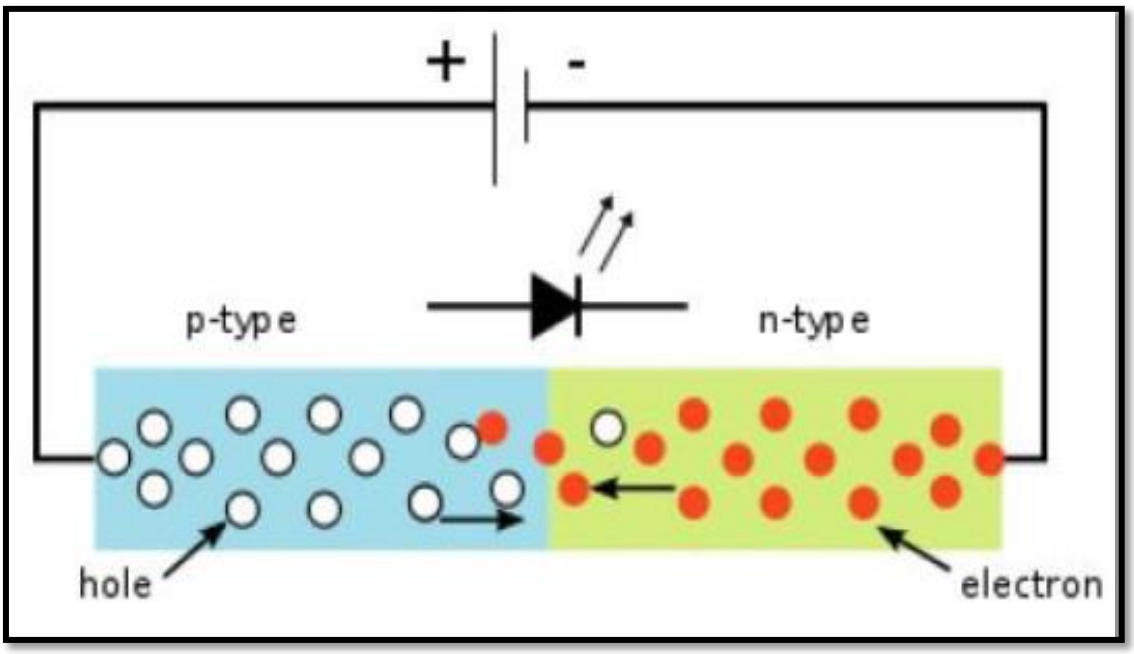

Figure (2-3): Forward bias condition operation in the LED[1].

White LEDs are currently made by using two different techniques (i) combining GaN (Gallium Nitride) LED and YAG (Yittrium Aluminum Garnet) phosphor in the blue range (i.e.; 450nm-470nm) to glare white (ii) combining three types of LEDs (red, green and blue)to realise a white colour.

There are three main characteristics that must be considered when selecting the light source. There are: Power efficiency, luminous efficiency and light bandwidth. The power efficiency of a LED light is the ratio between the optical power output and the electrical power input. This is expressed as follows:

$$\eta_{power} = \frac{Optical\ Power\ O/\ P\ from\ LED}{Electrical\ \ I/P\ Power} \qquad (2.1)$$

The luminous efficiency (η_{lu})is used to express the LED characteristics inside the visible spectrum. This parameters normalize the power efficiency η_{power} by a factor related to the radiation pattern within human eye sensitivity as shown in figure(2-4)[44].

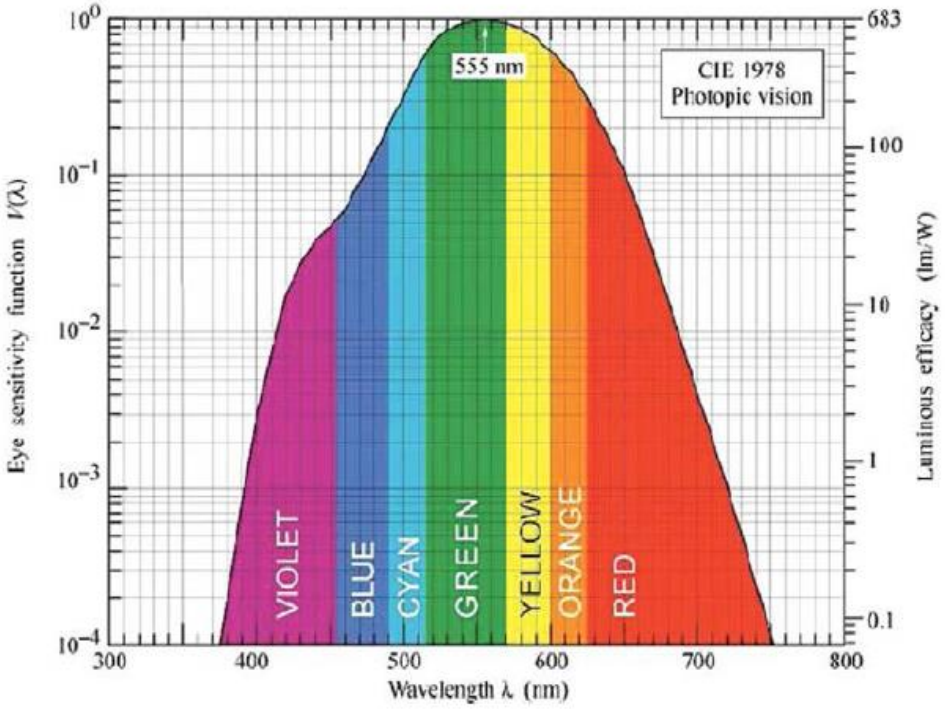

Figure (2-4): Human eye's response based on the 1978 CIE data[44].

The luminous flux (lumens) can be defined as the total emitted flux scaled to reflect the human eye's sensitivity to different light wavelengths. The luminous flux is described by:

$$\Phi_{flux} = 683 \int_{375}^{780} V(\lambda)\, P_{optical}(\lambda) d\lambda \qquad (2.2)$$

where $V(\lambda)$ is the normalization factor based on the eye response and $P_{optical}(\lambda)$ is the LED light's radiated power spectrum. The luminous efficiency of the LED is given by

$$\eta_{lu} = \frac{683 \int_{375}^{780} V(\lambda)\, P_{optical}(\lambda) d\lambda}{Electrical\ \ I/P\ Power} \qquad (2.3)$$

Finally, the light bandwidth will determine the modulation bandwidth and, consequently, the maximum data rate the system can achieve. In general, LEDs have a low pass transfer function that is modelled as:

$$H(j\omega) = \frac{1}{1+j\omega RC} \quad (2.4)$$

This is an equivalent first-order jRC low-pass filter. R and C are the resistance and junction capacitance of the LED. Hence, the 3 dB modulation bandwidth of the LED is given by

$$f_c = \frac{1}{2\pi RC} \quad (2.5)$$

In general, the LED angular distribution of the radiation intensity pattern is represented using a generalized Lambertian radiant intensity distribution pattern[42].

2.1.2 Light Detectors

On the receiver side of a VLC system, a photodetector (PD) is utilized to convert the modulating light intensity into electric signals. The photoelectric effect in the depletion region creates an electrical current when intense light is incident on its surface. Photon absorption results in the formation of electron-hole pairs, with electrons traveling to the N side and holes traveling to the P side of the junction, as shown in figure (2-5). There is a proportional square relationship between the received optical power and the photodetectors' output over a much wider dynamic range. There are the two kinds of photodetectors available: photodiodes and phototransistors. Semiconductor PN junctions, PIN photodiodes, and Avalanche PDs (APDs) are all examples of photodiodes. The size and gain of the depletion layer change between these types. APDs, for instance, have gained while PINs have not, and each has a different bandwidth. Compared to photodiodes, phototransistors have an additional n-type area and a slower response time.

In the essential steady-state operation, the following expression can be used to represent the average photocurrent I_p [1]:

$$I_p = q\eta_i \frac{P_p}{hv} \tag{2.6}$$

where q is the electronic charge, η_i is the quantum efficiency of the device in electrons per photon, hv is the photon energy, h is the Planck constant (eVs), and v is the photon frequency (m/s). The photocurrent-to-received-optical-power ratio, which represents the photodetector responsivity (R_{PD}) in A/watt, can be calculated as follows[1]:

$$R_{PD} = \frac{\text{No. of electron–hole pairs generated/sec}}{\text{No.of incident Photons/sec}} = \frac{I_p}{P_i} = \frac{q\eta_i}{hv} \tag{2.7}$$

The responsivity may be recast using the relationship between the power and the length x of the semiconductor (i.e. $exp(-\alpha x)$) as shown equation below[1]:

$$R_{PD} = \frac{q\lambda}{hv}(1 - R_f)\big(exp(-\alpha x_1) - exp(-\alpha x_2)\big) \tag{2.8}$$

where λ is the light wavelength, R_f is the reflectivity at the photodiode entry, and α is the absorption coefficient. When a photon hits the photodiode's active area, the quantum efficiency measures how likely it is that an electron-hole pair will form. This value typically falls between 0.7 and 0.9. This means that APD's responsivity can be greater than unity because the gain can reach up to 300[1].

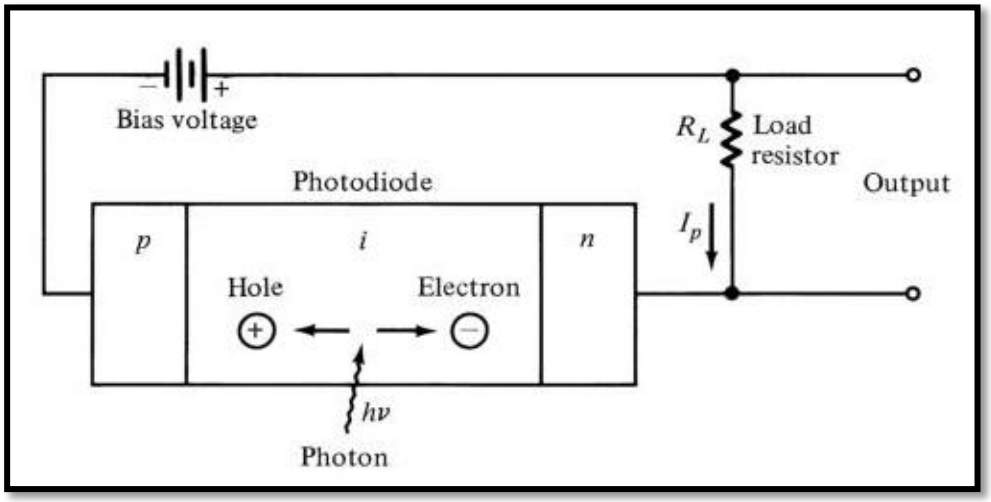

Figure (2-5): PIN photodiode diagram[1].

2.1.3 Modulations Scheme

Previous research has proposed several modulation approaches and thoroughly examined the imposed limits[45]. VLC systems rely on the IM/DD scheme which is used by the vast majority of practical ones. The carrier signal's amplitude, frequency, and phase are modulated by an information signal in RF systems. These are LED-based and appropriate for VLC systems[46]. The following are the primary criteria for choosing a modulation scheme:

i. **Bandwidth efficiency**: Theoretically, there is no limit to the amount of bandwidth available. Multipath propagation, on the other hand, restricts the channel bandwidth, whereas the photodetector area does not restrict the receiver bandwidth. Modulation techniques have an impact on inter-symbol interference (ISI). The ratio of the achievable bit rate (Rb) to the IR transceiver's bandwidth B is known as the bandwidth efficiency ηB[1]:

$$\eta_B = \frac{Rb}{B} \tag{2.9}$$

The power efficiency is the second parameter. Bandwidth efficiency and average duty cycle γ over a given time period are defined as the relationship between the two [1]:

$$\eta_P = \frac{\eta_B}{\gamma} \tag{2.10}$$

ii. **Transmission reliability**: Reliability necessitates a certain level of error tolerance. The phase jitter due to fluctuations in signal power, pulse extensions, and pulse deformation must be overcome by modulation methods.

iii. **Power efficiency**: The average optical power transmitted for each modulation scheme is constrained by regulatory standards and illumination design considerations. The term power efficiency is defined

as the relationship between the pulse energy E_{pulse} and the average energy per bit E_b:

$$\eta_P = \frac{E_{pulse}}{E_b} \tag{2.11}$$

It is necessary to take these characteristics into account when selecting a modulation scheme based on bandwidth and power needs. The simplest modulation approach is OOK, which is the lowest order of M-PAM, has the lowest bandwidth efficiency, and is the easiest to apply. The optical output's intensity is directly proportional to the electrical current's amplitude in this technology. There are two levels in OOK, where pulse energy is used to transmit binary one, while a lack of energy is used to represent bit zero as shown in the following relationship:

$$P(t) = \begin{cases} P_0 & if\ 0 \le t < T_b \\ 0 & elsewhere \end{cases} \tag{2.12}$$

where $P_0 = 2P_{avg}$, P_{avg} is over the symbol interval and T_b is the bit duration. Two sub-techniques of the OOK technique namely return-to-zero (RZ) and non-return-to-zero as shown in figure(2-6). The OOK signal can be represented by [1]:

$$\emptyset_{OOK}(t) = \frac{1}{\sqrt{T}}\ rect(\frac{t}{T}) \tag{2.13}$$

where

$$rect\ (t) = \begin{cases} 1 & 0 \le t < T \\ 0 & otherwise \end{cases} \tag{2.14}$$

The basis function can represent the time-varying optical intensity as:

$$x(t) = \sum_{k=-\infty}^{\infty} 2P\sqrt{T}\ A[k]\emptyset_{OOK}(t - kT) \tag{2.15}$$

Where $A[k] \in [0, 1]$, and it must be uniform.

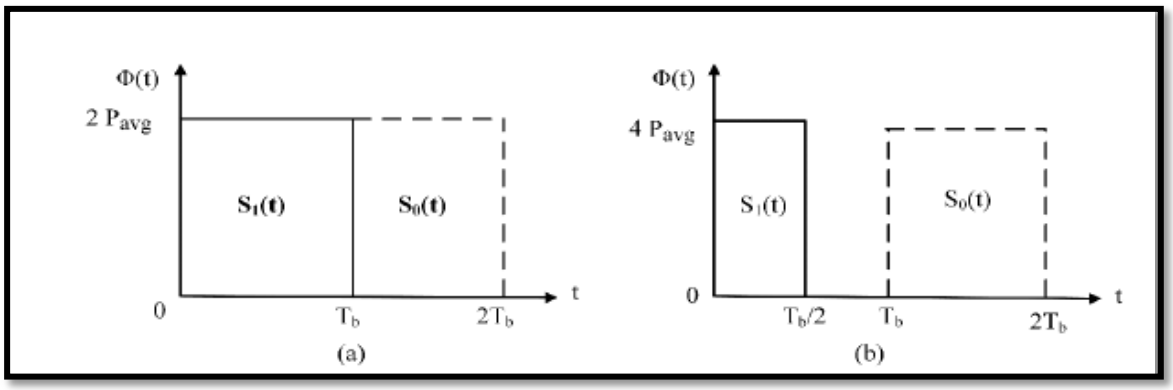

Figure(2-6): OOK signal OOK signal in which S1(t) stands for binary one and S0(t) stands for binary zero. (a) NRZ scheme (b) RZ scheme (γ = 0.5)[41].

As the name implies, the data is communicated in OOK modulation by switching the LED on and off alternately. Lights that are in the "on" condition indicate a digital '1," whereas lights that are off represent a digital '0." The advantage of employing OOK modulation is that it is straightforward to generate and decode; as a result, throughout the actual experiment, this thesis employs the OOK-NRZ modulation method.

2.2 Light Propagation Model

In general, the total received electrical power at the receiver is expressed as in equation (2.16):

$$P_{r-total} = R_{PD}P_t(H_{LOS} + H_{NLOS}) + \sigma^2 \quad (2.16)$$

where $P_{r-total}$, R_{PD}, P_t ,H_{LOS} and H_{NLOS} is the total received power by the user, the responsivity of the photodetector, the transmitted power by LED source and the channel gain part of line-of-sight (LOS) link, the non-line-of-sight (NLOS), respectively. Finally, the σ^2 is the channel noise modelled as additive white Gaussian noise (AWGN) and discussed in section 2.3[42].

2.2.1 LOS Mathematical Modelling

When a direct path links the transmitter and receiver, as shown in figure (2-7), a LOS model is available. In the LOS scenario, the VLC channel's impulse response is given by [47].

$$H_{LOS}(0) = \begin{cases} \frac{1}{r^2} R_{LOS}(\theta_1) A_{PD} \cos(\psi_1) T_s(\psi_1) g(\psi_1) \delta\left(t - \frac{r}{c}\right) \\ 0 \le \psi_1 \le FOV \\ otherwise \end{cases} \quad (2.17)$$

With

$$R_{LOS}(\theta_1) = \frac{(m+1)}{2\pi} cos^m(\theta_1) \quad (2.18)$$

where $R_{LOS}(\theta_1)$ is the transmitter radiant intensity for the LOS scenario, θ_1 is the angle of irradiance, ψ_1 is the angle of incidence, $T_s(\psi)$ is the optical filter gain, $g(\psi)$is the optical concentrator gain, A_{PD} is the detector effective area, $r = d(T_x, R_x)$ is the distance between transmitter and the receiver, FOV is the field of view of the receiver, and m is the Lambertian emission, which is given as

$$m = \frac{-\ln(2)}{\ln(\cos(\theta_{1/2})} \quad (2.19)$$

with $\theta_{1/2}$ being the semi angle at half luminance of the LED.

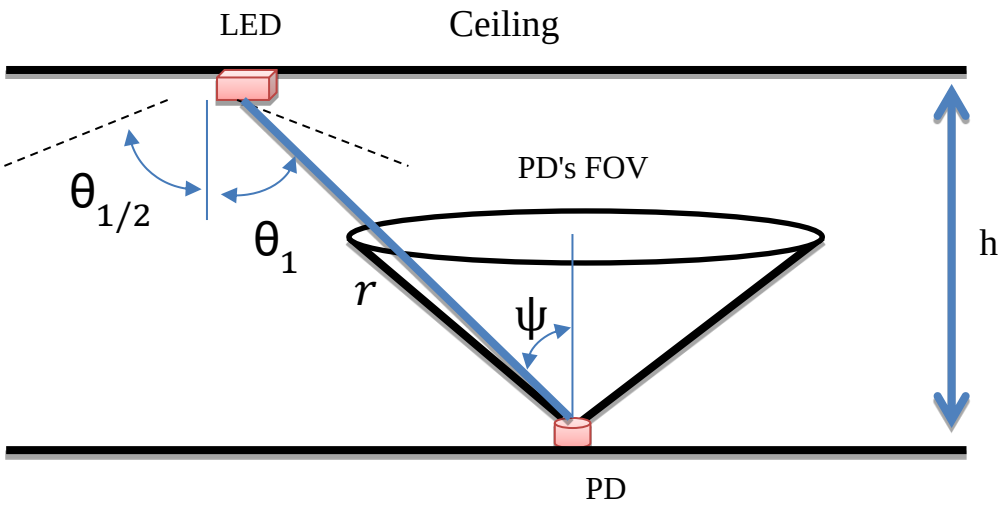

Figure (2-7) LOS link modelling[47] .

2.2.2 NLOS Mathematical Modelling

The NLOS model is depicted in figure (2-8) by a ray incident from the transmitter on a wall and subsequently from the reflective element to the

receiver. The VLC channel's impulse response in the NLOS situation is described as.

$$H_{NLOS}(0) = \begin{cases} \frac{1}{(r_1+r_2)^2} R_{NLOS}(\theta_2) A_{PD} \cos(\psi_2) T_s(\psi_2) g(\psi_2) \mu\delta\left(t - \frac{(r_1+r_2)}{c}\right) & 0 \le \psi_2 \le FOV \\ 0 & otherwise \end{cases} \quad (2.20)$$

With

$$R_{NLOS}(\theta_2) = \frac{(m+1)}{2\pi} cos^m(\theta_2) \quad (2.21)$$

$$\mu = \frac{\rho dA_{wall}}{\pi} \cos(\alpha) \cos(\beta) \quad (2.22)$$

Here μ is the coefficient based on Fresnel reflection, where μ is the first reflection factor, $R_{NLOS}(\theta_2)$ is the transmitter radiant intensity for the scenario of NLOS, ρ is the factor of reflectance, dA_{wall} is the small region reflective area, α is the reflective point angle of irradiance, and β is the angle of multipath of irradiance to the receiver [41].

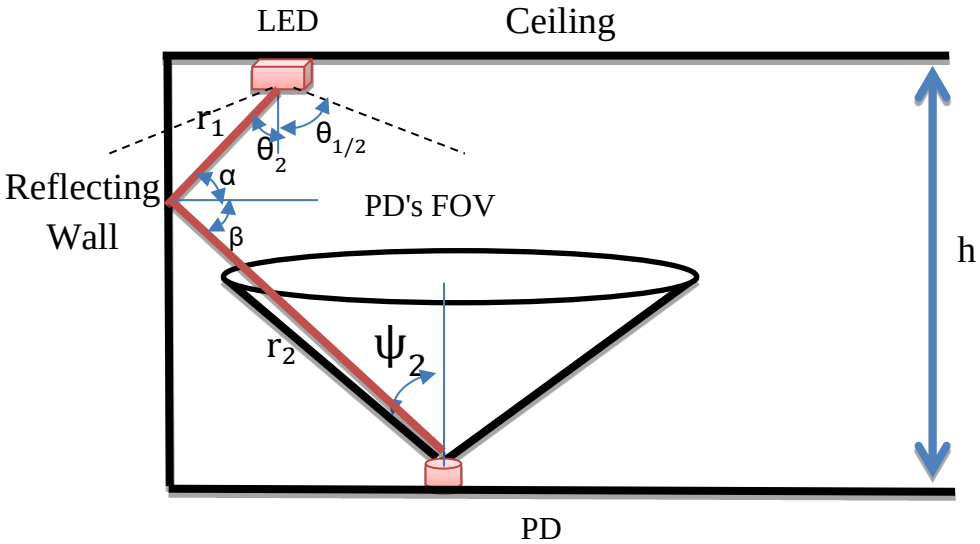

Figure (2-8) NLOS link modelling[47].

2.3 Noise Model

Noise is inherently present in all communication channels. The received signal has the least amount of power on the receiver side, while the amount of noise on the transmitter side is the most near the end of propagation. When it comes to most noise sources (outside of APD), there are three main ways that it can be produced.

2.3.1 Dark Current Noise

When no light is incident on the photodetector surface, the dark current noise is induced by the dark current generated in the circuit. Due to the reverse bias operation, a slight reverse saturation current flow through the device. A small amount of reverse saturation current flows through the device as a result of the reverse bias operation. For Si PIN photodiode and Si APD, the amplitude of the dark current is typically 100 pA and 10 pA, respectively.

2.3.2 Shot Noise

The shot noise is the noise due to the environment factor for example sun or sky luminosity. It found in all-optical receivers and is the primarily caused of noise in photodetectors and also known as background noise. The shot noise variance is given by.

$$\sigma_{shot}^2 = 2qI_{bg}I_2B_n + 2qR_{PD}P_{r-total}B_n \quad (2.23)$$

q is the electric charge, I_{bg} is the background current, I_2 and I_3 denotes the noise bandwidth factor B_n is the bandwidth, R_{PD} denotes the photodetector responsivity[48]**.**

2.3.3 Thermal Noise

For all electronic devices (active or passive), the load resistance (RL) is an important factor. A random motion of electrons generates thermal energy, even when no optical power or voltage is applied to a photodetector. The

Johnson is another name for it. Besides that, it is white noise, and its distribution is Gaussian with zero means, and the variance can be calculated as shown[48].

$$\sigma_{Thermal}^2 = \frac{8\pi k T_K A_{PD} I_2 B_n^2}{Go} + \frac{16\pi^2 k \Gamma T_k}{gm} C_f^2 A_{PD}^2 I_3 B_n^3 \quad (2.24)$$

where k stands for the Boltzmann Constant, C_f is the fixed capacitance per unit area, T_K is the absolute temperature, A_{PD} is the PD effective area, Go is the open-loop gain, Γ is the FET channel noise factor, and gm is the FET transconductance and $I_3$is the FET channel noise factor[48].

The dark current noise is minimal and can be neglected. So, the total noise variance (σ^2) can be characterized by the following equation[42]:

$$\sigma^2 = \sigma_{shot}^2 + \sigma_{Thermal}^2 \quad (2.25)$$

The VLC system is being evaluated by the computed optical and electrical SNR value, which can be expressed as given below [49].

$$OSNR = \frac{P_{r-total}}{\sigma^2} \quad (2.26)$$

and

$$ESNR = \frac{(R_{PD} P_{r-total})^2}{\sigma^2} \quad (2.27)$$

2.4 VLC Applications

VLC technology has numerous applications in which it could fit in. Hereafter, some of the most relevant applications for healthcare monitoring system based on VLC are discussed. This applications include light-fidelity technology and Indoor positoning system.

2.4.1 Light-Fidelity

For data sharing, social activities and education, interaction, communication, and knowledge updates, different people connect through a network. Wireless Fidelity (Wi-Fi) offers, around offices, schools, homes and even in public places, wireless internet access. But, as different technologies have restrictions , Wi-Fi faces several challenges and impacts in availability, capacity, security and efficiency, since incremental demand for wireless [50]. Since Wi-Fi is able to cover a whole place, its bandwidth is limited to several hundred of Mbps. The Wi-Fi speed is not enough for transmitting and receiving huge files such as video games, HD movies, and music gathering. Based on media servers or cloud for storing files, more data rate and bandwidth are required[51].

One of the most important applications envisioned for VLC is providing Li-Fi or optical Wi-Fi as an alternate or solution to Wi-Fi limitations. Basically, it is data transmission via the illumination using LEDs and a photo detector to detect signals. Li-Fi is a low cost technique, highly impressive and could be considered as a healthy environment compare to the Wi-Fi. Li-Fi uses light spectrum from infrared (IR) to ultraviolet (UV) consisting the visible light (VL) as an alternate of radio waves for data replacing [52]. Harald Haas is the head of mobile communication at the Edinburgh University who has been mentioned as the of Li-Fi inventor. He presented a manifestation of a Li-Fi model at the TED Global conference in Edinburgh in 2011. This technique is implemented as a part of the electromagnetic such as telecommunication algorithms and different networks then presents a short-distance wireless communication [6]. The principle of Li-Fi is a communication of data on the high light frequencies that is not observed by human eye. However, it is concentrated on a photo diode which converts the on-off state into digital data. If the LED is on state , a binary 1 is transmitted, and when it is off , a 0 binary is transmitted, then they are able to be switched on and off fast, which provides a kindly convenient

moment for transmitting data[53]. Up to 10 Gbps obtained as a high data rate transmission through Li-Fi which offers more security and privacy, since it covers a short range and not penetrates the walls, and it has higher frequency than radio and does not interfere in sensitive electronics, putting it in an efficient mean for implementations in different environments such as hospitals and aircraft[50].

Table (2-1): Li-Fi and Wi-Fi comparison.

Property	**Li-Fi**	**Wi-Fi**
Transmission and reception medium	IR or UV or VL	Radio waves
Maximum bit rate	$> 10\ Gbps$	$6\ Gbps$ utilizing IEEE 802.11 ad
Infrastructure Cost	Low	Very High
Interference level	Low	High
Distance	Short	Short to long
Security	High	Low
Standards	802.15.7	802.11b
Services	Lightening when using visible light & Communicating	Communicating
Noise sources	Light from the sun and other ambient sources	All electrical/electronic devices
Power consumption	Low	High
Movement	Limited	Unlimited
Coverage	10m	Up to 100m
Health risk	No health risks involved in VLC	Harmful when high power is used for transmission

2.4.2 Indoor Positioning System using VLC technology

For many years, radio-band satellite-based positioning technologies (such as Global Positioning System (GPS)) have been widely used, primarily for outdoor purposes. Due to severe signal degradation by walls and enclosed objects (homes, factories, offices, tunnels, etc.)[54]. Furthermore, for interior applications requiring greater precision, commercial GPS systems with position errors of a few meters are unsuitable. RF wireless technologies such as wireless local area networks (WLAN), Wi-Fi, and Bluetooth can be used to locate people indoors, with varying precision, coverage, and costs[55], [56].

RF-based positioning systems perform position estimation by exchanging signals between nodes with defined positions (called anchor nodes) and nodes whose locations need to be estimated (called target nodes). Likewise, in a VLC system, LED transmitters, which have established positions and are often affixed to the ceiling of a room in indoor environment, also serve as anchor nodes. On the other hand, VLC receivers with PD attempt to establish their location using LED signals detected by PD [57].

For location estimation in a VLC system, several ways can be used, divided into two categories: direct positioning and two-step positioning (see figure(2-9)). The direct positioning approach utilizes all of the available information from received signals to estimate the receiver’s position without first considering position-related factors. Instead of relying on additional parameter estimation steps, this approach directly addresses the issue of localization[58].

On the other hand, the two-step method accomplishes position estimation in two stages. Position-related parameters are extracted in the first stage. Then algorithms and methodologies for estimating receiver position are employed in the second stage depending on those parameters. The two-step positioning method is less complex than the direct positioning method (which necessitates

a large amount of data storage and transmission capacity), resulting in a poor solution. It does not immediately utilize the received signals[58].

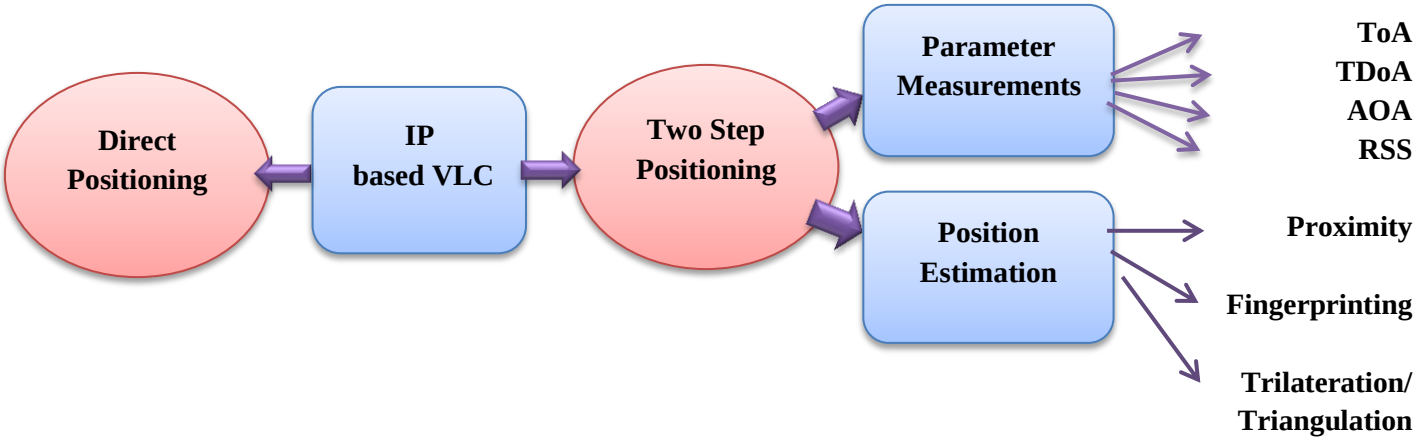

Figure (2-9): Positioning techniques for VLC systems[58].

The research in the literature investigates many position-related parameters in the context of two-step positioning, such as:

a. Time of Arrival (TOA), The propagation speed of an electromagnetic signal is constant. If the signal propagation time between an LED and a target can be determined, ToA can determine the distance between the LED and the target, as shown in figure(2-10). As a result, the distance (d) is obtained as shown:

$$d = C.t \qquad (2.28)$$

Where C is the speed of light (i.e., 300,000km/s) and t is transmission time of the signal, respectively. Using the measurements of ToA has limitations. It requires a high degree of synchronization and precise time measurements, making these metrics relatively expensive in practical applications[59].

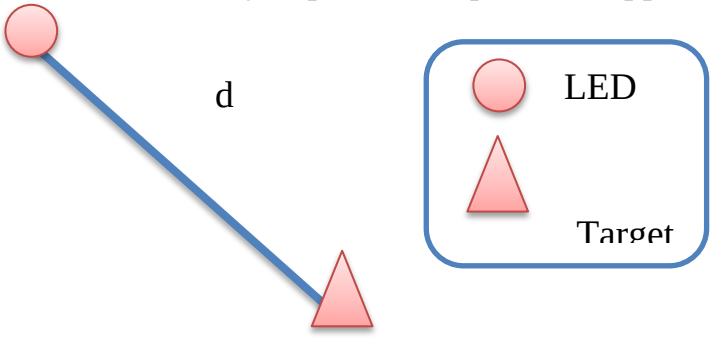

Figure (2-10): ToA-Measurement[59].

b. Time Difference of Arrival (TDoA), It is similar to the ToA but has an advantage over it in that it does not needs an absolute time reference, is capable of using low-cost antennas, and is impervious to mistimed timing signals. Time difference between two signals with different propagation speeds (C1 and C2) is all that TDoA takes into account when determining distance. The time difference t_{Diff} and distance d is given by the following expression:

$$t_{Diff} = t_2 - t_1 = \frac{d_1}{c} - \frac{d_2}{c} \tag{2.29}$$

This means that only the receiver needs to be synchronized with the system, rather than the entire system[59].

c. Angle of Arrival (AOA) the angle at which the transmitted signal impinges on the receiver is estimated using antennae arrays on the receiver side, as shown in figure(2-11) [59][60].

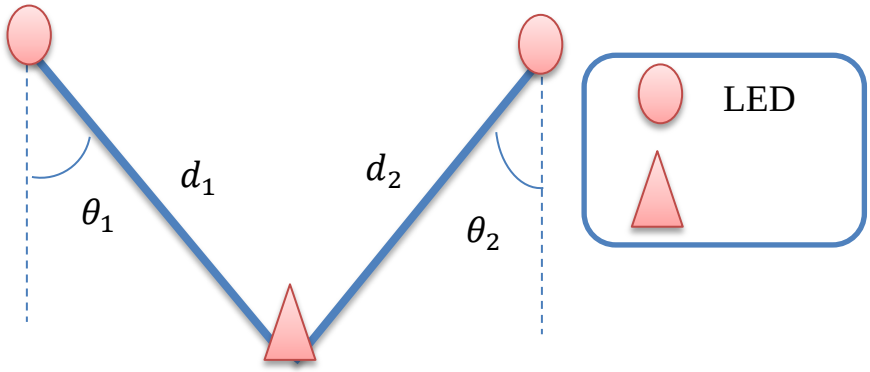

Figure (2-11): AoA-Measurement [59].

However, AOA requires highly directional antennas or antenna arrays. It is a promising metric for VLC systems and can be used effectively in the localization process. Based on the received signal direction, AOA based systems can benefit from LOS connections between the LED transmitters and the VLC receiver and are able to perform localization adequately.

d. Received Signal Strength (RSS), In VLC systems, RSS is a widely used method. This method uses the received power (the received signal strength) levels determined at the receiver to estimate the transmitters' distances. The RSS parameter, unlike time-based parameters such as TOA and TDOA,

does not necessitate synchronization. Furthermore, the RSS parameter used in VLC systems is significantly more accurate than that in RF systems[57]. Multipath effects in RF-based systems are the primary cause of this issue. Specifically, RF-based systems are plagued by multipath interference and typically lack a LOS path between the transmitter and receiver. As opposed to RF-based system, multipath effects are not as critical in VLC systems since VLC systems commonly have LOS paths between LED transmitters and VLC receivers. Diffuse components resulting from multipath scattering are significantly weaker than the LOS component.

Even though both VLC and RF-based localization systems use the same types of position-related parameters, the information they carry can differ greatly.

After obtaining position-related parameters in the first stage of the two-step positioning strategy, a VLC system can use various algorithms and approaches to complete the localization process in the second step. The following are the algorithms and tactics used to achieve this goal:

i. **Proximity algorithm:** accomplish localization for a fixed node and a mobile node depending on transmission range. If the power level is low, the mobile node may be out of transmission range in this situation[41].
ii. **Trilateration/triangulation algorithm** uses the geometrical dependencies between the user and transmitters. In contrast, the trilateration method uses distances, and the triangulation method uses the angles between the mobile node and transmitters [61].
iii. **Fingerprinting methods**, the user's position is calculated in two stages: The predicted signal's channel parameters, SNR, and probability distribution are determined in the first stage, which is an offline learning or training stage. Second, the VLC receiver's online measurements are compared to the offline dataset, and the receiver's position in the system is determined using a matching algorithm[62] .

Alternative approaches to improving the localization performance of VLC systems can be used in addition to the algorithms and techniques utilized in the second step of the two-step positioning scheme. Cooperation among the entities in a VLC system can improve localization accuracy[63], just as it can in RF-based positioning systems.

2.5 Trilateration in 3D using RSS

Figure (2-12)shows our respected IPS-based VLC. A large-scale building [hospital in our work] is observed, and fixed position transmitters are placed in a grid layout, which is a conventional layout for recessed lighting fixtures, to measure their positions. Prior to the event taking place, a mobile target is expected to get the database including all LED position coordinates and store them on his or her device.

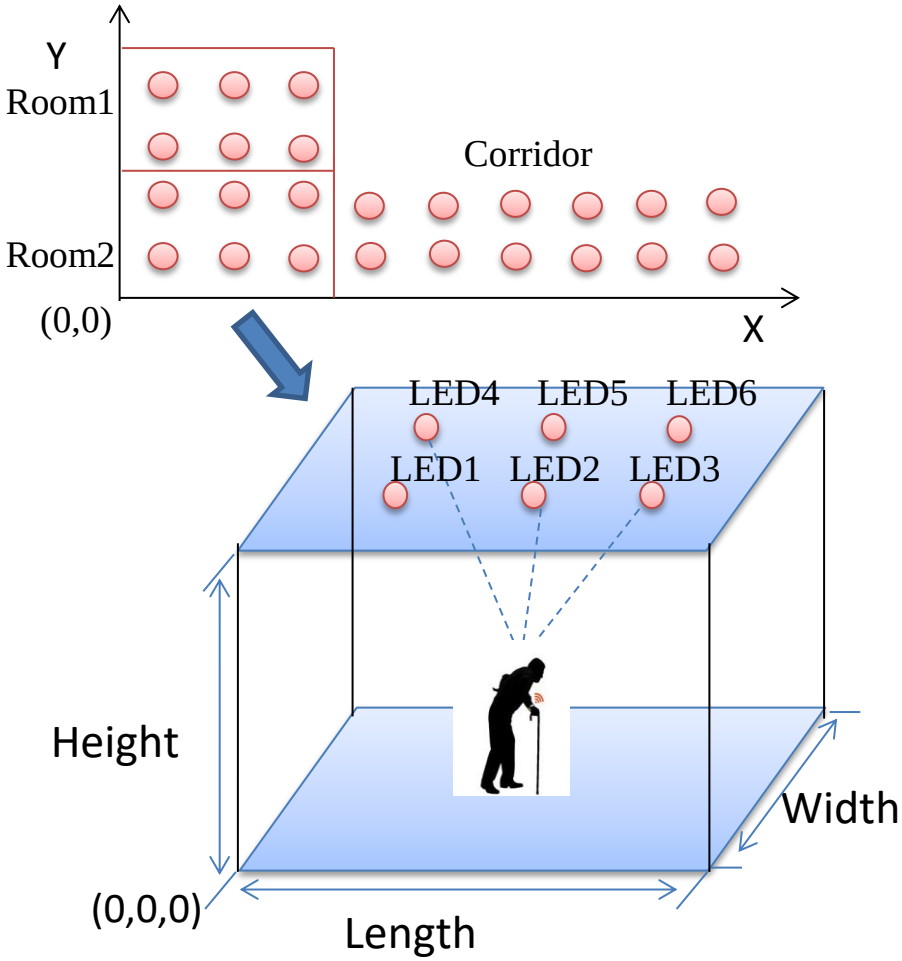

Figure (2-12): IPS based VLC [34].

It's assumed that the lighting infrastructure has been installed so that the target device can always receive signals from at least four LEDs. The trilateration method can be used to locate the user based on these signals. The method's central idea is to estimate the distances between the user and the four LED transmitters, as shown in figures (2-13).

Let P= (x, y, z) denotes the position of the target in Cartesian coordinates. Additionally, $L_i = (Lx_i, Ly_i, Lz_i)$ presents the positions of the LEDs. $i = 1, \ldots . n$, where i expresses the LED index. In general, the actual distances between *i*th LED and the target is presented in the following equation.

$$r_i^2 = (Lx_i - x)^2 + (Ly_i - y)^2 + (Lz_i - z)^2 \qquad (2.30)$$

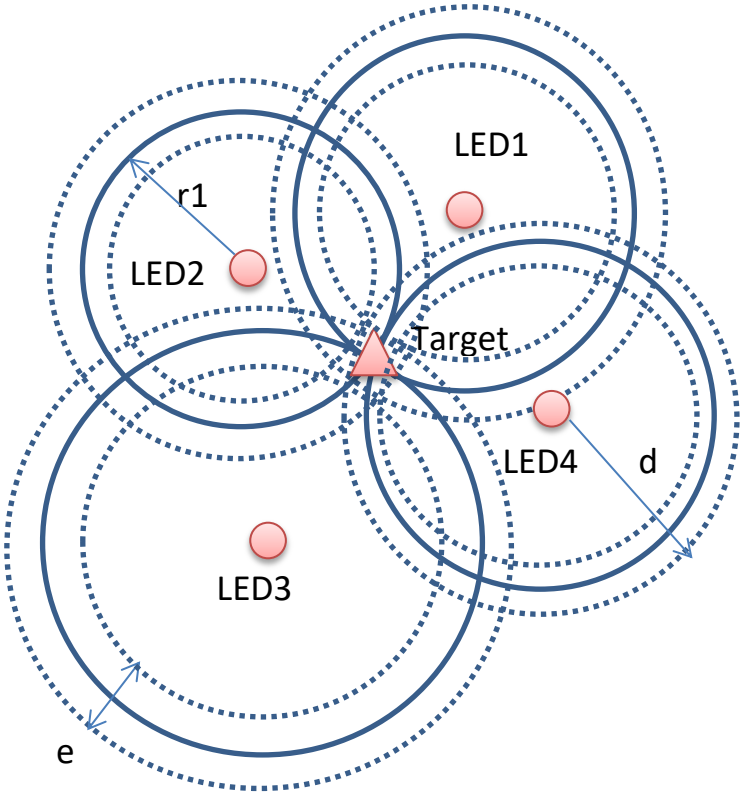

Figure(2-13): Trilateration method[34].

At a transmitter side, assume that the average transmitted optical power P_t is known and constant. Given the received electrical signal at the receiver

($P_{r-total}$) as in equation (2.16), The estimated distance d_i from the target to the ith LED is given by:

$$d_i = \left\{ \frac{(m+1)A_{PD}h^{m+1}P_t cos^m(\theta_1)\cos(\psi_1)T_s(\psi_1)g(\psi_1)}{2\pi P_{r-total_i}} \right\}^{\frac{1}{2}} \quad (2.31)$$

2.6 Separation Received Signal

It should be noted that previous works examined positioning methods for typical room sizes (e.g, a few meters each dimension) with the assumption of using time division multiplexing (TDM), for signal separation at the receiver [[28],[29] and [33]. In practice, it is quite obvious that indoor positioning would be more useful in large areas, such as supermarkets, hospitals, stations or airports. Thus, IPSs are expected to be predominantly deployed in a large-scale fashion. Moreover, the use of TDM poses several drawbacks for practical implementation. Firstly, it requires a perfect synchronization between the transmission times of LEDs. An additional transmission procedure is therefore necessary to ensure the constant illumination provided by the LEDs. Secondly, since the signals are transmitted in different time slots, the receiver may need to spend a long time obtaining signals from at least four LEDs, which renders real-time navigation more challenging. Authors in [34],used Optical orthogonal codes (OCCs) as a multiplexing techniques for signal separation with a unique location identification (ID). Hence, received signals at the receiver can be simultaneously distinguished. For the large-scale design, a code re-use strategy was employed to efficiently use the OCC resource. The OOC concept and code reuse strategy will be explained below.

2.6.1 Optical Orthogonal Code (OOC).

Generally, two serious problems when using RSS, namely, signal isolation and power estimation to determine the distance from the patient to the LED transmitter. In the beginning, the OOCs are used as to classify several

signals received at the receiver. An OOC, denoted by $(n, k, \lambda_a, \lambda_c)$, is a series of unipolar sequences (0,1). 0 and 1 are called chips. n and k are the code length and weight, which refer to the total number of chips and the number of chips "1", respectively. λ_a and λ_c denote the autocorrelation and cross-correlation constraints, which are given below[64]:

$$\sum_{t=0}^{n-1} x_t x_{t+\tau} \leq \lambda_a \tag{2.32}$$

$$\sum_{t=0}^{n-1} x_t y_{t+\tau} \leq \lambda_c \tag{2.33}$$

For any $x, y \in C$ and any integer $t, (0 \leq t < n)$. In the case that $\lambda_a = \lambda_c = 1$, the maximum number of codewords $|C_{max}|$ is expressed as:

$$|C_{max}| = \leq \left[\frac{n-1}{k(k-1)}\right] \tag{2.34}$$

While OOCs are used, the separated signals cause an unpredictable amount of interference. This requires the force of the target signal to be determined, not directly. However, we will note that the target signal's power is less than the interruption (mixture of more than two signals with same power as the desired one). A chip-level detection is used to determine the minimum level of chip power required to solve the problem. This method can be highly complicated in significant data rates that are typically not required for IPSs. Because of the low OOC cross-correlation (the number of cross-correlations between two codes is at most one, while the overall number of signals received is not too high, we can measure the signal strengths received separately, as seen in figure (2-14). We can assure that the RSS will not be affected by interference by selecting the lowest power chip. Only the limited cardinality (i.e., the maximum number of OOC codewords |C max |) remains a challenge. For example, the number of codes in C (341,5,1,1) is only 16, which is significantly less than the expected number of LEDs for a large-scale network. To increase

the code cardinality, a longer code length is needed, which increases the chip rate and decreases the amount of chip power. In order to solve this problem, a code reuse approach is used.

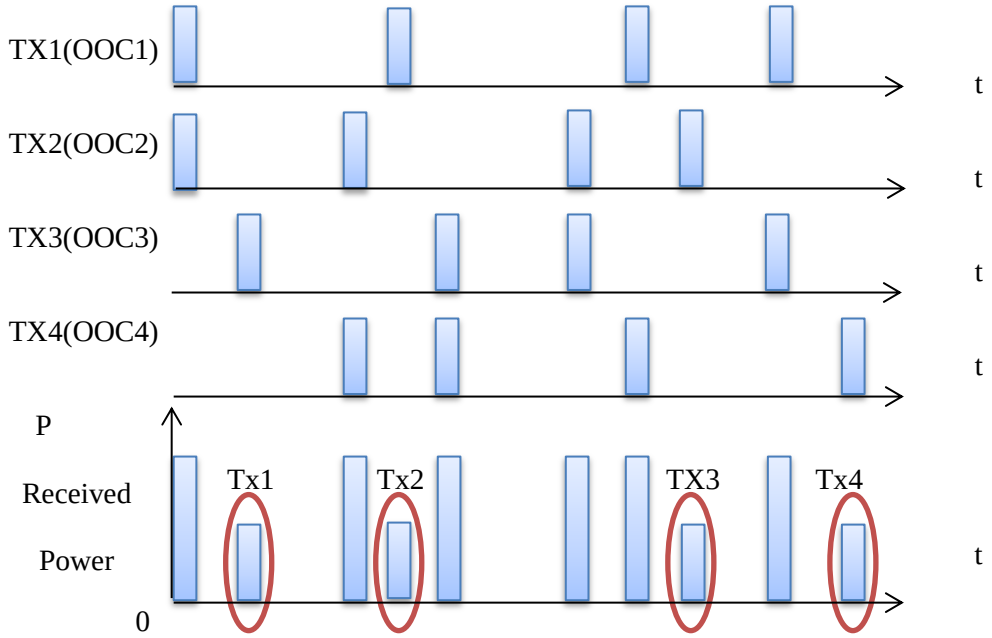

Figure (2-14): Example of RSS detection[34].

2.6.2 Code reuse strategy

In this method, for any network size, we need just six codewords to allocate. They are arranged so that the receiver will not interpret two signals of the same codeword simultaneously. Code reuse is depicted in figure (2-15) using the 6x6 LED grid as an example. One set of six codewords includes: (C1, C2, C3) and (C4, C5, C6). The first, third, and fifth column LEDs are assigned to (C1, C2, C3), while the second, fourth, and sixth column LEDs are assigned to (C4, C5, C6) in the following mode. For LEDs divided into two LEDs using different codewords, the same codeword is assigned to each column. Additionally, separate codewords are allocated to six LEDs in each row. The lighting field of two LEDs with the same codeword will not interfere with each other[34].

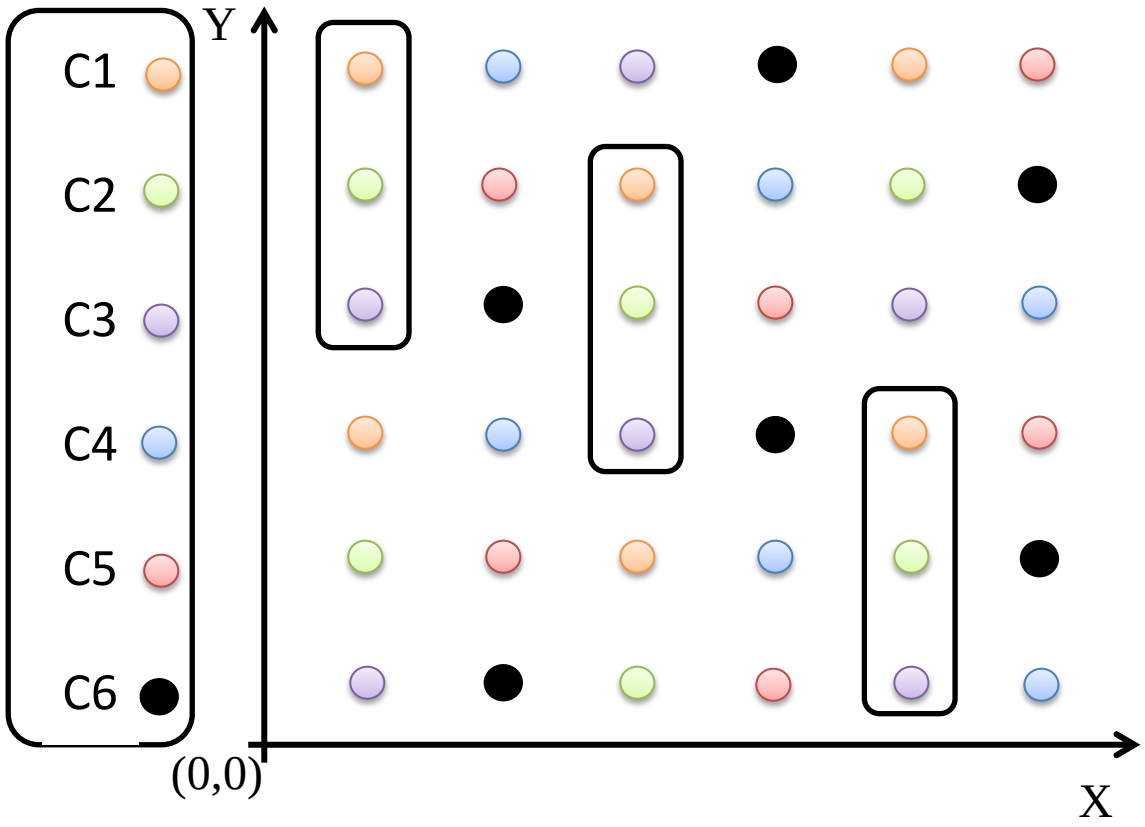

Figure (2-15): The code reuse strategy [34].

2.7 Position Estimation

Once the distances to various anchor nodes have been calculated, a positioning algorithm must be applied to calculate the mobile node's position. This thesis uses weight least square (WLS), maximum likelihood estimator (MLE), and modified MLE to find the target's position, explained in the following subsections.

2.7.1 Weighed Least Square Estimator

As previously stated, the actual distance is r, and the estimated distance is d, so the error will present and the four circles in figure(3-5) will not intersect at one point. This error can be calculated as shown below:

$$e_i = \sum_{i=0}^{i} r_i - d_i \qquad (2.35)$$

Multiple solutions appear in the system described by Eq. 2.16 because of the noisy range measurements. In this scenario, as discussed in[65][66], the

least square solution provides a standard approach to an approximate solution of the positioning system.

$$r_1^2 - r_i^2 = (Lx_1 - x)^2 + (Ly_1 - y)^2 + (Lz_1 - z)^2 - ((Lx_i - x)^2 + (Ly_i - y)^2 + (Lz_i - z)^2) \quad (2.36)$$

where $i = 2 \ldots\ldots\ldots n$. By adjusting equation (2.36) and computing estimated position in terms of estimated distance. Then, describing the system in the matrix form as

$$A\hat{P} = B \quad (2.37)$$

Where

$$\hat{P} = \begin{bmatrix} \hat{x} \\ \hat{y} \\ \hat{z} \end{bmatrix} \quad (2.38)$$

$$\mathrm{A} = \begin{bmatrix} Lx_2 - Lx_1 & Ly_2 - Ly_1 & Lz_2 - Lz_1 \\ Lx_3 - Ax_1 & Ly_3 - Ly_1 & Lz_3 - Lz_1 \\ \vdots & \vdots & \\ Lx_n - Lx_1 & Ly_n - Ly_1 & Lz_n - Lz_1 \end{bmatrix} \quad (2.39)$$

And the measurement vector as shown in

$$B = 0.5 \begin{bmatrix} Lx_2{}^2 + Ly_2{}^2 + Lz_2{}^2 + d_1^2 - d_2^2 \\ Lx_3{}^2 + Ly_2{}^2 + Lz_2{}^2 + d_1^2 - d_3^2 \\ \vdots \\ Lx_3{}^2 + Ly_2{}^2 + Lz_2{}^2 + d_1^2 - d_n^2 \end{bmatrix} \quad (2.40)$$

The least squares solution to the system is given by

$$\hat{P} = (A^T A)^{-1} A^T B \quad (2.41)$$

To enhance the positioning accuracy, the equation (2.41) could be modified using the variance of the measured distance and the new algorithm is named the weighted least squares (WLS) method [67]. The weights used in the WLS algorithm are changed by taking into consideration the inverse of the variance of the relevant distance measurements, as indicated in the weight matrix (W) below.

$$W = \begin{bmatrix} var(d_1^2) + var(d_2^2) & var(d_1^2) & \dots. & var(d_1^2) \\ var(d_1^2) & var(d_1^2) + var(d_3^2) & \dots. & var(d_1^2) \\ & \vdots & & \\ var(d_1^2) & var(d_1^2) & var(d_1^2) + var(d_n^2) & \end{bmatrix} \quad (2.42)$$

where $var(d_1^2)$ is the variance of a square estimated distance between the reference LED and P and $var(d_n^2)$ is the variance of a square estimated distance between all remaining LEDs and the P. Then, in the WLS's final equation, use the inverse of W.

$$\hat{P} = \begin{bmatrix} \hat{x} \\ \hat{y} \\ \hat{z} \end{bmatrix} = (A^T W^{-1} A)^{-1} A W^{-1} B \quad (2.43)$$

2.7.2 Maximum Likelihood Estimator

The target position is computed using the WLS estimator by reducing the squared error of distance estimation from known anchor nodes (i.e. LEDs). However, in the minimization issue, the probability distribution of the measurement error is ignored. The measurement error of various signal properties can have a different probability distribution. Furthermore, in a complicated signal transmission environment, the measurement error variance can be considerable. Consequently, lowering the mean square error of distance measurement without taking into account the error probability model will not lead to optimal estimation of the target position[68].

Maximum Likelihood Estimation (MLE) maximizes the joint probability of obtaining a collection of independent and identically distributed observed data to estimate unknown parameters in a statistical model. Let X is denoting the observed data samples $(x_1, x_2, \cdots, x_n)$ and θ denoting the statistical model parameter set to be estimated. Therefore, if we have n observations, we can represent the joint probability density function as[68]:

$$P(X|\theta) = P(x_1|\theta).P(x_2|\theta) \dots .. P(x_n|\theta) \quad (2.44)$$

where $P(x_n|\theta)$ is the conditional probability of having the observed data sample x_n when the parameter vector is θ. In practice, equation(2.44) is typically converted to log-likelihood function as:

$$L(X|\theta) = \sum_{i=1}^{n} \ln(P(x_n|\theta)) \quad (2.45)$$

Then the unknown parameters in the statistical model can be estimated through minimizing the log-likelihood function in (2.45) with respect to θ. In wireless location estimation, the observed data samples correspond to those measured position dependent parameters from the anchor nodes.

The unknown parameter vector θ corresponds to the unknown target position $(\hat{x}, \hat{y}, \hat{z})$. Let $D = (d_1, d_2, \cdots, d_n)$ denote the measured position-dependent parameters from n different anchor nodes, equation (2.45) becomes[68]:

$$L(D|\hat{x}, \hat{y}, \hat{z}) = \sum_{i=1}^{n} \ln(p(d_i|\hat{x}, \hat{y}, \hat{z})) \quad (2.46)$$

As previously stated, $e_i = \sum_{i=0}^{i} r_i - d_i$. Hence equation (2.46) becomes

$$L(D \left| \hat{x}, \hat{y}, \hat{z}) = \sum_{i=1}^{n} \mathrm{E}_i(\hat{x}, \hat{y}, \hat{z}) \right. \quad (2.47)$$

Where $\mathrm{E}_i(\hat{x}, \hat{y}, \hat{z}) = \ln(p(r_i - d_i)$. Therefore, the target position can be estimated as

$$\hat{P} = (\hat{x}, \hat{y}, \hat{z}) = argmin_p L(D|\hat{x}, \hat{y}, \hat{z})) \quad (2.48)$$

Figure (2-16) depicts an example of the MLE algorithm's localization process. Signal characteristics between LEDs and target are captured and transmitted to the data center. The target's position is determined using MLE, which is based on a statistical model of signal measurement error[68].

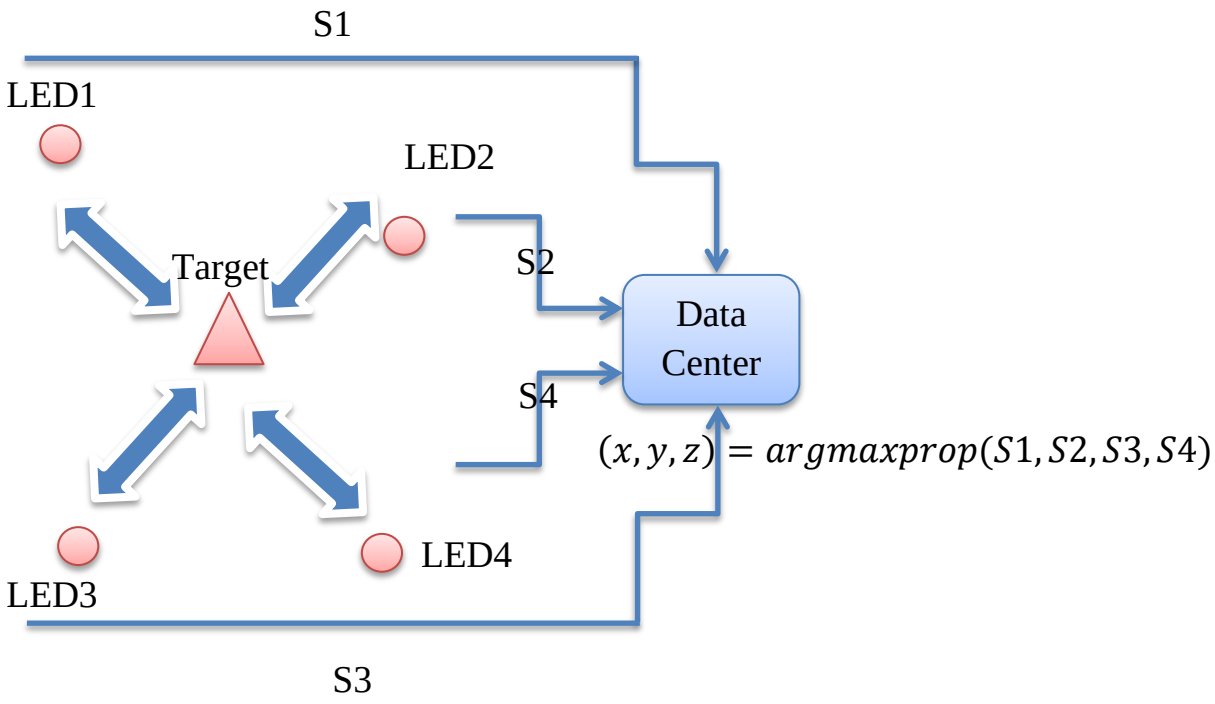

Figure (2-16): Position estimation using the MLE algorithm[68].

Position estimation will be more accurate than trilateration-based positioning thanks to the use of ML. The probability distribution of measurement errors between the target and reference nodes is used to minimize the mean square error.

In the conventional ML, the initial point is fixed and randomly selected. But, in this work, the initial point is carefully selected based on the MSE for all estimated positions of the target computed by each LEDs group using WLS.

2.8 Anchor selection

After installing N LEDs in the ceiling for a generic scenario of IP with VLC system, N' LEDs are selected from the total number of LEDs (N) where $N' \leq N$ (we chose N'=6). After that, the combination method is used, a clustering method to create different groups of LEDs. So,

$$\text{The total number of groups} = \binom{N'}{4} + \binom{N'}{5} + \cdots \binom{N'}{6} \tag{2.49}$$

Where

$$\binom{N'}{6} = \frac{(N'+6-1)!}{6!\ (N'-1)!} \tag{2.50}$$

Based on [69], the authors have shown that the positioning accuracy is not increased dramatically when increasing anchor nodes and typically from four to six anchor nodes is enough. Then, the target position of each group is estimated using WLS. The positioning accuracy of each group is checked using the MSE evaluation metric and select the group Having minimum MSE among other groups as given [69]:

$$MSE = \min\{MSE(i)\} \tag{2.51}$$

The conventional MSE, which needs actual and estimated target values, could be written generically as:

$$MSE = E\left\{\left\|P - \hat{P}\right\|^2\right\} \tag{2.52}$$

where P and $\hat{P}$ denote the actual and estimated positions of the target. However, in this work, we need to make an MSE flexible in working with live statues to check the positioning accuracy of each anchor node group based only on the measured distances. The MSE used in this work, modified by[70], does not need an actual value and could be used to find the positioning accuracy of a positioning system online based only on the measured distances, as shown below:

$$MSE(T_x) = \left[\sum_{i=1}^{n-1} \frac{E\{\varepsilon_i\}}{det}\left((k_{11}\sum_{i=2}^{n} x_i - x_1) - (k_{12}\sum_{i=2}^{n} y_i - y_1) - (k_{13}\sum_{i=2}^{n} z_i - z_1)\right)\right]^2 \tag{2.53}$$

Additionally, MSEs for y and z coordinates, equation (2.54) and equation (2.55), are similar to x-coordinates and only will have the change to the index of k in equation (2.53)

$$MSE(T_y) = \left[\sum_{i=1}^{n-1} \frac{E\{\varepsilon_i\}}{det}\left((-k_{12}\sum_{i=2}^{n} x_i - x_1) + (k_{22}\sum_{i=2}^{n} y_i - y_1) - (k_{23}\sum_{i=2}^{n} z_i - z_1)\right)\right]^2 \quad (2.54)$$

$$MSE(T_z) = \left[\sum_{i=1}^{n-1} \frac{E\{\varepsilon_i\}}{det}\left((k_{13}\sum_{i=2}^{n} x_i - x_1) - (k_{23}\sum_{i=2}^{n} y_i - y_1) + (k_{33}\sum_{i=2}^{n} z_i - z_1)\right)\right]^2 \quad (2.55)$$

Where ε is computed in Appendix 1, subsection B for every coordinate in the reference[70]. Where $i = 2 \ldots n$ denotes the index of the anchor node, and n indicates the total number of anchor nodes. Finally, the compact Equation of the derived MSE is expressed as:

$$MSE(\hat{T}) = \frac{MSE(\widehat{T_x}) + MSE(\widehat{T_y}) + MSE(\widehat{T_z})}{3} \quad (2.56)$$

2.9 Internet of Things (IoT)

The Internet of Things (IoT) is a paradigm in which a continuous network of uniquely addressable things communicates globally to construct dynamic networks [71]. The IoT is a network of uniquely identified connected devices with computer services, such as objects, sensors, and everyday household items. The idea of connecting computers and networks to monitor and manage items has existed for decades, but the phrase “Internet of Things” is new. By the late 1970s, for example, remote monitoring of electrical grid meters over telephone lines had become commonplace. Advanced wireless technology has enabled machine-to-machine enterprise and industrial solutions for equipment monitoring and operation, using closed purpose-built networks or proprietary industry-specific standards instead of Internet Protocol (IP) and Internet

standards. Since the early 2000s, when IP was first used to connect devices, a thriving field of research and development into smart object networking has created the IoT's basis. The phrase "internet of things" (IoT) is now widely used to describe scenarios in which internet connectivity and computing power are extended to a variety of objects[72]. As indicated in the figure(2-17), the IoT concept could also be expressed. The A's stand for technology's globalization (anytime, anywhere, any device, any network, etc.), while the C's stand for IoT qualities like collections, convergence, connection, computation, and so on. On the other hand, Today's IoT has already exceeded the range of A's and C's.

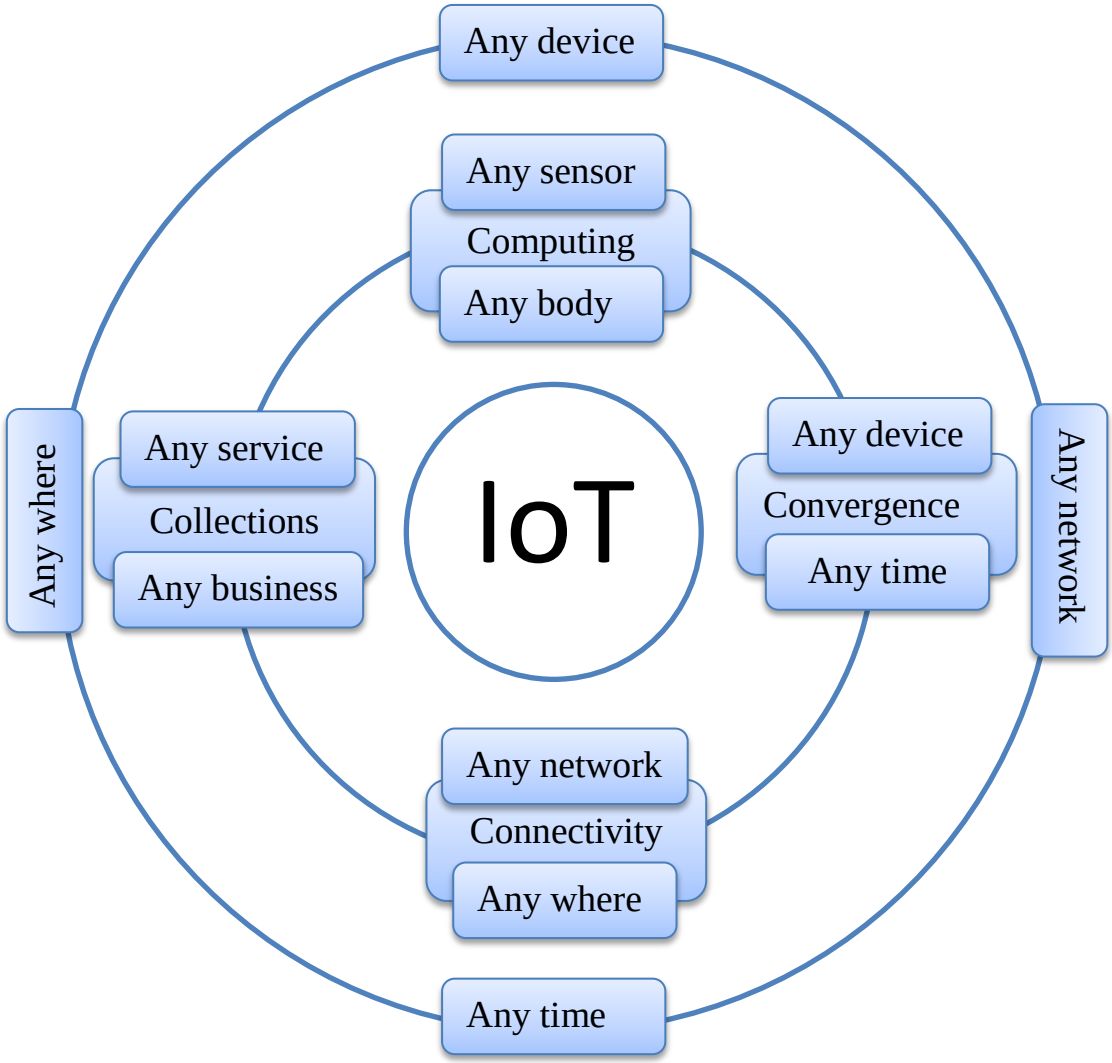

Figure(2-17) : A's and C's concept in IoT [10].

2.9.1 IoT Definitions

The IoT is difficult to define accurately. It describes a world in which everything is interconnected and can communicate intelligently. To better understand the IoT terminology, various standard development organizations (SDOs) have developed definitions of IoT, which are listed below.

- **International Organization for Standardization (ISO) and the International Electrotechnical Commission (IEC) Definition** [73]**:** "It is an infrastructure of interconnected objects, people, systems and information resources together with intelligent services to allow them to process information of the physical and the virtual world and react."
- **International Telecommunication Union (ITU-T Y.2060) Definition**[74]**:** "A global infrastructure for the information society, enabling advanced services by interconnecting (physical and virtual) things based on existing and evolving interoperable information and communication technologies."

Note 1 – The IoT makes full use of things to give services to all types of applications while ensuring that security and privacy requirements are met by utilizing identification, data collecting, processing, and communication capabilities.

Note 2 – The IoT can be perceived as a vision with technological and societal implications in a broad perspective. "Things: Concerning the Internet of things, these are an object of the physical world (physical devices) or the information world (virtual things), which are capable of being identified and integrated into communication networks."

- **Institute of Electrical and Electronic Engineering (IEEE) Definition** [75]**:** "The Internet of Things (IoT) is a framework in which all things have a representation and a presence on the internet. More specifically, the Internet of Things aims at offering new applications and services bridging the physical and virtual worlds, in which Machine-to-Machine (M2M) communications

represents the baseline communication that enables the interactions between Things and applications in the Cloud."

2.9.2 IoT Architecture

There is no widely accepted architecture for the Internet of Things at the present time. Various researchers have recommended a variety of different architectural designs. Many academics working in the subject of Internet of Things (IoT) employ the concept of networking layers to design IoT architecture. Each layer is distinguished by the function it performs as well as the devices that it makes use of. As illustrated in figure(2-11), the most fundamental architecture of the Internet of Things is a three-tier architectural framework in terms of the devices and technologies that comprise each layer. The following are the fundamental functions of each layer[76][77] :

(i) **The perception layer** is the physical layer, which involves the sensing and acquisition of information about the surrounding environment. It can detect certain physical characteristics in the environment and recognize other smart objects in the environment. It takes data from the environment and communicates it to the network layer with the use of sensors and actuators, which are embedded in the system.

(ii) **The network layer** is capable of connecting to other intelligent things, network devices, and servers. Its capabilities are also put to use in the transmission and processing of sensor information. The network layer of IoT serves the function of data routing and transmission to different IoT hubs and devices over the internet. At this layer, cloud computing platforms, Internet gateways, switching, routing devices, etc., operate utilizing the newest technologies. The network gateways act as a mediator between multiple Internet of Things nodes, gathering, filtering, and transferring data to and from various sensors on the network.

(iii) **The application layer** is responsible for delivering application-specific services to the user. The Internet of Things can be used for a variety of purposes, including smart homes, smart cities, and smart hospitals, among other things. Data integrity, authenticity, and privacy are the responsibility of the application layer. At this layer, the IoT or the creation of a smart environment is achieved.

The three-layer architecture provides an overview of the Internet of Things for the audience. In spite of this, many Internet of Things researchers believe it is insufficient because research is frequently focused on more attractive features of the Internet of Things. Thus, a new five-layered architecture, which includes the processing and business layers, has been defined. The five layers are perception, transport, processing, application, and business layers as depicted in figure (2-18). The perception and application layers play the same role as the three-layered architecture in terms of function. The functions of the remaining three layers are discussed as following[78]:

(i) **The transport layer** transfers the sensor data from the perception layer to the processing layer and vice versa through networks such as Wi-Fi, 3G, LAN, Bluetooth, and RFID (**Li-Fi in our work)**.

(ii) **The processing** The middleware layer is another name for this layer. From the transport layer, it collects, analyzes, and processes massive amounts of data. A variety of services can be provided to the lower layers by this layer. It utilizes a wide range of technologies, including databases, cloud computing, and data processing modules.

(iii) **The business layer** manages the overall IoT system, including the applications, business and profit models, and users' privacy. Based on the data received from the application layer, it creates various business models, graphs, and flowcharts. This layer will aid in the formulation of future plans and strategies by analyzing the data gathered.

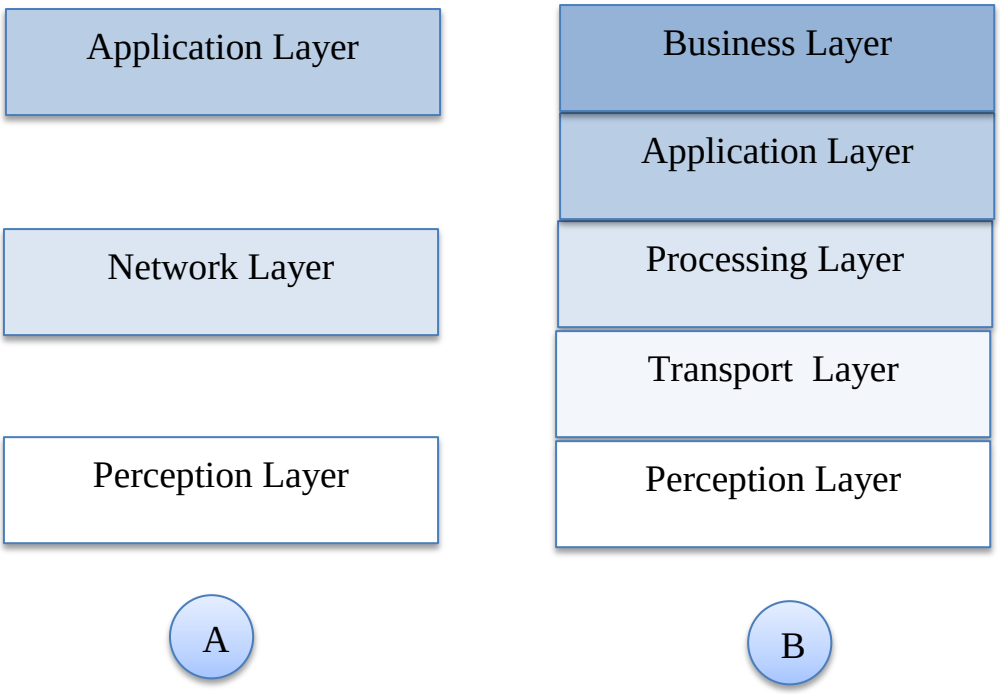

Figure (2-18): IoT architecture A) Three Layer architecture. B) Five Layer architecture[77]**.**

2.9.3 ThingSpeak IoT Platform

ThingSpeak is an open-source software written in Ruby which allows users to communicate with internet enabled devices. It facilitates data access, retrieval and logging of data by providing an Application Programming Interface (API) to both the devices and social network websites. ThingSpeak eliminates the need to set up servers for cloud storage and analysis. ThingSpeak allows users to build applications around data collected from IoT devices such as temperature sensors, heartbeat sensors, and various microcontrollers. It is a Matlab-supported IoT platform for analyzing and visualizing data. Processed data could also be used to send tweets and other alerts to users.

There are so-called channels for storing data, and each channel can hold up to 8 fields with a total of 255 alphanumeric characters. Other fields include: Description, Latitude, Longitude, and Elevation for location information. Time and date stamps are added to each piece of data that arrives, and each piece of

data is assigned a unique ID number. Using the ThingSpeak API, a unique alphanumeric string known as a "write key" can be used to publish data from a newly created channel. Thus, a "read key" is used to access channel data if it is set to keep its data private (the default setting). To make a channel accessible by anyone without a read key, simply set the channel to "public"[79].

Thingspeak has a wide range of capabilities, among which are the following:

- Simple configuration: Thingspeak can be configured to receive data from any IoT-enabled device using standard IoT protocols.
- Visualization: sensor data can be visualized in real-time using this feature.
- Aggregation: on the request of third parties, data can be aggregated data.
- Analyze: run the IoT analytics automatically based on the events or timetables.
- Prototyping: build and prototype IoT systems without the need for servers or web software.
- Automation: Third-party services such as Twitter® and Twilio® can be used to automate data manipulation and communication.

Chapter Three

Proposal Designs for Healthcare Monitoring System

Chapter Three

Proposal Designs for Healthcare Monitoring System

3.1 Proposed Smart Healthcare Monitoring System using Li-Fi technology-based IoT Description

With the help of the block diagram in figure(3-1), one can develop a prototype for a remote health monitoring system using Li-Fi technology-based IoT. The proposed system monitors vital parameters like temperature and heart rate using temperature and heart rate sensors. The sensors data is passed through the Li-Fi transmitter section near the patient. Then the data is transmitted through a Li-Fi channel, which is LED light. This light passed to optical receivers which is assumed to be created in the room's ceiling. The received signal is traveled through different propagation links (direct LOS, non-direct LOS, and diffuser) and ambient noise(may be sunlight or Fluorescent lamps).

This data is presented in a PC called the central nurse station and uploaded to the ThingSpeak IoT cloud platform using python code. The internet is connected to the computer via an Ethernet cable, so the use of Wi-Fi technology will be dispensed. This data is constantly being added to the database. Data is retrieved from the database and displayed by the ThingSpeak platform. The doctor can stay up to date on the patient's condition in real-time. An automated notification will appear in the doctor's laptop or android mobile application if a patient's parameter exceeds a predetermined threshold value. The System design is divided into two parts: Used Hardware and Used software with the platforms, the description for each part is explained in the following sub-sections.

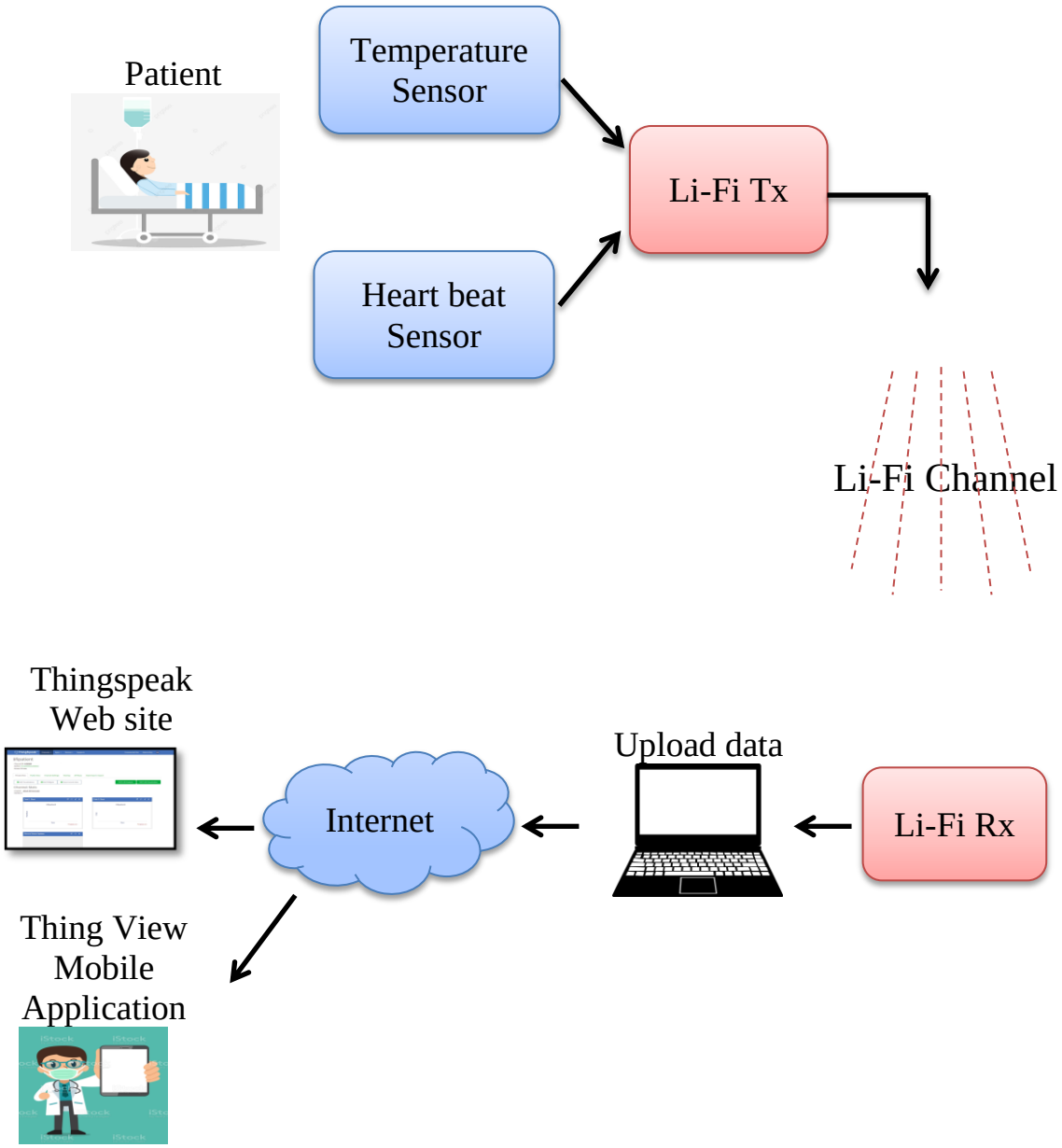

Figure(3-1): Proposed System Block Diagram.

3.1.1 Used Hardware:

The used hardware included two sections for the proposed prototype: the transmitter section and the receiver section.

A. Transmitter Section

The transmitter section is shown in figure(3-2) with the following hardware:

i. **Battery.**
ii. **Arduino-Uno [Appendix A].**
iii. **MLX90614 IR Temperature Sensor.**
iv. **DFRobot heart rate sensor.**
v. **BC547 NPN Transistor.**
vi. **LED.**

Each of the sensors is connected to **Arduino-Uno** and converted into digital form. A linear relationship between current and light intensity made **LED** an excellent choice. The intensity of the LEDs can be changed in various ways. The simplest way to represent data is through on-off keying (OOK). To indicate the extremes, the logical values are used 1 and 0. Thus, the LED is turned off to transmit a zero (i.e., no light is sent), while the LED is turned on to send the bit number (i.e., a bright light is emitted). There isn't enough current flowing through the Arduino ports to produce bright, fast light. Using a **BC547 NPN Transistor** instead of the Arduino Board's built-in switch, we could switch a higher current more quickly while still enabling us to turn on and off the LED at will. The Arduino's pin is used to control this transistor. In addition, it is possible to vary the distance between the transmitter and receiver for testing purposes. To prevent data loss, variable resistance is used to adjust the LED brightness.

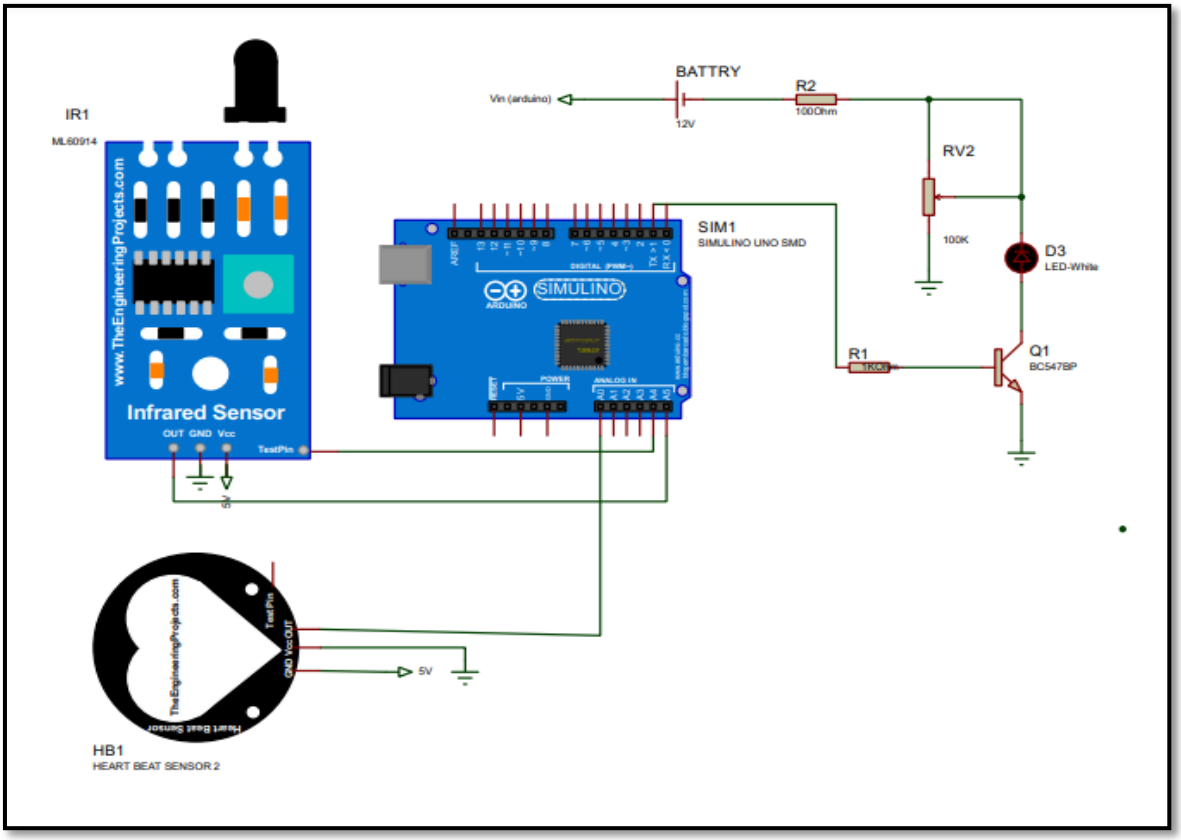

Figure (3-2): Transmitter Section.

The description of each component is given below:

i. **Battery**: Each circuit needs an electric source to operate. This circuit is equipped with a battery of 12V. This battery is small in size and rechargeable. Need this battery to operate the LED and Arduino-Uno board.

ii. **MLX90614 IR Temperature Sensor:** The MLX90614 is a Contactless Infrared (IR) Temperature Sensor that can be used in a wide temperature range: from $-40^{o}C$ to $125^{o}C$. The MLX90614's most important characteristic is a high level of precision and contactless IR temperature sensor. As a result of its extreme precision, it is also widely utilized in various business and healthcare applications, including monitoring of room and body temperatures.

The Stefan-Boltzmann principle asserts that all objects and living beings emit IR energy. The intensity of this emitted IR energy is precisely proportional to the temperature of that object or living being. The

MLX90614sensor works on this concept. So the MLX90614sensor measures the amount of IR energy emitted by an item to determine its temperature.

A company by the name of Melexis produces the MLX90614Temperature sensor. To speed up development, the sensor is pre-calibrated and can be used as a plug-and-play sensor module. The MLX90614 combines the functions of two separate devices. The sensor's sensing unit is contained in a processing unit, both of which are integrated into one sensor [see figure(3-3)]. The sensing part is a Thermo detector operating using Infrared to sense the temperature. The processing one is a Single adjustment ASSP to convert the sensor's signal into digital form and transfers using the I2C protocol. Low noise amplifier, "17 – bit ADC", and robust DSP helps the MLX90614 sensor achieve high resolution and accuracy.

Figure (3-3): MLX90614 IR Temperature Sensor.

To demonstrate how to connect the MLX90614 IR Temperature sensor to an Arduino-UNO. Any Arduino board with an I2C port will work because the MLX90614 sensor provides temperature output on the I2C bus. The pinout configuration of the MLX90614 sensor will be shown in table (3-1).

Table (3-1)MLX90614 Pinout Configuration.

Pin No.	Pin Name	Description
1	Vdd(Power Supply)	Vdd can be used to power the sensor, typically using 5V.
2	Ground	The metal can also act as ground
3	SDA-Serial Data	Serial Data pin used for I2C communication
4	SCL-Serial Clock	Serial Clock pin used for I2C communication

First, connect the temperature sensor's power supply pin (Vin) to the 5V pin on Arduino and the MLX90614's GND pin to the Arduino UNO's GND pin. Then, to transport data serially, connect the SDA and SCL pins of the sensor to the Arduino-UNO's A4 and A5 pins. The interfacing between the MLX90614temperature sensor and Arduino is shown in figure (3-4).

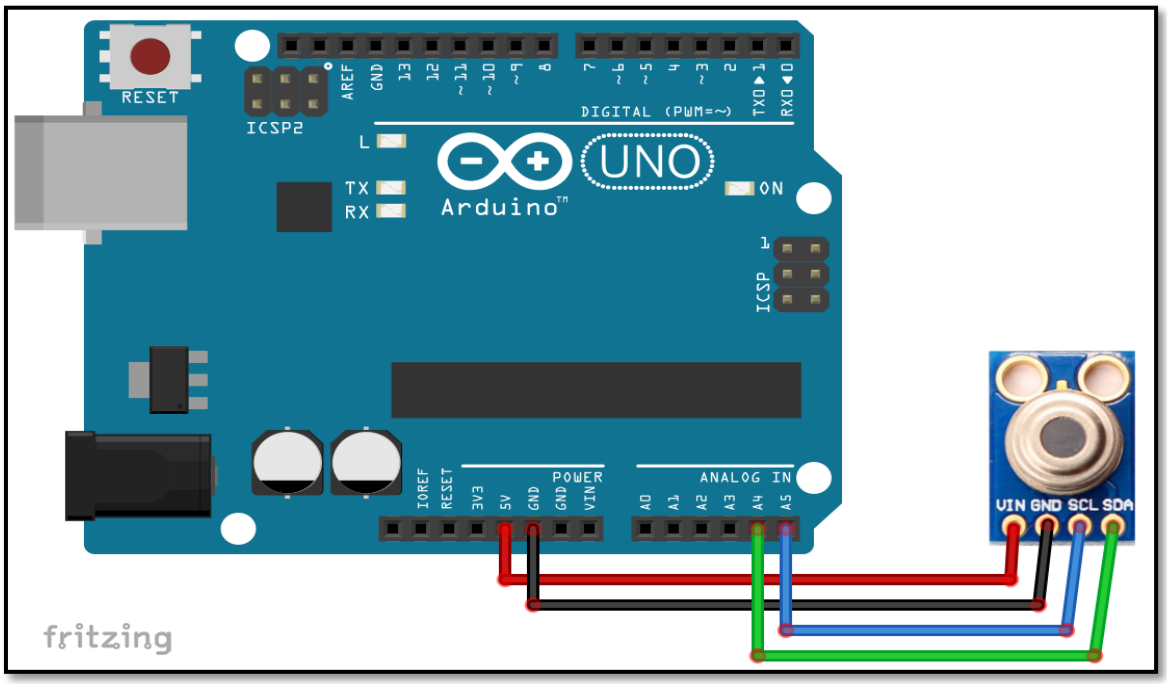

Figure (3-4): Interfacing between the MLX90614 temperature sensor and Arduino-Uno.

iii. **DFRobot heartrate sensor:** The DFRobot heartrate sensor is a heart rate monitor designed with the size of the thumb. It allows for simple plug-and-play connectivity thanks to the Gravity interface. Photo Plethysmo Graphy (PPG) techniques are the basis of this sensor's development. These techniques are optical, inexpensive, and easy to use to detect blood volume changes in tissues' microvascular beds. According to this theory, the pulsatile element of the cardiac cycle is usually easy to identify. Belt attachment is made possible by two holes drilled into the sensor. So, the fingers and wrists and any other skin-contact areas can be wrapped in it, as shown in figure(3-5).

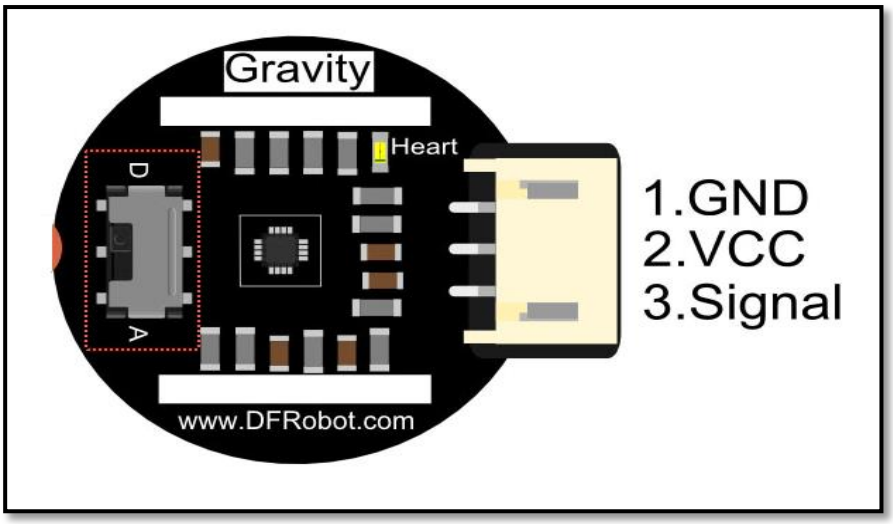

Figure(3-5): DFRobot heart rate sensor.

The interfacing of the DFRobot heart rate sensor with the Arduino-Uno board is shown in figure (3-6). It has three pins. If the front side is toward you, the left pin is the GND, and the center one is the input voltage, which will be linked to the Arduino's 5 volts. The final one will be used for electrical output and connected to the Arduino's analog bins.

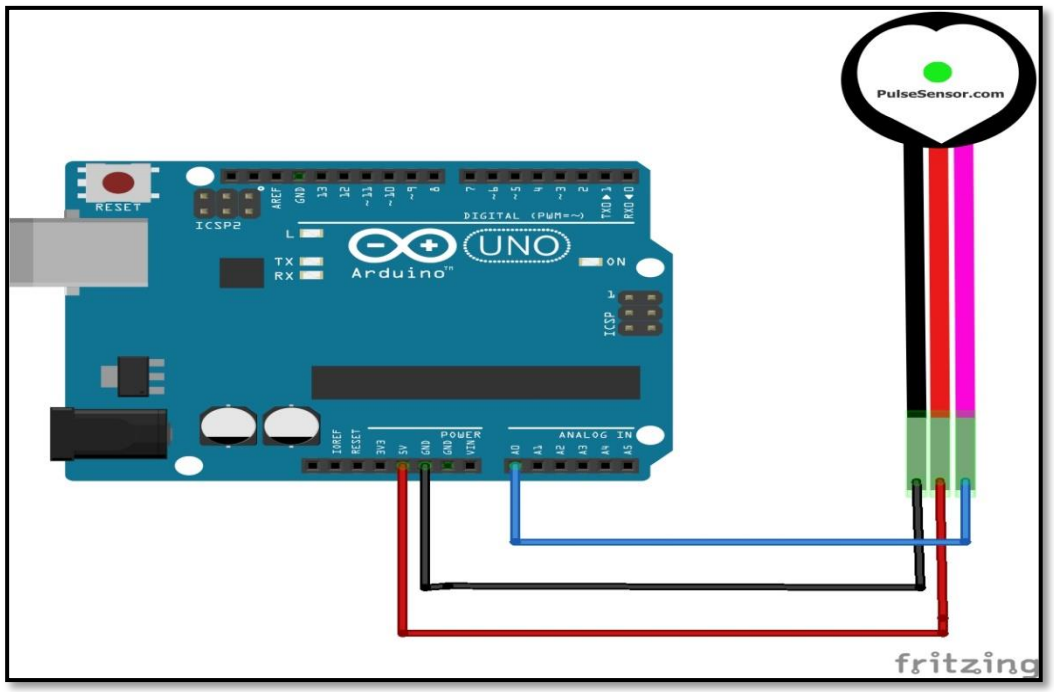

Figure (3-6): Interfacing between DFRobot heart rate sensor and Arduino-Uno.

iv. BC547 NPN Transistor: BC547 is an NPN Bipolar Junction Transistor with three pins: emitter, collector, and base. This transistor comes in a TO-92 package. The maximum throughput current of it is 100 mA. The low noise and high DC current gain of the BC547 make it an excellent choice for signal amplification applications. The standard saturation voltage of 90mv should be considered a favorable sign to utilize it for switching purposes.

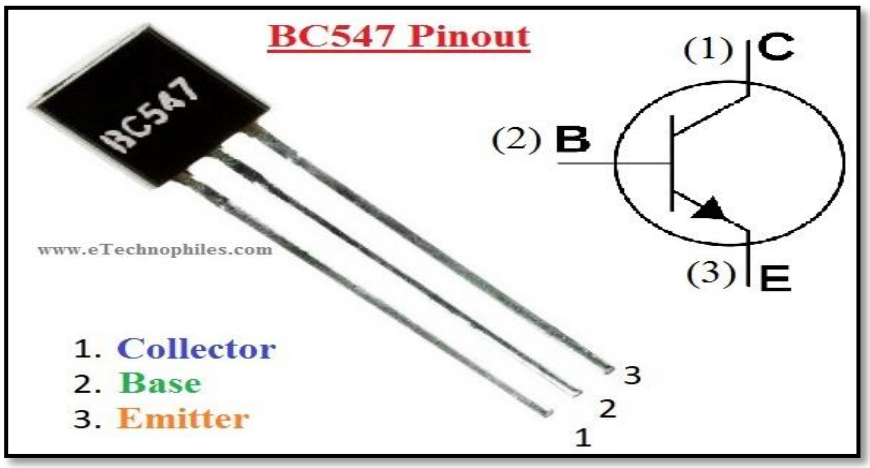

Figure(3-7): BC547 Transistor.

v. **LED:** The central part of this operation is the LED source which is used as a data transmission light. The principle of the working of the LED depends on the spectrum of the visible light, which ranges from 375nm to 780nm for visible light transmission. The LED used in this system was a commercial type with a power of 1W for dual used, lighting and data transfer. This LED operates at a voltage of 12V which consider very cheap and available in the market.

vi. **Convex lens**: A convex lens is used after the LED for focusing the light. The focal length for this lens was 25cm.

B. Receiver Section

The receiver section is shown in figure(3-8) with the following hardware:

i. **PIN Photodiode.**

ii. **Arduino-Uno.**

iii. **LM358 Operational Amplifier.**

iv. **Variable resistance (100Kohm).**

v. **Red LED with series Resistance.**

vi. **Green LED with series Resistance.**

The receiver task is to convert the light into current using a **PIN Photodiode**. Arduino cannot accept a high voltage for a digital signal. So, the electrical signals must be processed before by a circuit between an Arduino and a photodiode to read them accurately. Electrical current needs to be transformed into voltage for comparison and amplification purposes for receiver electronics. This is done using **LM358 Operational Amplifier**. The distance between the transmitter and receiver can be changed; however, a variable resistor is necessary to avoid too small or too high a signal. This component amplifies or decreases the input voltage depending on the desired output voltage.

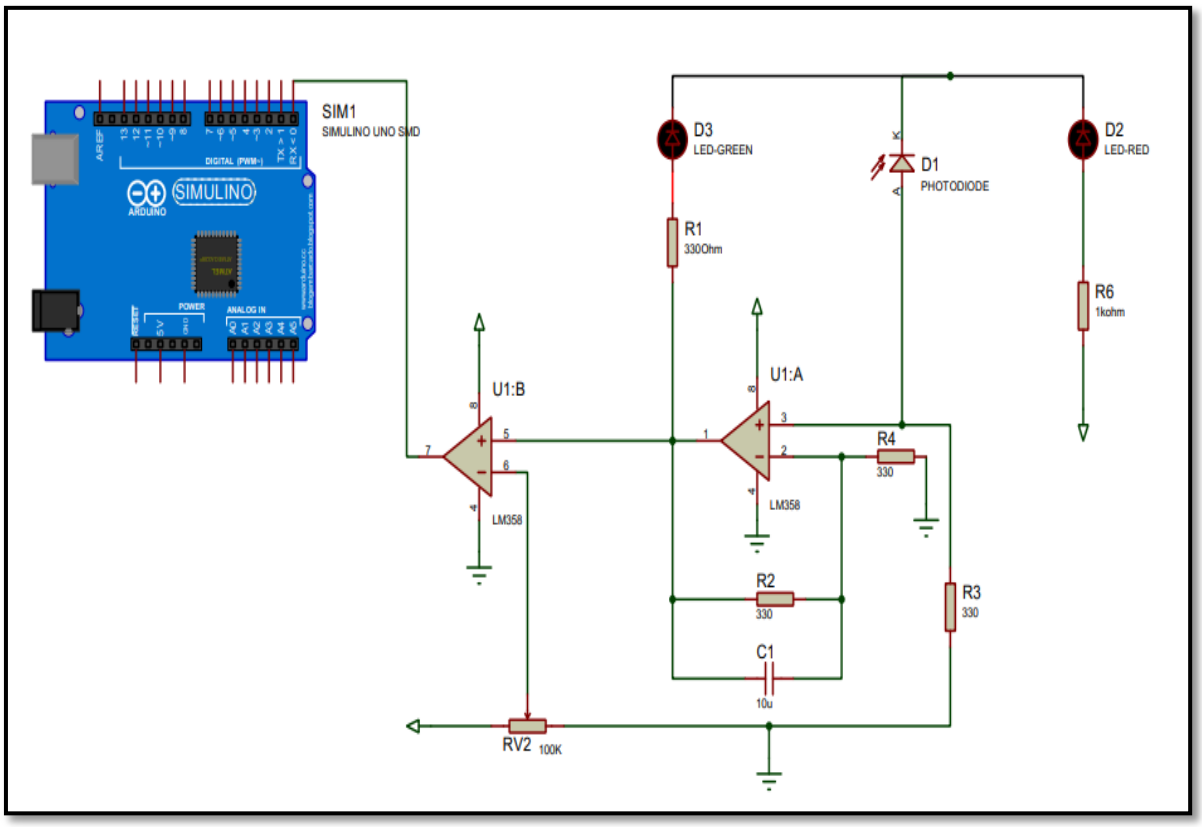

Figure(3-8): Receiver Section.

The description of each component is given below:

i. **Photodiode:** Light can be converted into electrical current by using a photodiode, a semiconductor device. The photodiode has three main requirements: a fast response time, high sensitivity to visible wavelengths, and a sizeable radiation-sensitive area. The used photodiode is SFH2030 which is an inexpensive general-purpose PIN diode. The spectral bandwidth is from 400 nm to 1100 nm and is ideal for the intended purpose. The light intensity to current ratio is linear, and the radiant sensitive area is 1 mm2. Switching times are short, which is typically 5 ns.

ii. **LM258 Operational Amplifier:** The trans-impedance amplifier used here is used to convert the photodiode's output current into the voltage. LM358 operational amplifier is used for this purpose which consists of two independent, high gain, internally frequency compensated operational amplifiers. It's made to work with a single power supply and a wide range of voltages, ranging from 3 to 32 volts. For this reason, it is widely used in a

variety of applications because it does not necessitate a negative power supply like most operational amplifiers. LM358 Pinout diagram shown below:

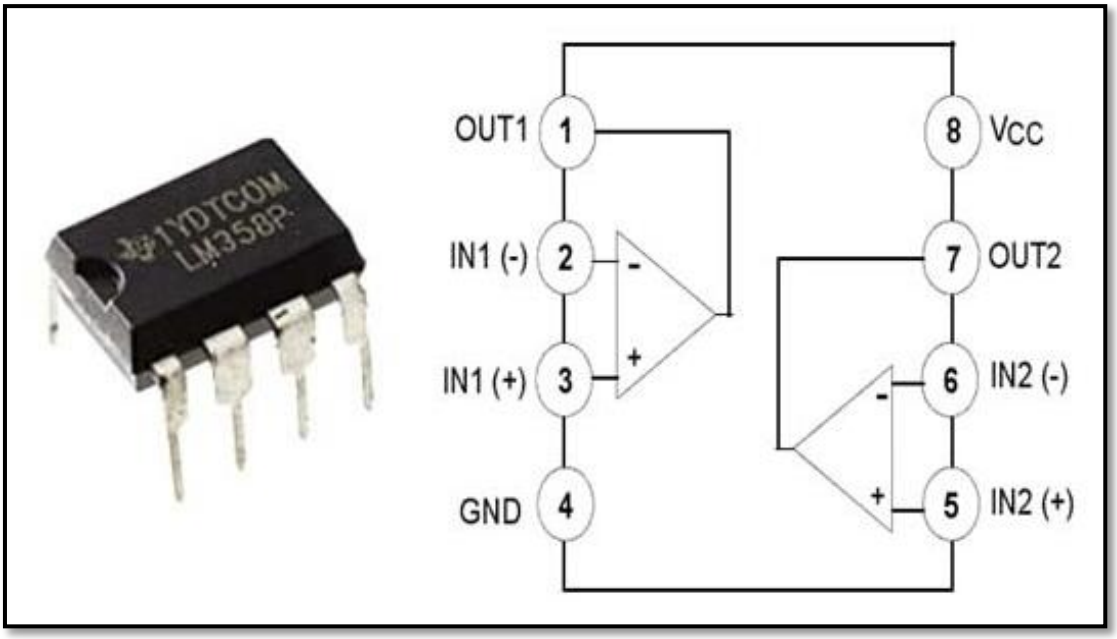

Figure(3-9): LM258 Op-Amplifier Pinout diagram.

Additionally, they can operate from dual power supplies ranging in voltage from 1.5V to 16V, depending on the application's needs. The outputs can generate a good amount of power, which can supply up to 30mA per channel and sink 20mA. These operational amplifiers are frequently used to buffer or amplify signals. They can be used in various circuits, including voltage comparators and voltage-controlled oscillators. They can handle frequencies up to 700KHz with a gain of up to 100 times.

iii. **Red LED with series Resistance:** indicates that the circuit is powered up. The series 330Ω resistance is a current limiting resistor.

iv. **Green LED with series Resistance:** indicates the photodetector is received data. The series 1kΩ resistance is a current limiting resistor.

3.1.2 Used Software and Platforms

The used Software and Platforms include:

i. **Arduino IDE**.
ii. **ThingSpeaks Platform**.
iii. **Python Language.**
iv. **Making Emergency Alert with IFTTT.**

The description for each part is given below:

i. **Arduino IDE**: Programming and uploading code to the Arduino board is made simple by the open-source Arduino Software (IDE). Linux, Windows, and OS X are all supported it. The environment is built using Java, based on Processing and open-source software. Any Arduino board can be used with this software[the used version is 1.8.13].

In this project, Arduino programming language was chosen. Arduino works with sensors, gets the values, and compiles it using the specific libraries that belong to the developer of the sensor. This microcontroller converts the analog sensor input to digital form then gives these data to Li-Fi Tx. For the reception, another code is used to convert the received digital data to analog one for retrieving the sensors' data as shown in figure(3-10). The Arduino programming language is more straightforward than most programming languages.

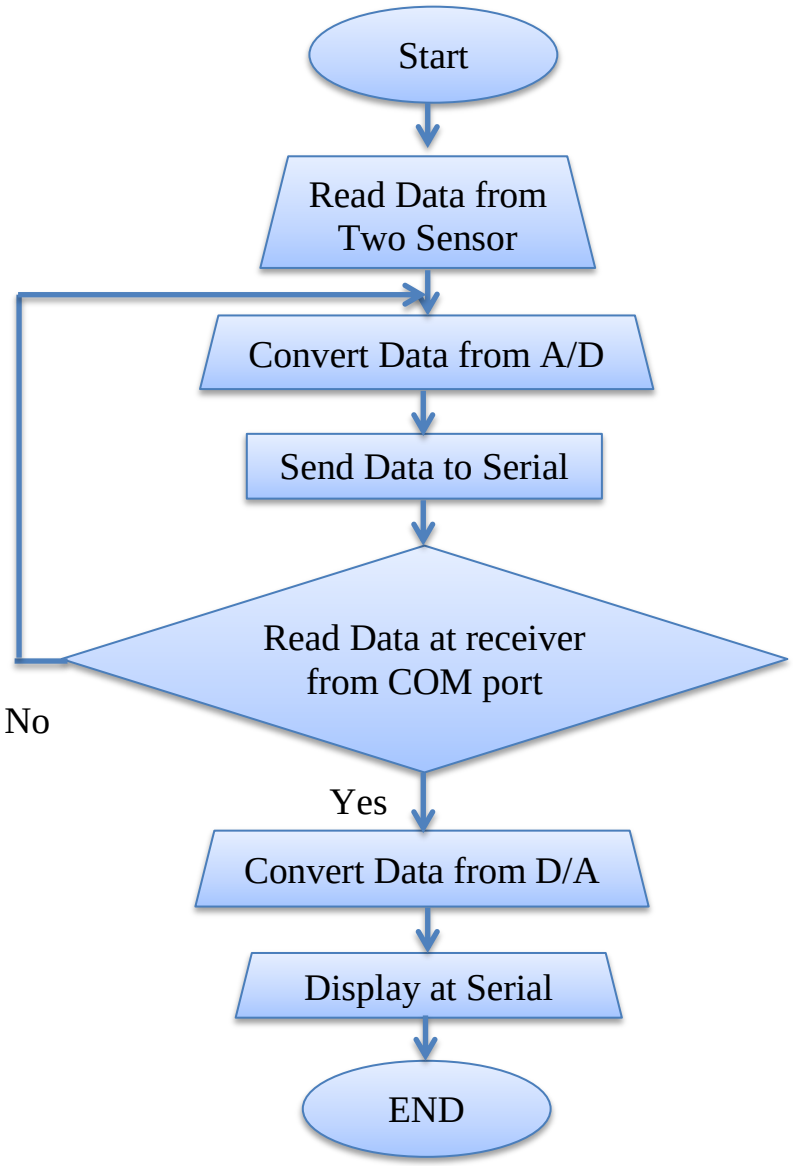

Figure(3-10): Flow Chart of Transmitter and Receiver Codes.

ii. ThingSpeak platform procedure :

Step 1: Start creating the channel

- Log in to ThingSpeak, using MathWorks or ThingSpeak account, or creating a new one.
- Press Channels and choose MyChannels.

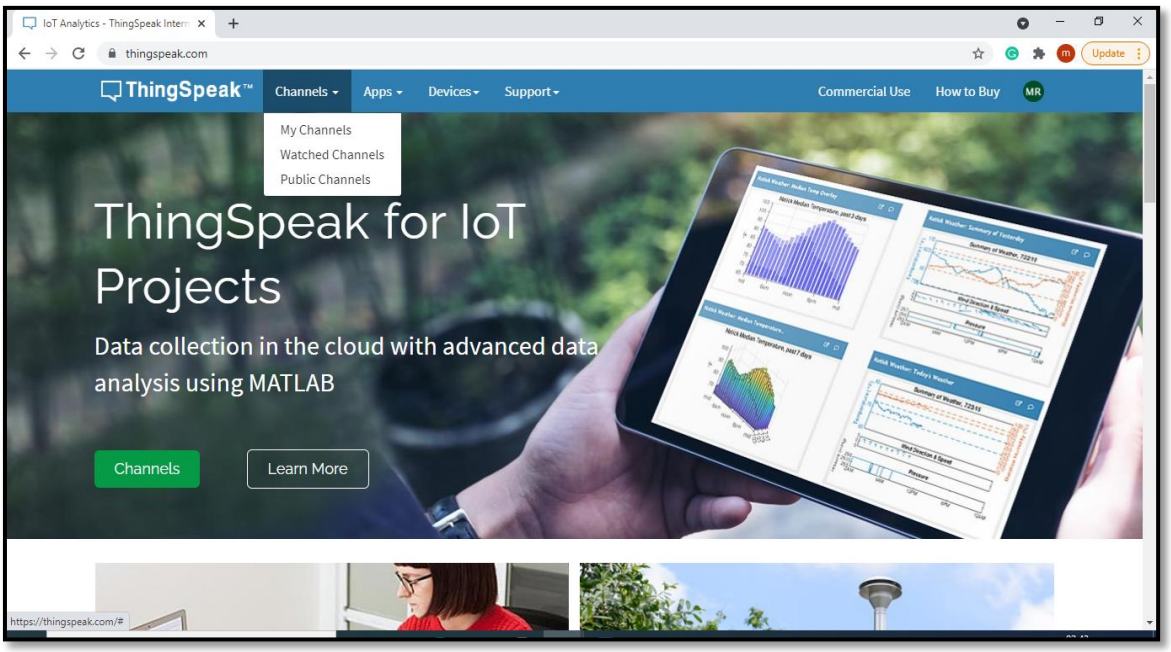

Figure (3-11): Creating channel on ThingSpeak.

- Press New Channel.
- After that, enter these setting values:
  - Name: Healthcare Monitoring System
  - Field 1: Temperature
  - Field 2: Heart-Rate

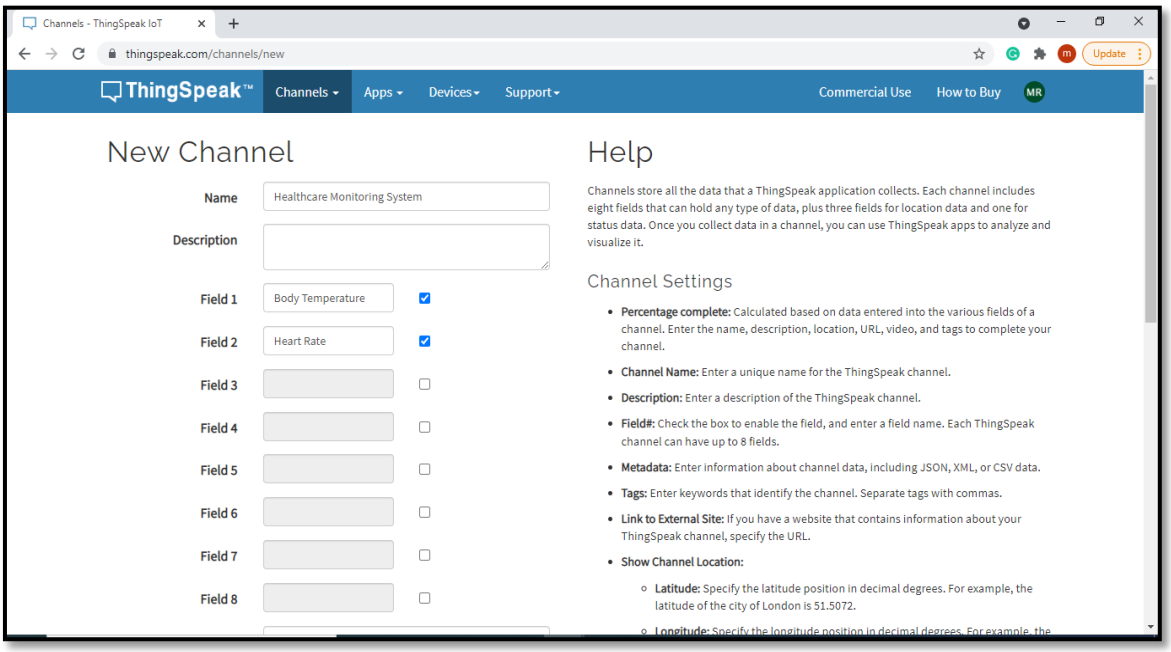

Figure(3-12): Creating Fields.

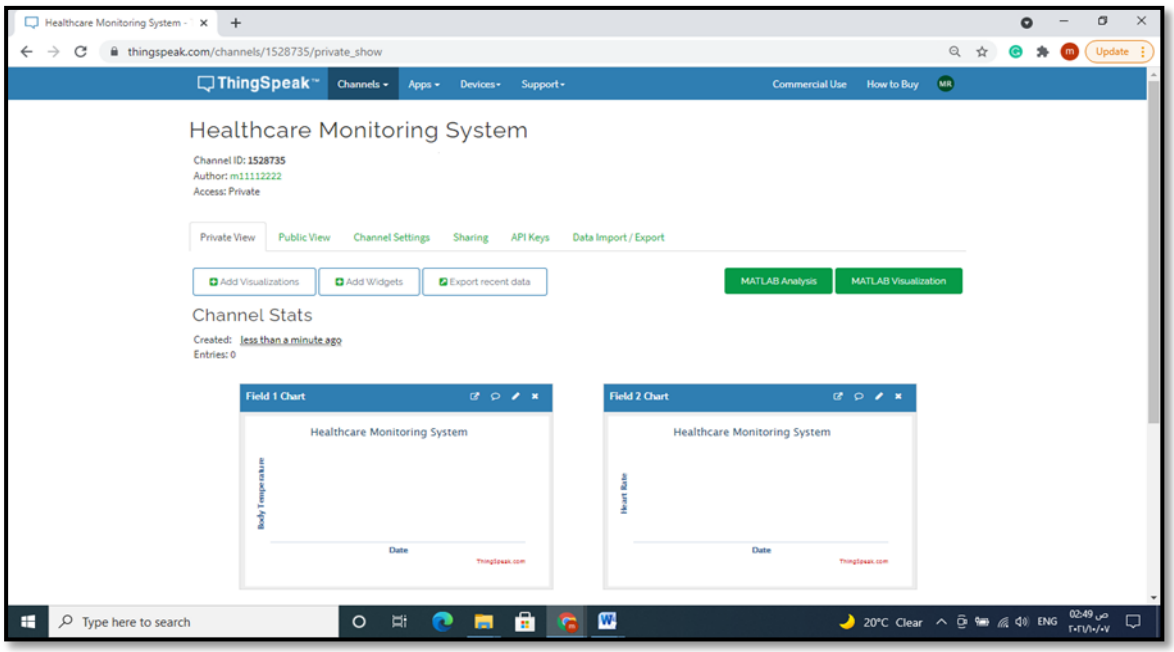

Figure(3-13): ThingSpeak Channel.

- After finishing, press Save Channel below the settings.

These tabs are now visible:

- **Private View**: This tab includes data about the channel that we can see.
- Public View: This tab is chosen to open up the channel for the general public.
- **Channel Settings**: This tab shows all the options you choose when creating a channel. Also, this tab allows us to edit or delete the channel.
- **API Keys**: The API keys for the channel can be found here. Using the keys, we can read and post to our channel.
- **Data Import/Export**: This tab makes importing and exporting channel data possible.

This channel can be accessed by pressing **Channels** and choosing My Channels.

Step 2: Find channel ID and API key

Just below the name of the channel (Healthcare Monitoring system in our project), we'll find channel ID and API Keys.

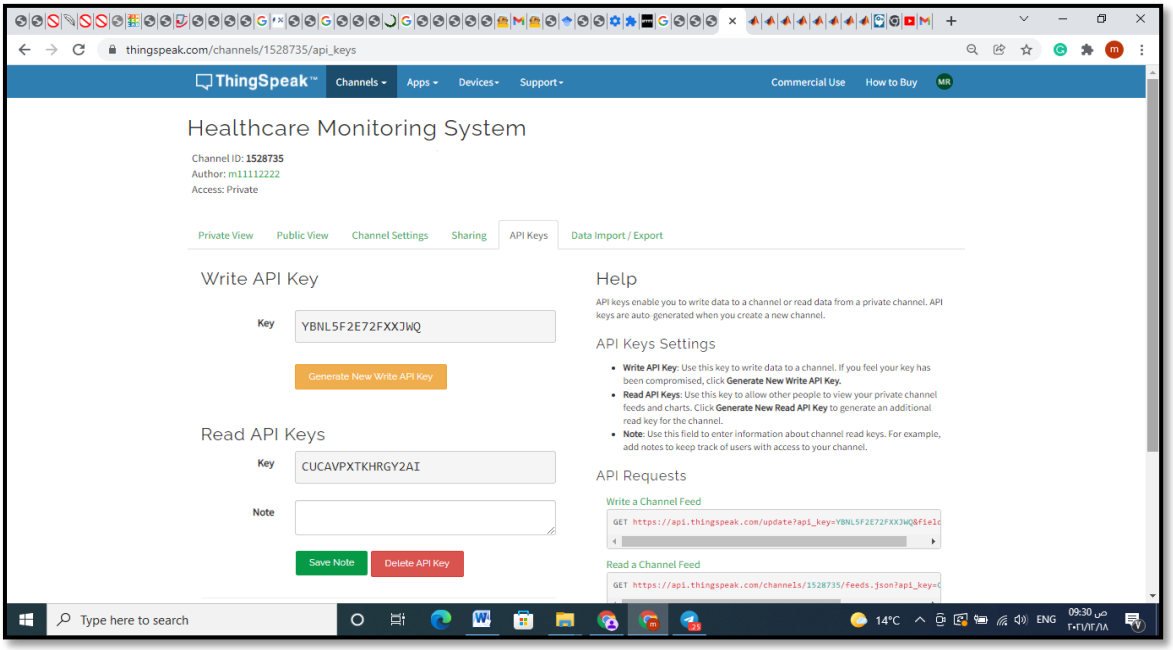

Figure (3-14): Generation of Channel ID and API Key.

This channel is also seen in the smartphone using the ThingView mobile application. This is done after inserting the channel ID and API key.

iii. Python code for uploading data to the ThingSpeak

After creating the channel, get Channel ID and API Key in ThingSpeak. The next step is to upload data to ThingSpeak cloud. For this purpose, python code is used as shown below in figure(4-15)

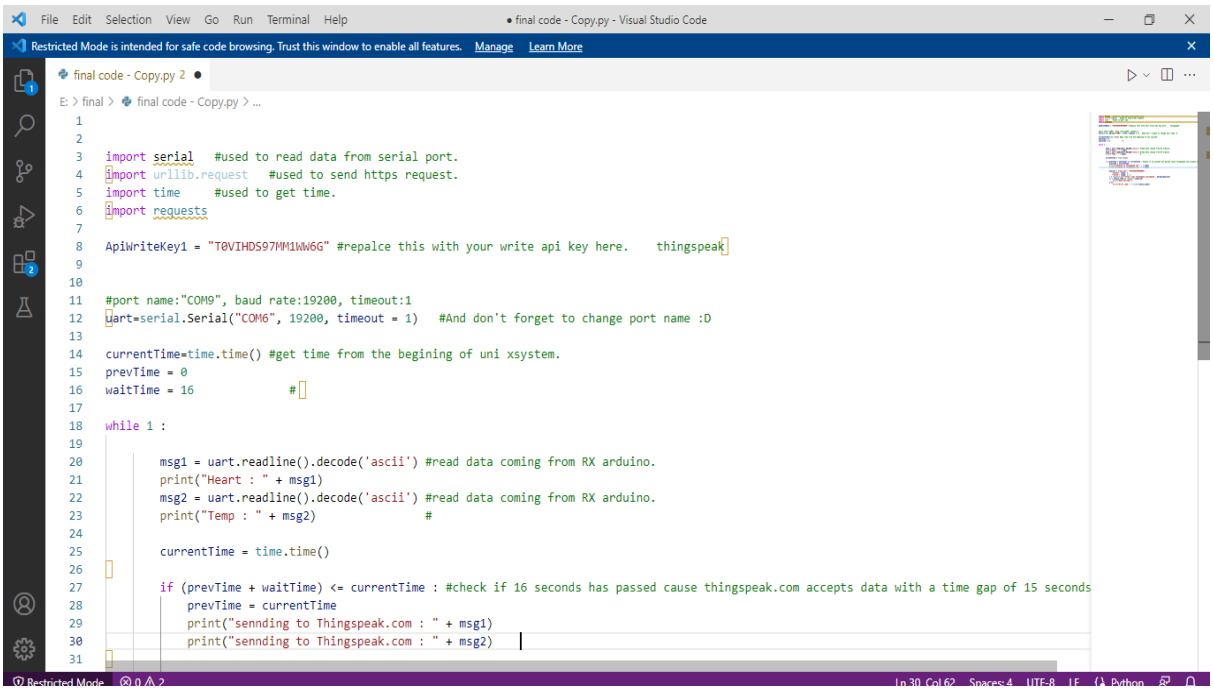

Figure(3-15): Python Code.

iv. Making Emergency Alert with IFTTT

It is impossible to have a health care observer on-call around the clock for every patient. In traditional methods, doctors must be notified in person if there is any abnormality. In the worst cases, even first-aid can't be provided; imperative that a responsible person responds to emergency calls on time. Therefore, an effective healthcare monitoring system should provide doctors or medical technicians with an extra efficient, high-speed, and timely alarm. The proposed system makes this possible using IFTTT.

For short, IFTTT stands for If This Then That. It initiates a cascade of changes to the website's behavior, all aimed at "making the internet working for our". People can use IFTTT to connect various websites and applications to complete a task by taking advantage of APIs provided by various websites with no need to write any code. IFTTT enables us to receive or focus on the most important information by connecting all kinds of information via process and afterwards centrally presenting it. According to IFTTT, "this" represents behavior on a specific website as a "Trigger," while "that" represents another behavior "action" induced by the series of reactions. Those triggers and actions are all based on a specific website, which is referred to "channel" in IFTTT. The whole "if this then that" action is defined to be "Task". For instance, once the data is uploaded to Thingspeak, when it reaches a certain threshold, the trigger will be activated so that the designated action can be taken: an email will be sent to doctor or medical technicians portable devices (all the steps that explained this is in Appendix B). The threshold values used here are shown in table (3-2).

Table(3-2): Threshold values.

Component	**Normal Range**
Temperature	$36.5 - 37.5\ C^o$
Heartbeat rate	$60 - 100$ beats/min

3.2 System Building and Implementation

To build the proposed system, the required connections are made. Then program file is uploaded to the Arduino-Uno. Finally, the health monitoring system is ready to measure heart rate and body temperature using Li-Fi technology as shown in figure(3-16).

For the IoT part, run python code for data uploading to ThingSpeak. Then open ThingSpeak website. After that, Search channel ID. It is easy to see the related channel, and it is enough to click on it to see the graphical visuals and gauges of numerical values coming from the sensors. Besides this, the ThingView application can be used to see these results. Also, IFTTT is used to make notifications at abnormal cases.

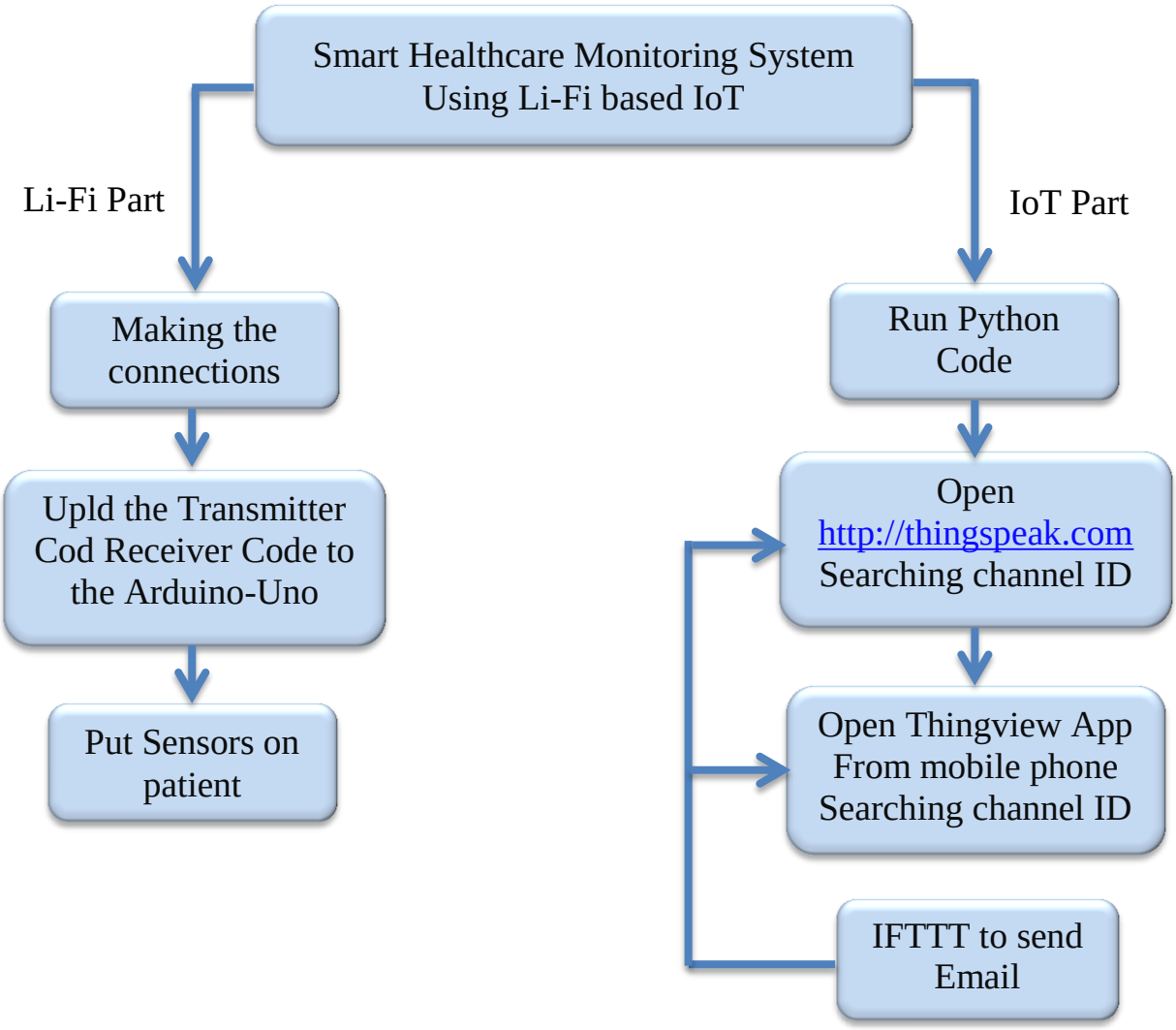

Figure(3-16): Steps for building the Patient Health Monitoring System.

Finally, with the help of diagrams that depict all the components and code, the hardware-implemented as described precisely in this thesis. A diagram of the proposed system's electronic circuitry is shown below in figure (3-17). The Lab experiment has been performed within the dimensions of length, width, and height (7 m x 4 m x3m). Also, a light power meter has been used to measure the received power and ambient noise at various links and for different distances.

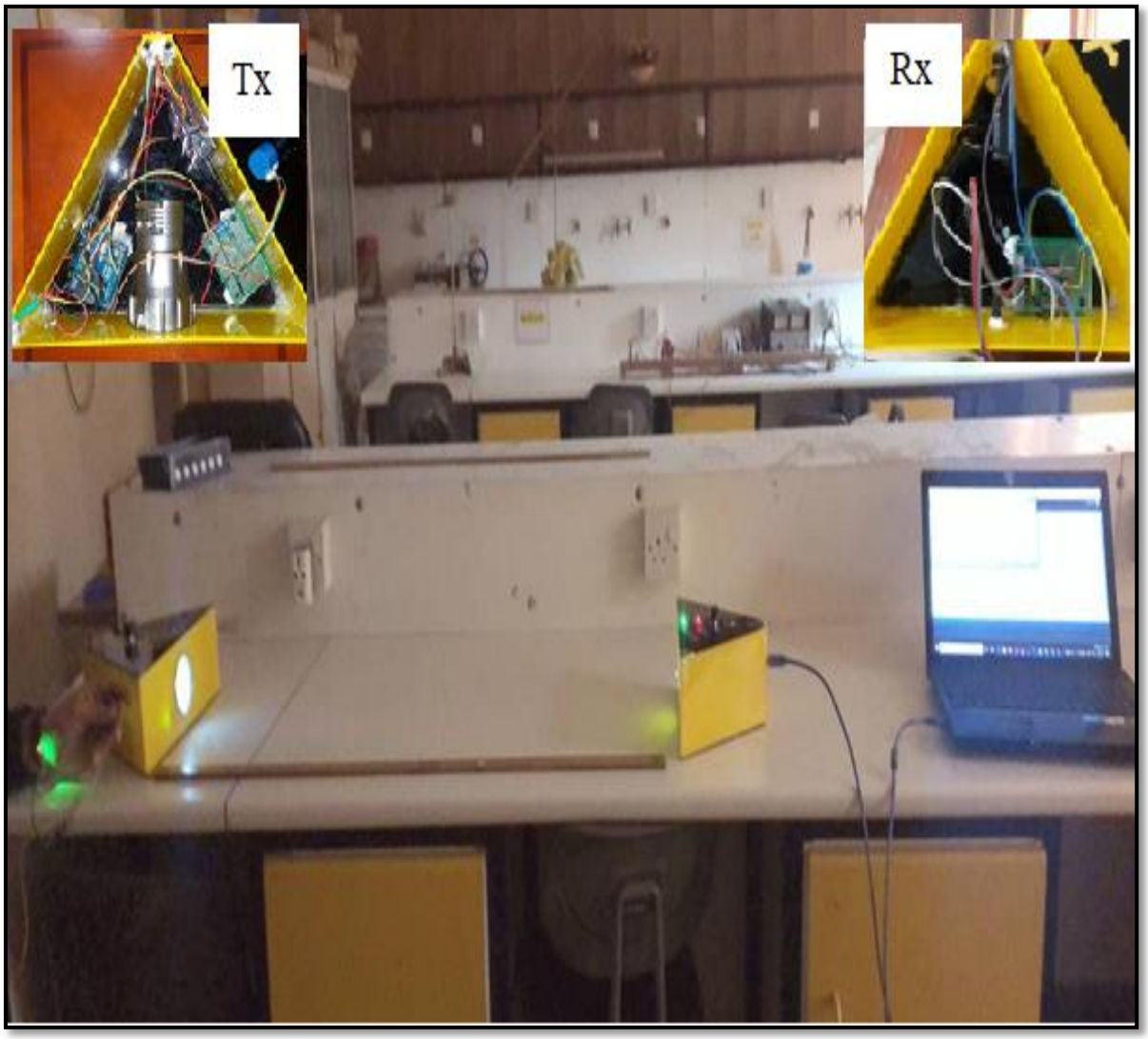

Figure (3-17):Implemented Proposed System.

3.3 Proposed IPS using VLC technology Description

This section presents a description of the Proposed Indoor Positioning System. The description of this system is done with two main parts: System Block diagram and System parameters. Each part is presented in the following subsections.

3.3.1 System Block Diagram

In this subsection, we present the algorithm and block diagram of the entire model of the created system, as shown in figure(3-18).

Algorithm 1 Positioning algorithm

1. **Procedure** Anchor nodes installation

Install n LEDs in the ceiling as anchor nodes. → In this experiment $n = 6$.

End procedure

2. **Procedure** Create the transmission algorithm.

Every LED sends information about its location (ID) to the detector.

End procedure

3. **Procedure** Channel impulse response
    a. Calculate actual distances(using equation(2.30))
    b. **LOS Case** (using equation(2.17))
    c. **NLOS Case** (using equation(2.20))
    d. **Total impulse Response**

End procedure

4. **After Photodiode, Measure power for each LED with noise** (using equation(2.16))
5. **Select 4 to 6 LEDs that having highest received power**
6. **Separate received signals →Optical Orthogonal Codes (OOC)**
7. **Procedure** Clustering nodes (P) → combination method (using equation(2.49))

    End procedure

8. **Procedure** Compute distances (using equation(2.31))

End procedure

9. **Procedure** Target (patient) location → WLS (using equation(2.43))

   End procedure

10. **Procedure** Compute derived MSE for each group. → based on the measured distance (using equation(2.56))

    End procedure

11. **Procedure** Anchor selection →Select the group Having minimum MSE among other groups. (using equation(2.51))

    End procedure

12. **Procedure** Patient Relocation→ Using **modified** ML algorithm→ Dynamic initial point (done with fminsearch function in matlab) (using equation(2.48))

    End procedure

End algorithm

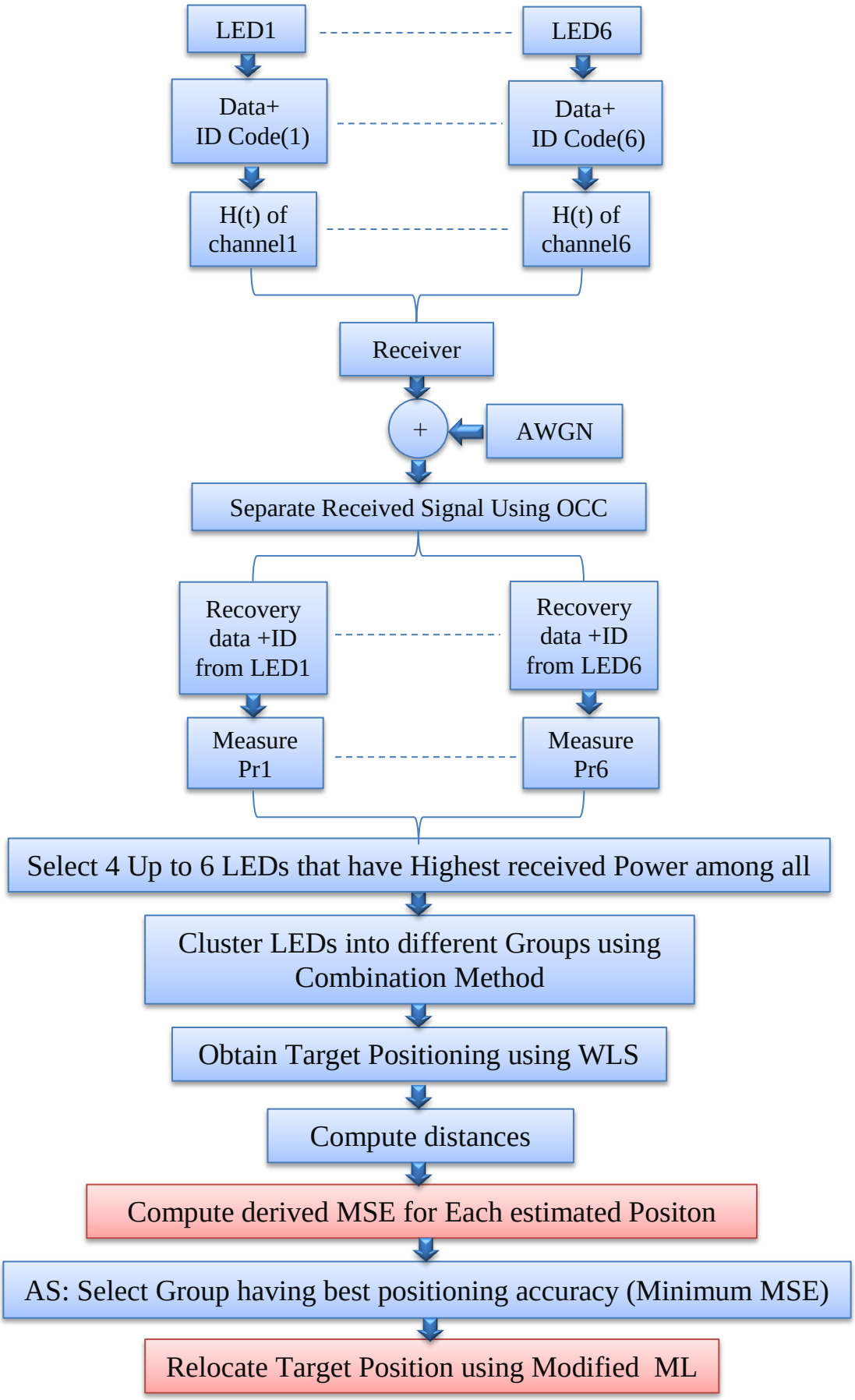

Figure (3-18): Block diagram of the proposed system.

3.3.2 System Parameters

This thesis presents a new indoor positioning system using a hybrid technique of different indoor positioning algorithms to get a reliable system with convenient accuracy, less complexity, and time conception. The created system is implemented using MatLab simulation. In this work, we presume a patient was walking through a room size 5 ×5 ×3 m and a corridor of 20 m. The lighting system consists of two scenarios, as shown:

a. **Scenario 1:**The first scenario uses 6 LEDs in the room and 18 LEDs for the corridor. The LEDs positions in the room at coordinates of (0.5, 0.5, 3), (2.5, 0.5, 3), (4.5, 0.5, 3), (0.5, 2.5, 3), (0.5, 4.5, 3), and (4.5, 4.5, 3), . In the corridor, the positions at (0.5, 0.5, 3), (2.5, -0.5, 3), (4.5, 0.5, 3), (4.5, 0.5, 3), (4.5, 0.5, 3), and so on as shown in figure(3-19a).
b. **Scenario 2:** The second scenario uses 9 LEDs in the room and 24 LEDs for the corridor. The LEDs positions in the room at coordinates of (0.5, 0.5, 3), (2.5, 0.5, 3), (4.5, 0.5, 3), (0.5, 2.5, 3), (2.5, 2.5, 3), (2.5, 4.5, 3), (0.5, 4.5, 3), (2.5, 4.5, 3), and (4.5, 4.5, 3) . In the corridor, the positions at (6, 1.5, 3), (6, 3.5, 3), (8, 1.5, 3), (8, 3.5, 3), (10, 1.5, 3), (10, 3.5, 3), and so on as shown in figure(3-19b).

The patient wears PD in his hand and could receive the location code if optical light is incident within its FOV. Based on the proposed scenarios, the receiver at least will receive 4 signals inside the room or the corridor based on the highest power. We assumed that the hand's orientation would not affect the bracelet reception since the receiver always has 4 up to 6 signals coming through different propagation channels (LOS and NLOS). Besides, the OCC is used to separate the received signals as an assumption. Table (3-3) presents the simulation parameters considered for this work.

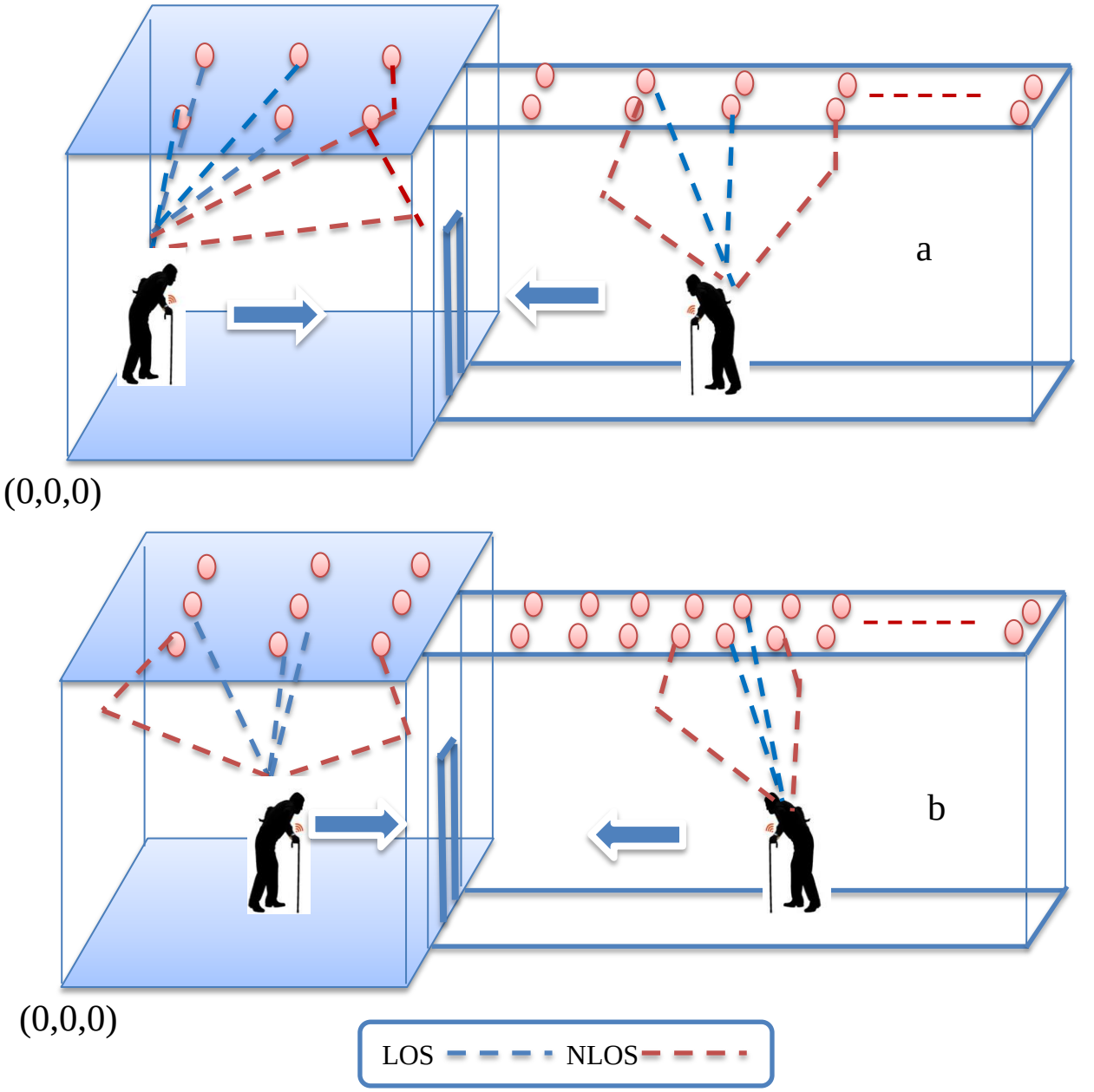

Figure(3-19): Experimental activities inside the room and corridor (a) Scenario1, (b) Scenario2.

Table (3-3) Simulation Parameters for proposed system

Transmitter Parameters	
Parameter	**Value**
Room size	$5 \times 5 \times 3m^3$
Corridor length	$20 \times 3 \times 3m^3$
Wall Reflectivity ρ	0.25
Reflecting element area dA_{wall}	$1cm^2$
Lambertian mode m	1
LED transmitter Power P_t	$4W$
Response Rate of PDs R	$0.4\ A/W$
Optical filter gain T_s	1
Concentrator gain g	1
Receiver Parameters	
Surface Area of the PD A_{PD}	$1cm^2$
Receiver Plane h	$0.85m$
FOV of the receiver	$80\ deg$
Noise Parameters[47]	
Current of daylight I_{bg}	$5100 \times 10^{-6}\ A$
Noise Bandwidth factor I_2	$0.562\ A$
I_3	$0.0868\ A$
Open-loop voltage gain G_o	10
Noise Bandwidth B_n	$10^8\ pulses/s$
Absolute temperature T_K	$298K$
FET transconductance g_m	$30mS$
FET Channel noise factor Γ	1.5
Fix capacitance C_f	$112pF/cm^2$

Chapter Four

Practical and Simulation Results with Discussion

Chapter Four

Practical and Simulation Results with Discussion

4.1 Performance of Smart Healthcare Monitoring system using Li-Fi technology-based IoT

This chapter begins with the performance of the proposed smart healthcare monitoring system using Li-Fi technology-based IoT. The system results are described in two sub-section. Firstly, the performance of the Li-Fi system is given, then the results of ThingSpeak platform and mobile application.

4.1.1 Li-Fi System Result

After the Arduino program writing, the written program is compiled and uploaded using Arduino IDE. Then the smart healthcare monitoring system using Li-Fi technology is powered. Sensors are connected to the patient's body. The serial Monitor of Arduino IDE at the receiver is opened to see heart rate and body temperature values.

The proposed system is tested over various propagation links (direct LOS, non-direct LOS, and NLOS) and ambient noise. Evaluation and validation of the system in this experiment are performed using a variety of measurements. These measurements include the transmitted power, received power, OSNR, ESNR, the transmitted half-angle, and the distance from the transmitter to the receiver.

Firstly, the performance evaluations' findings for the LOS link under low and high ambient noise (sunlight and fluorescent lamps) are presented in figure(4-1),to (4-6) tables (4-1) and (4-2).

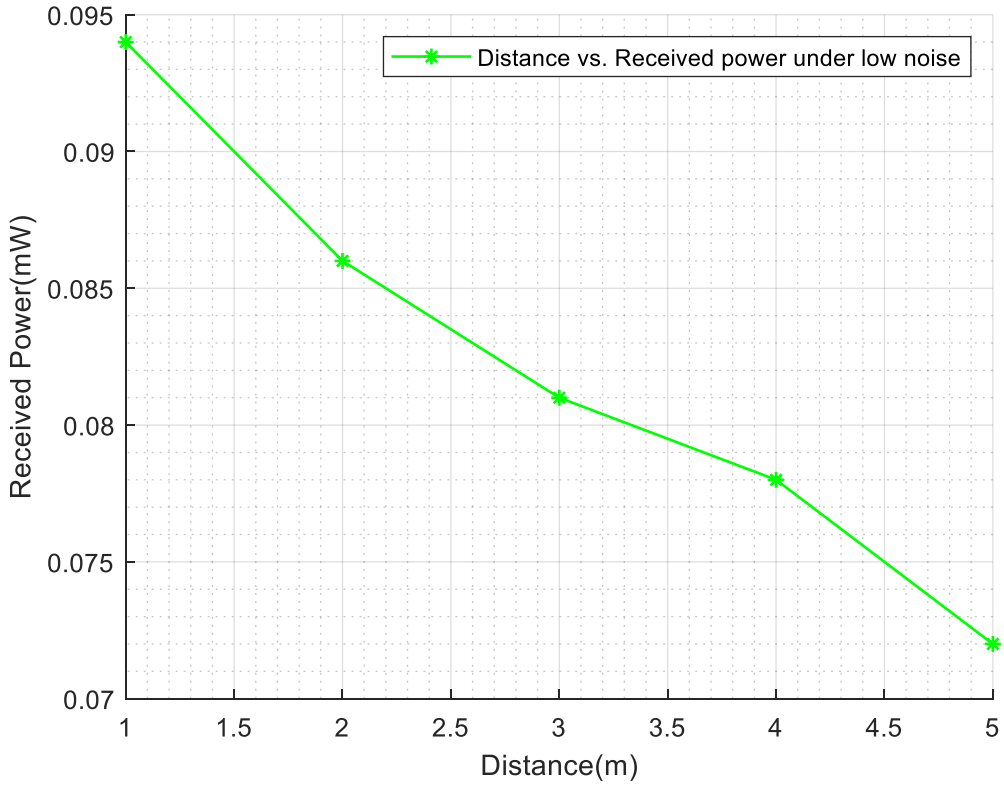

Figure (4-1): Distance vs. Received power for direct LOS under low ambient noise.

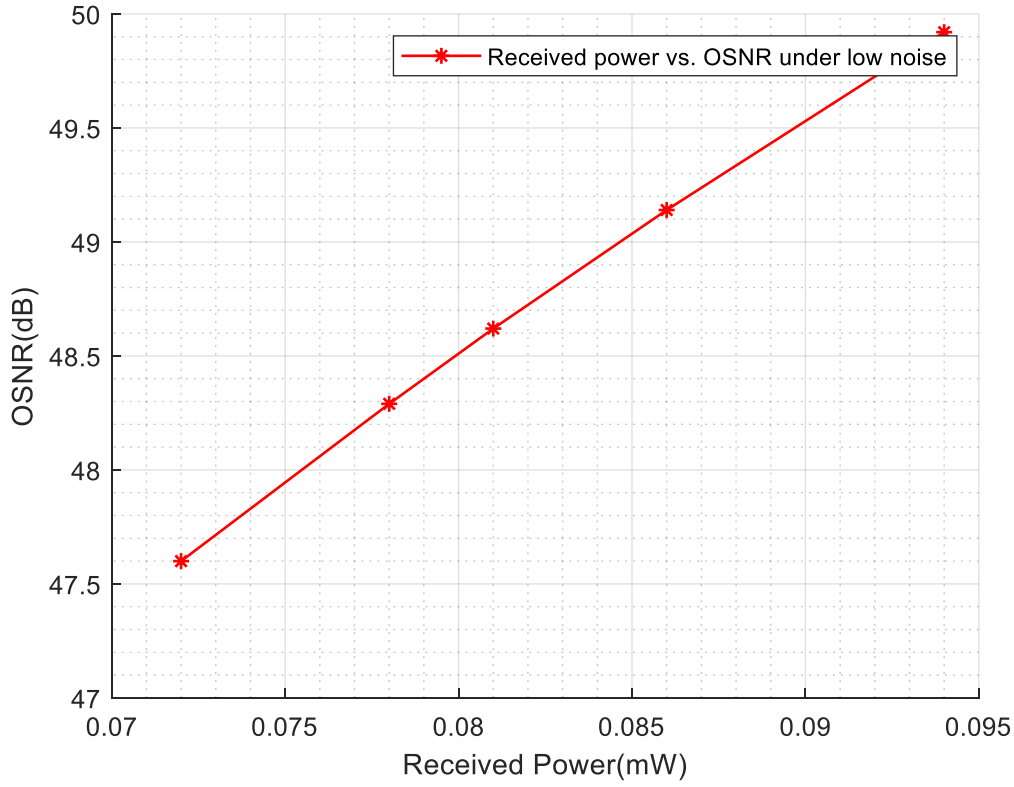

Figure (4-2): Received power vs. OSNR for direct LOS under low ambient noise.

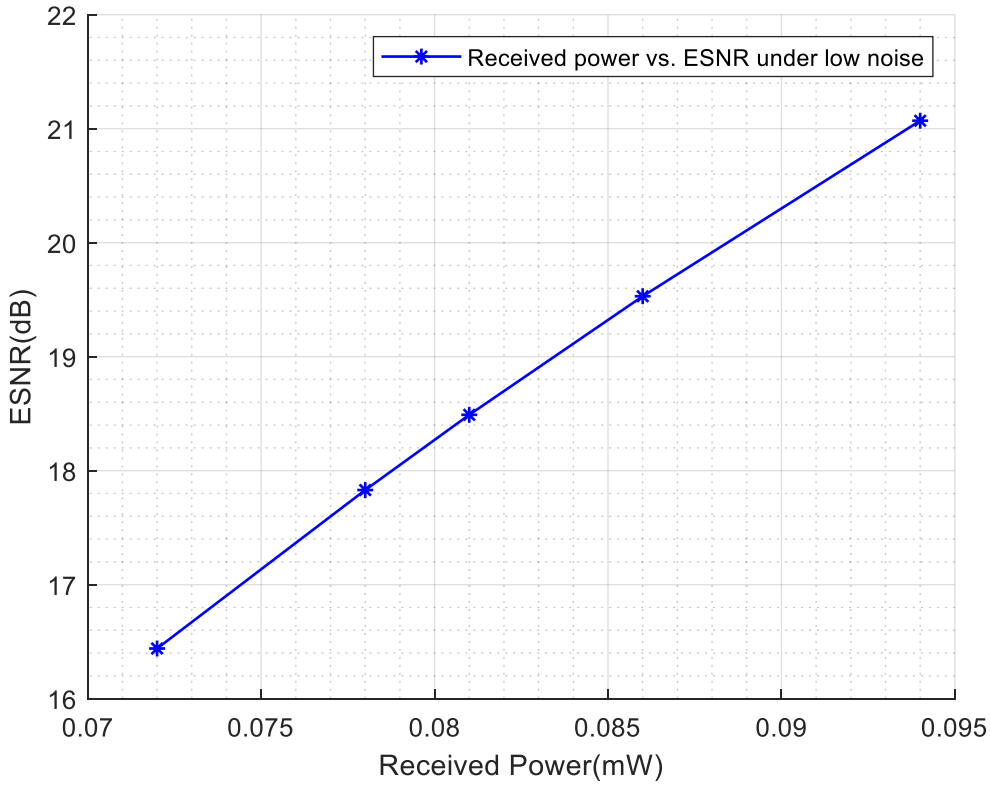

Figure (4-3): Received power vs. ESNR for direct LOS under low ambient noise.

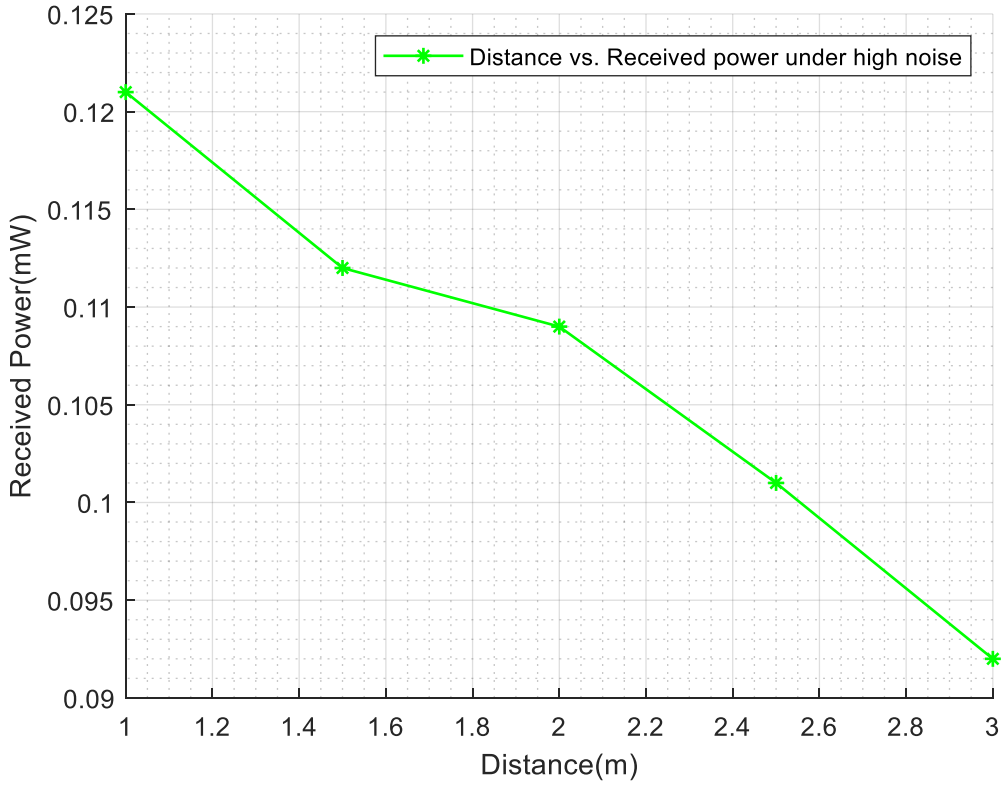

Figure (4-4): Distance vs. Received power for direct LOS under high ambient noise.

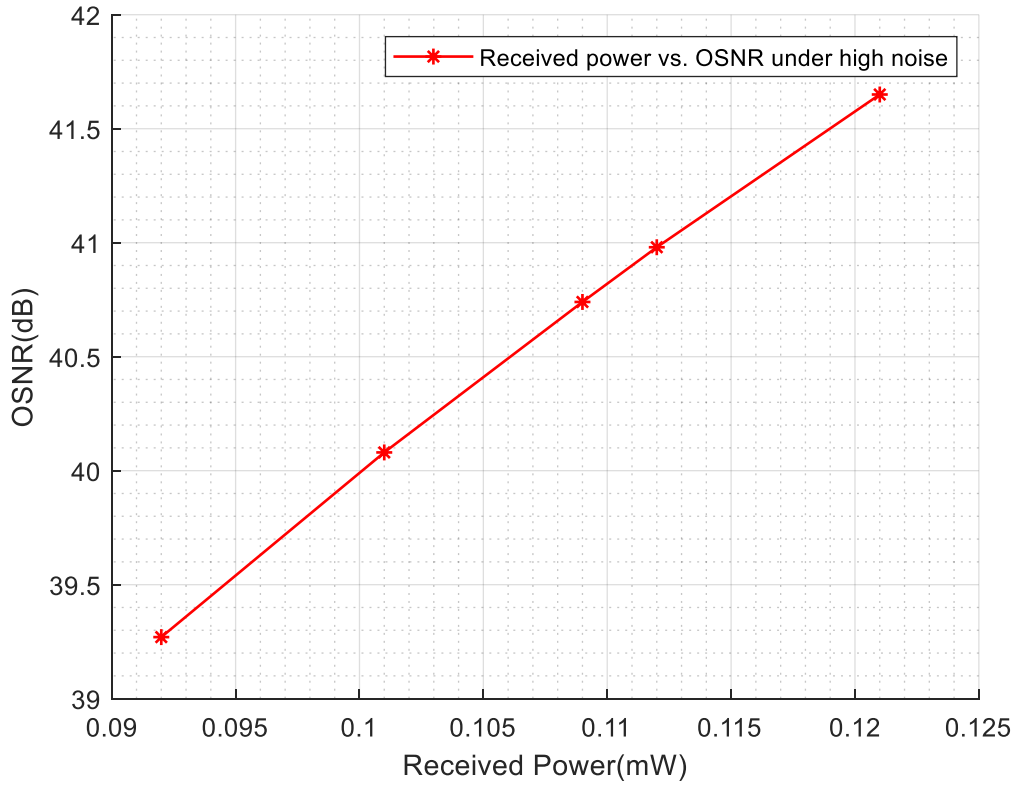

Figure (4-5): Received power vs. OSNR for direct LOS under high ambient noise.

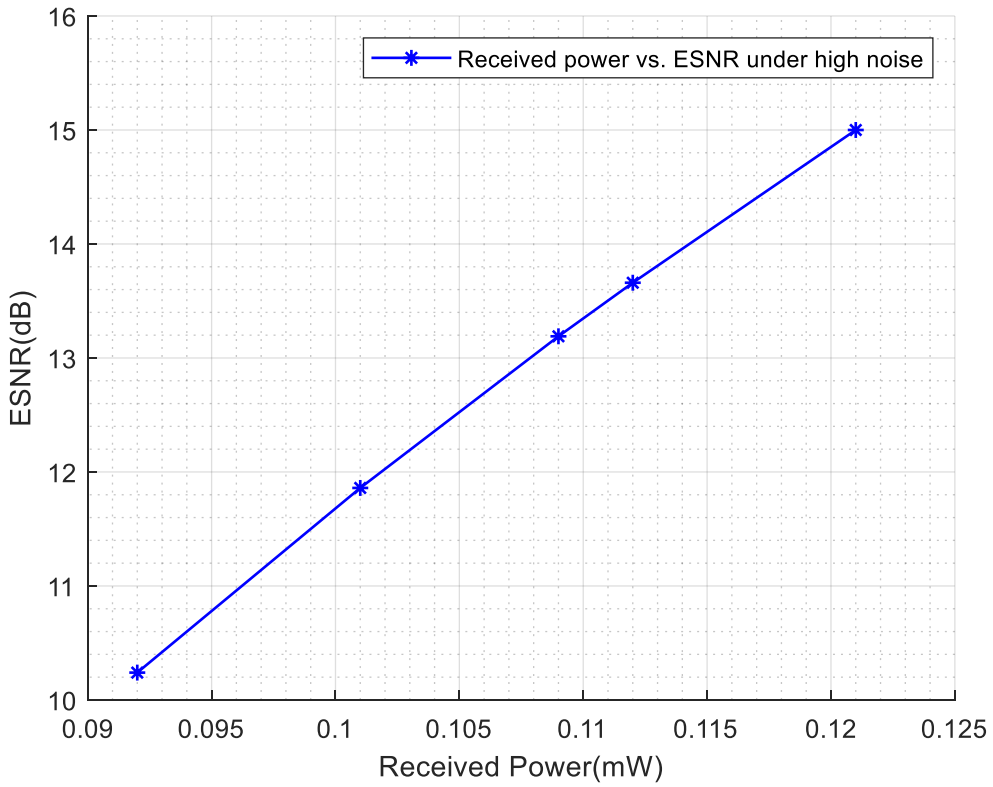

Figure (4-6): Received power vs. ESNR for direct LOS under high ambient noise.

Table (4-1): Direct-LOS link measurements under low ambient noise.

Distance (m)	Transmitted Power(mW)	Received Power(mW)	OSNR (dB)	ESNR (dB)
1	0.15	0. 094	49.92	21.07
2	0.4	0. 086	49.14	19.53
3	0.7	0. 081	48.62	18.49
4	1.1	0. 078	48.29	17.83
5	1.5	0. 072	47.60	16.44

Table (4-2): Direct-LOS link measurements under high ambient noise.

Distance (m)	Transmitted Power(mW)	Received Power(mW)	OSNR (dB)	ESNR (dB)
1	0.3	0.121	41.65	15.00
1.5	0.6	0.112	40.98	13.66
2	0.9	0.109	40.74	13.19
2.5	1.2	0.101	40.08	11.86
3	1.5	0.092	39.27	10.24

As shown in table(4-1) and table(4-2), OSNR is varied from 47.60 dB to 49.92dB and ESNR from 16.44 dB to 21.07dB for a distance of up to 5 meters in the direct-LOS link under low ambient noise. On the other hand, the OSNR is changed from 39.27dB to 41.65 dB and ESNR from 10.24dB to 15.00 dB for a distance of up to 3 meters in the same link under high ambient noise (sunlight and fluorescent lamp). It is observed that ambient sources profoundly impact the receivers of Li-Fi communication. The distance is restricted to 3m under ambient light sources while 5m under dim lighting.

The outcomes of the non-direct LOS link at a distance of 2 m with varied half-transmitted angles (5°-20°) under the two cases of ambient noise is presented in the figures from (4-7) to (4-12), table (4-3) and (4-4).

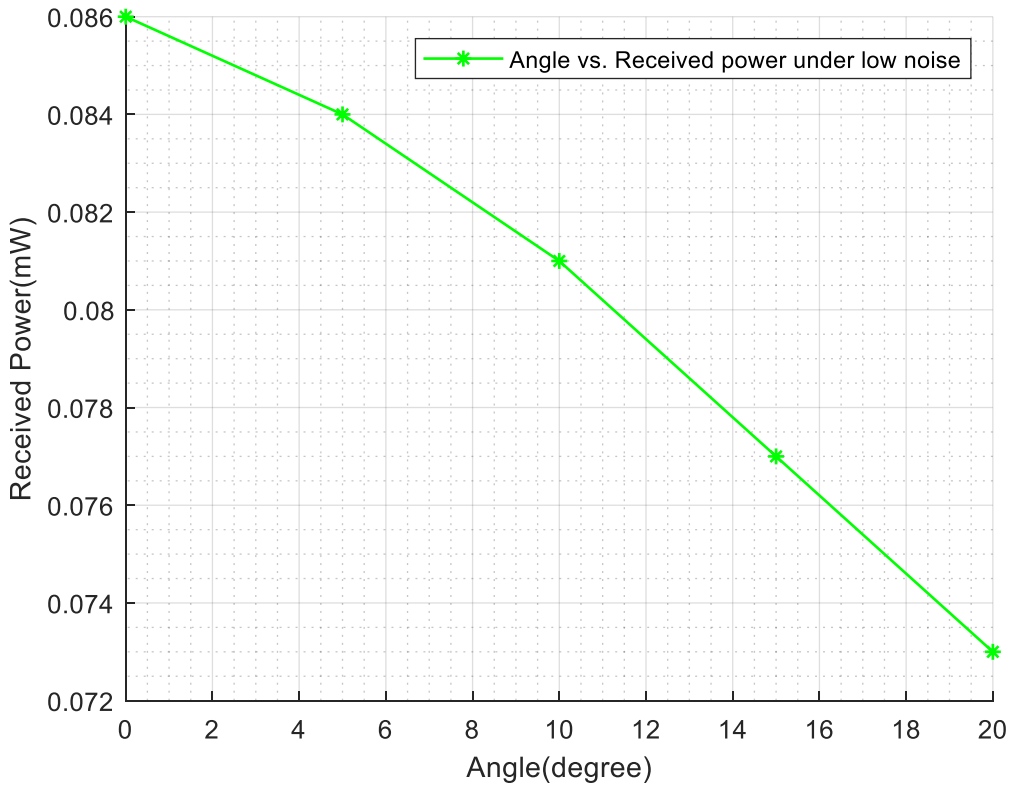

Figure (4-7): Angle vs. Received power for non- direct LOS under low ambient noise.

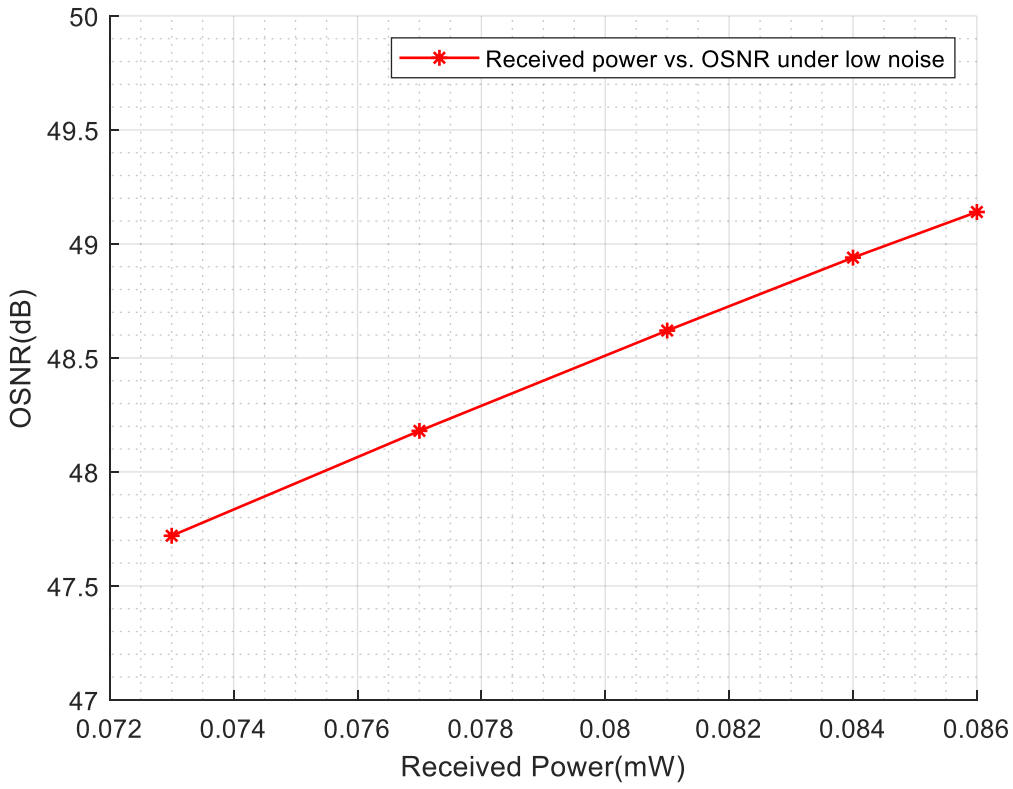

Figure (4-8): Received power vs. OSNR for non-direct LOS under low ambient noise.

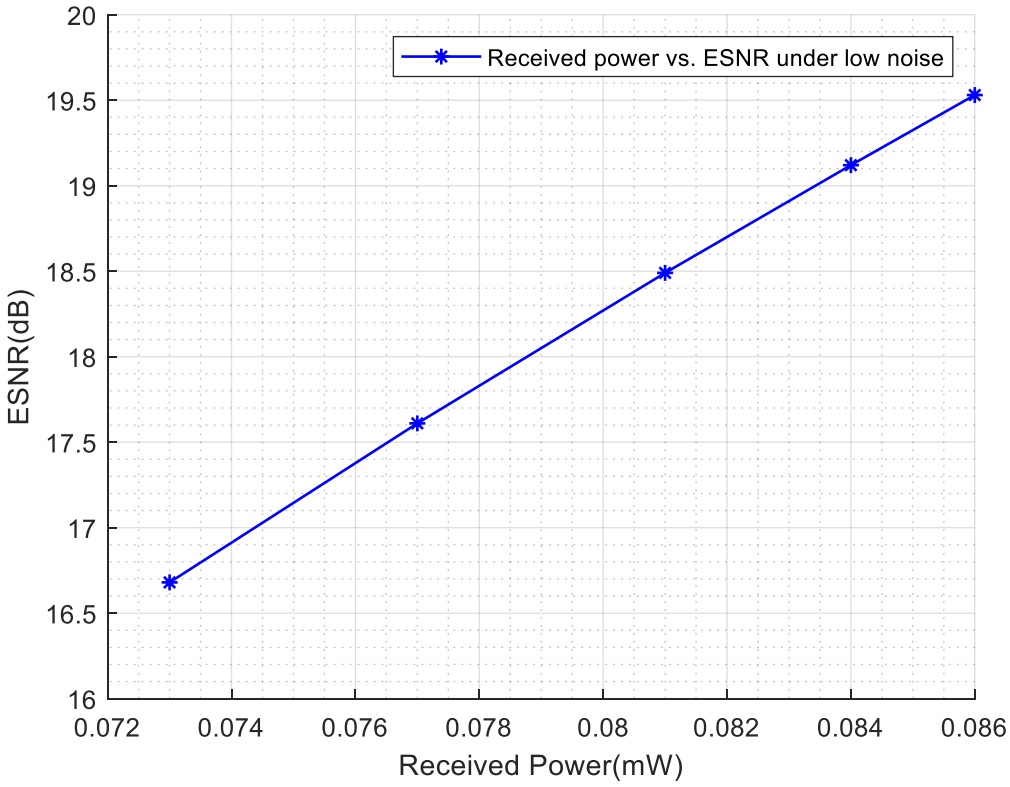

Figure (4-9): Received power vs. OSNR for non-direct LOS under low ambient noise.

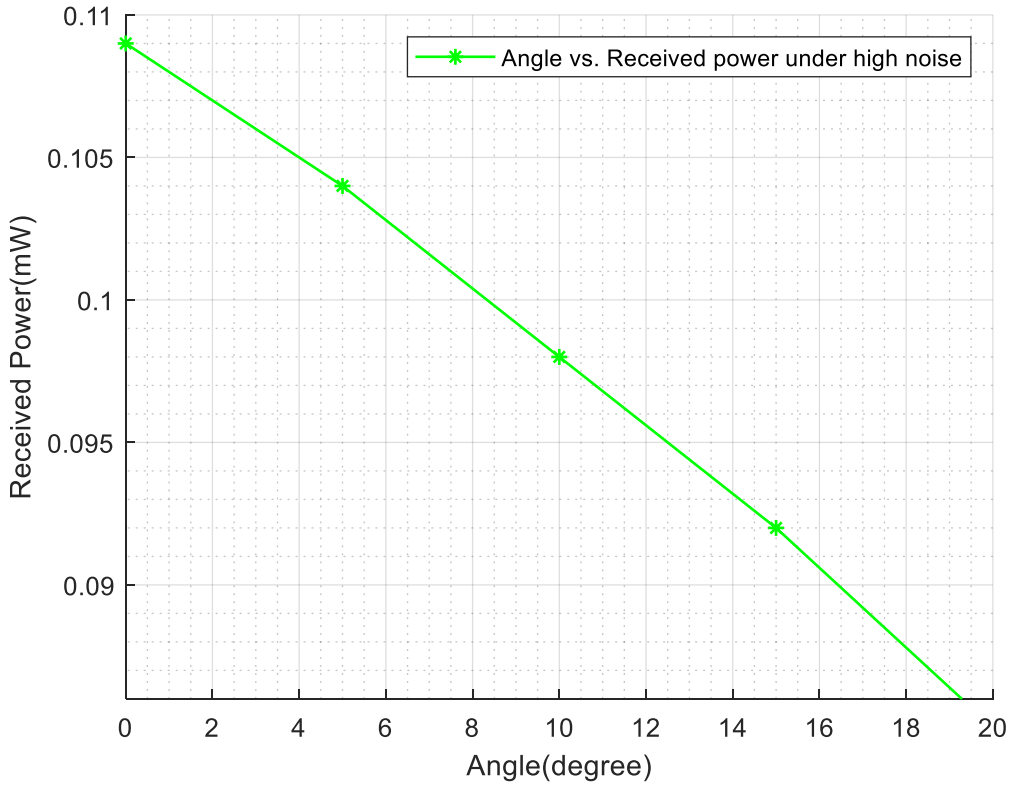

Figure (4-10): Angle vs. Received power for non-direct LOS under high ambient noise.

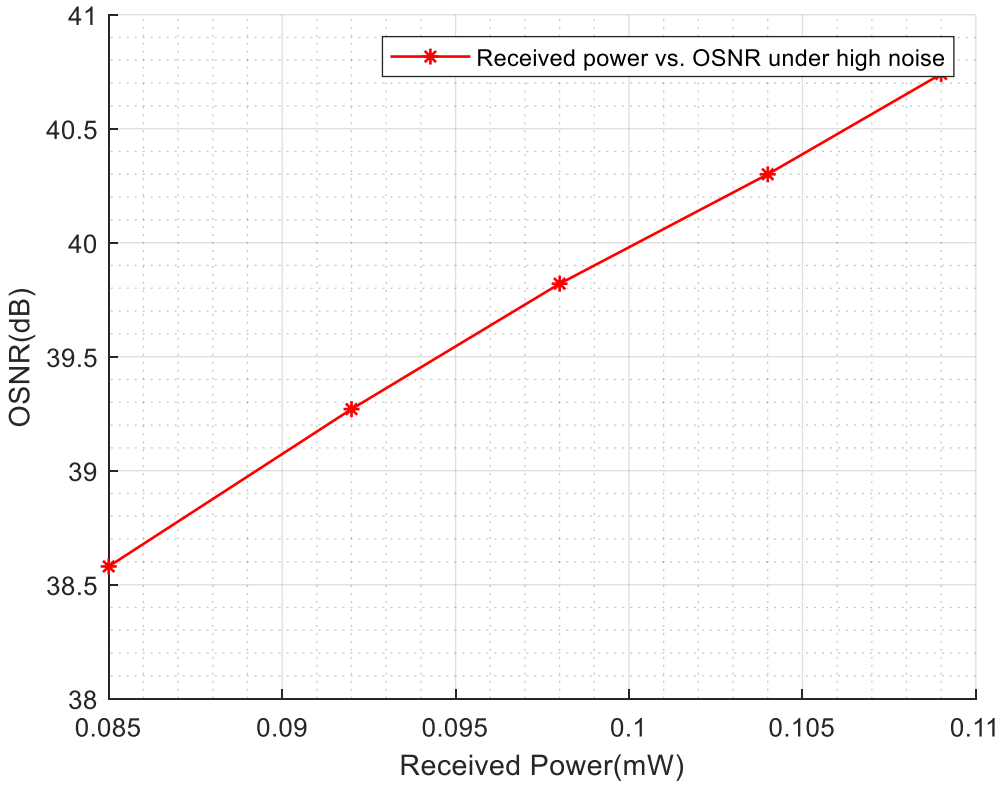

Figure (4-11): Received power vs. OSNR for non-direct LOS under high ambient noise.

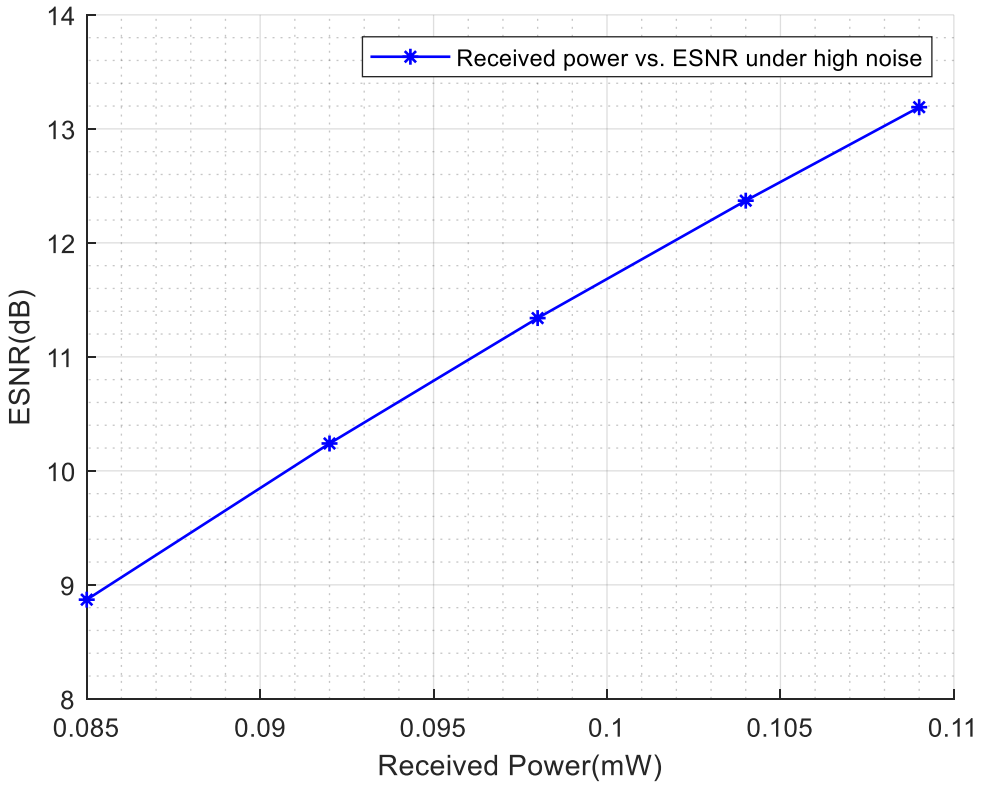

Figure (4-12): Received power vs. ESNR for non-direct LOS under high ambient noise.

Table(4-3): Non-direct LOS link measurements under low ambient noise.

Angle	Received Power(mW)	OSNR (dB)	ESNR (dB)
0 (Direct-LOS)	0. 086	49.14	19.53
5	0.084	48.94	19.12
10	0.081	48.62	18.49
15	0.077	48.18	17.61
20	0.073	47.72	16.68
25	-	-	-

Table(4-4): Non-direct LOS link measurements under high ambient noise.

Angle	Received Power(mW)	OSNR (dB)	ESNR (dB)
0 (Direct-LOS)	0.109	40.74	13.19
5	0.104	40.3	12.37
10	0.098	39.82	11.34
15	0.092	39.27	10.24
20	0.085	38.58	8.87
25	-	-	-

For the non-direct LOS link, the obtained OSNR is variable from 47.72 to49.14dB, and ESNR from 16.68 to 19.53dB, which is still acceptable. For other cases of noise, the obtained OSNR is variable from 38.58 to40.74dB, and ESNR from 8.87to 13.19dB. At angle 25^{o}, the green led in the experiment is off, and the data is lost.

Finally, figures from (4-13) to (4-18), tables (4-5), and (4-6) show the results of the proposed system at various distances for the NLOS links for two statuses of the ambient noise.

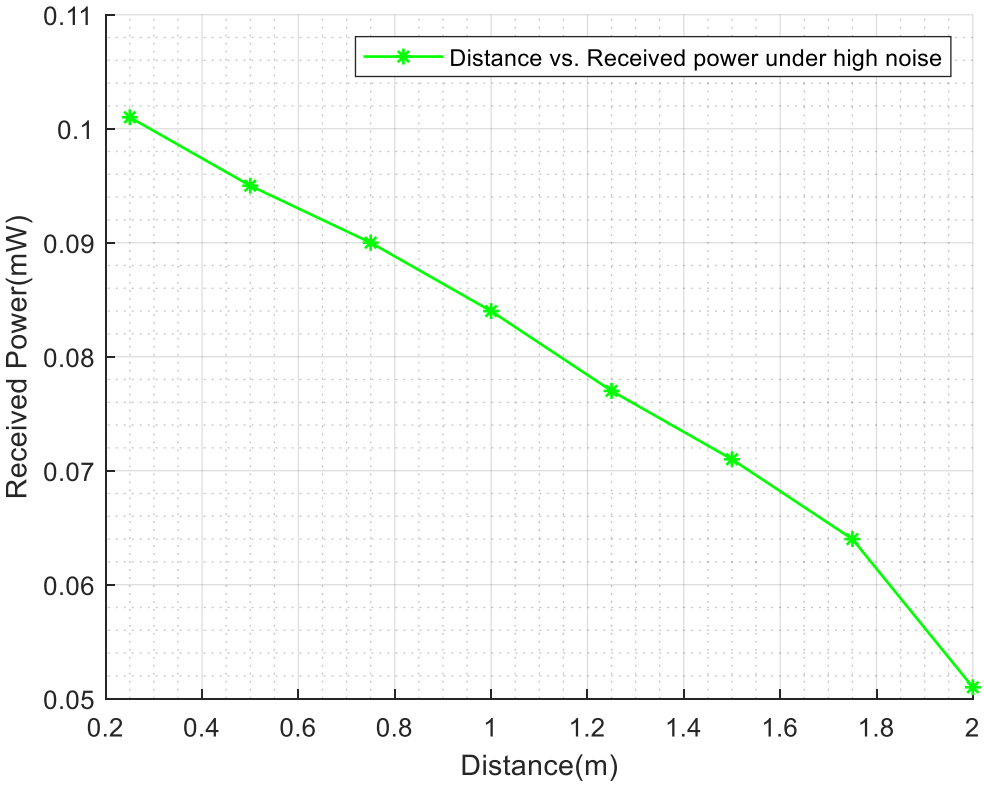

Figure (4-13): Distance vs. Received power for NLOS under low ambient noise.

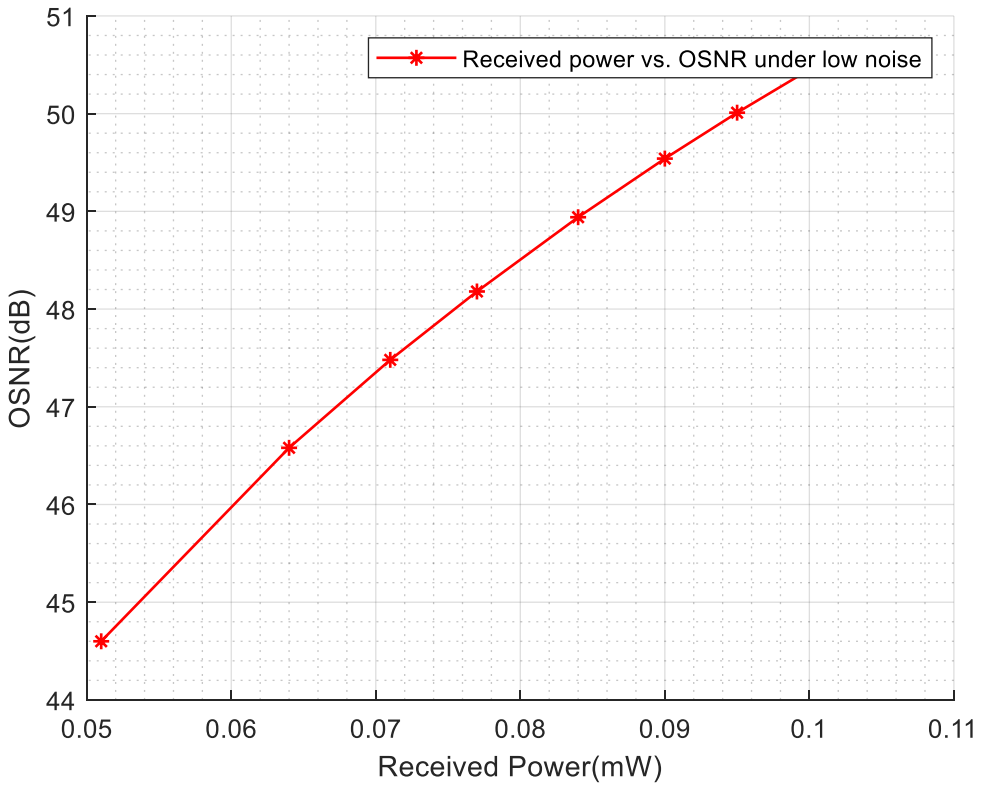

Figure (4-14): Received power vs. OSNR for NLOS under low ambient noise.

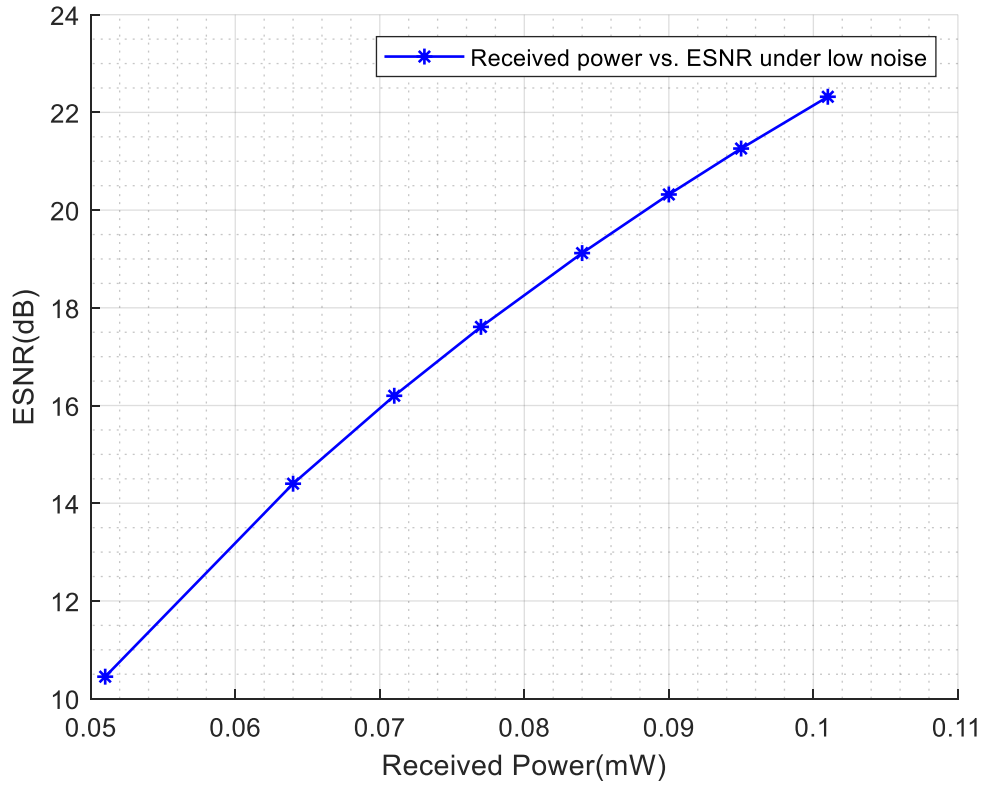

Figure (4-15): Received power vs. ESNR for NLOS under low ambient noise.

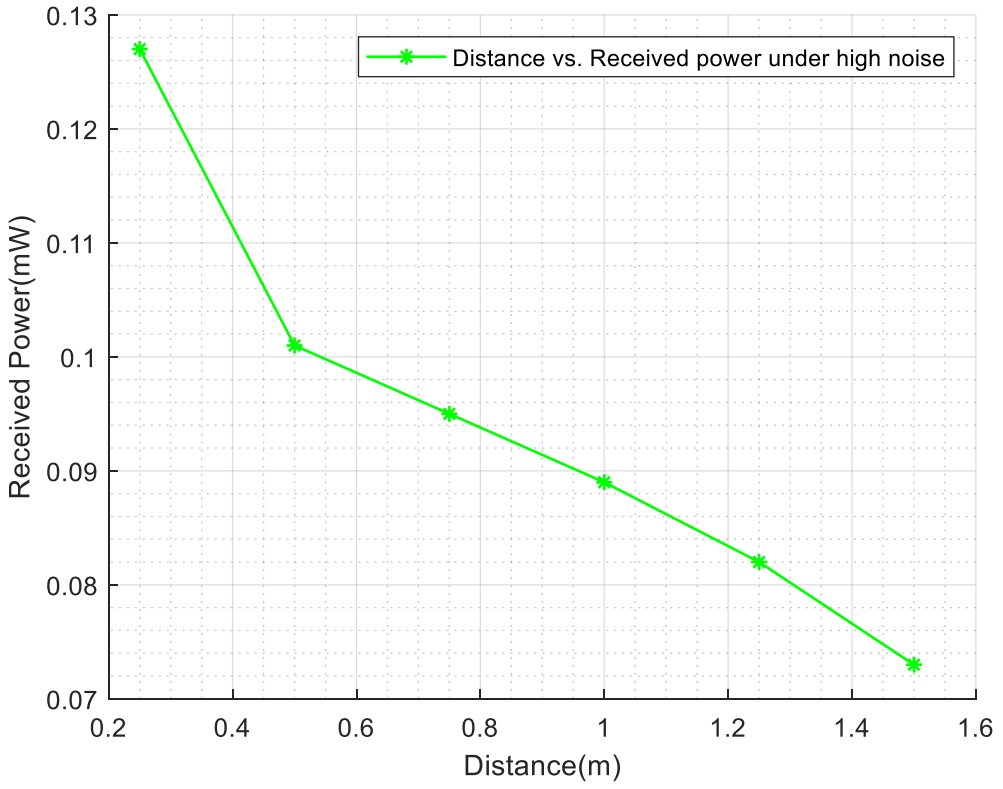

Figure (4-16): Distance vs. Received power for NLOS under high ambient noise.

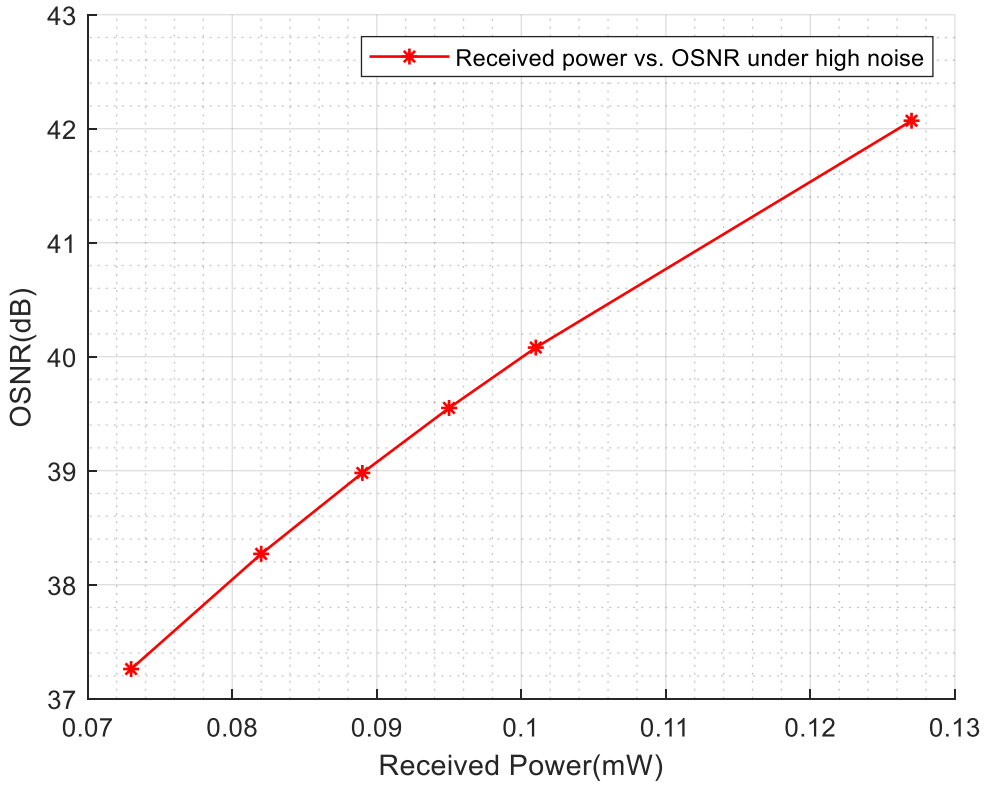

Figure (4-17): Received power vs. OSNR for NLOS under high ambient noise.

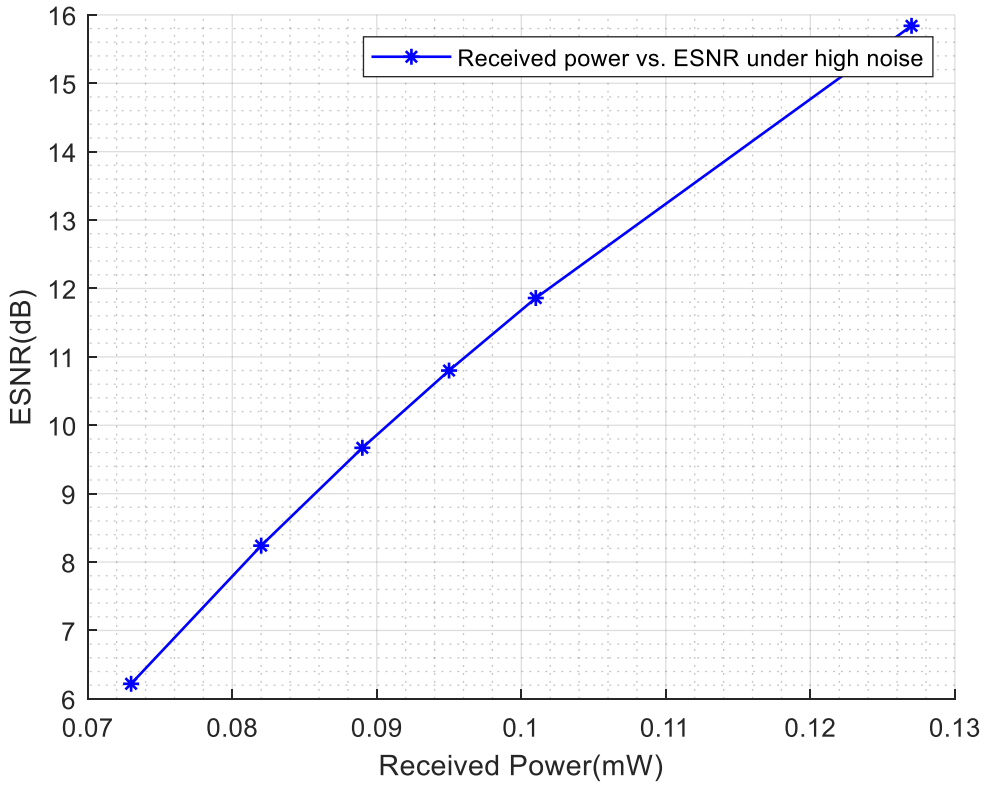

Figure (4-18): Received power vs. ESNR for NLOS under high ambient noise.

Table(4-5): NLOS link measurements under low ambient noise.

Distance (m)	Transmitted Power (mW)	Received Power (mW)	OSNR (dB)	ESNR (dB)
0.25	0.25	0. 101	50.54	22.32
0.5	0.4	0.095	50.01	21.26
0.75	0.55	0.09	49.54	20.32
1	0.7	0.084	48.94	19.12
1.25	0.95	0.077	48.18	17.61
1.5	1.1	0.071	47.48	16.20
1.75	1.25	0.064	46.58	14.40
2	1.5	0.051	44.60	10.45

Table(4-6): NLOS link measurements under high ambient noise.

Distance (m)	Transmitted Power (mW)	Received Power (mW)	OSNR (dB)	ESNR (dB)
0.25	0.4	0.127	42.07	15.84
0.5	0.65	0.101	40.08	11.86
0.75	0.9	0.095	39.55	10.80
1	1.1	0.089	38.98	9.67
1.25	1.3	0.082	38.27	8.24
1.5	1.5	0.073	37.26	6.22

Tables (4-5) and (4-6) show that the OSNR is varied from 44.60 to50.54dB and ESNR from 10.45to 22.32dB for the first case, whereas OSNR is varied from 37.26 to42.07dB and ESNR from 6.22to 15.84dB for the second case which obtained in the experiment. In this link type, it is noted that all the parameters worsen considerably.

In general, OSNR and ESNR are affected by the following factors: link type, distance, ambient noise, and transmitted half-angle. Hence, the received power reaching the receiver is concerned, which requires increasing the transmitting power to obtain acceptable values.

4.1.2 IoT Part Results

In the last step, the IoT part comes in. The proposed smart healthcare system is shown and utilized in intensive care of Al-Emam Al-Sadiq Hospital (figure(4-19)). Python code is running to send the measured heart rate and body temperature values to the ThingSpeak platform. The doctor or medical technician can monitor these values from related channels using laptops, Ipad, or mobile phones.

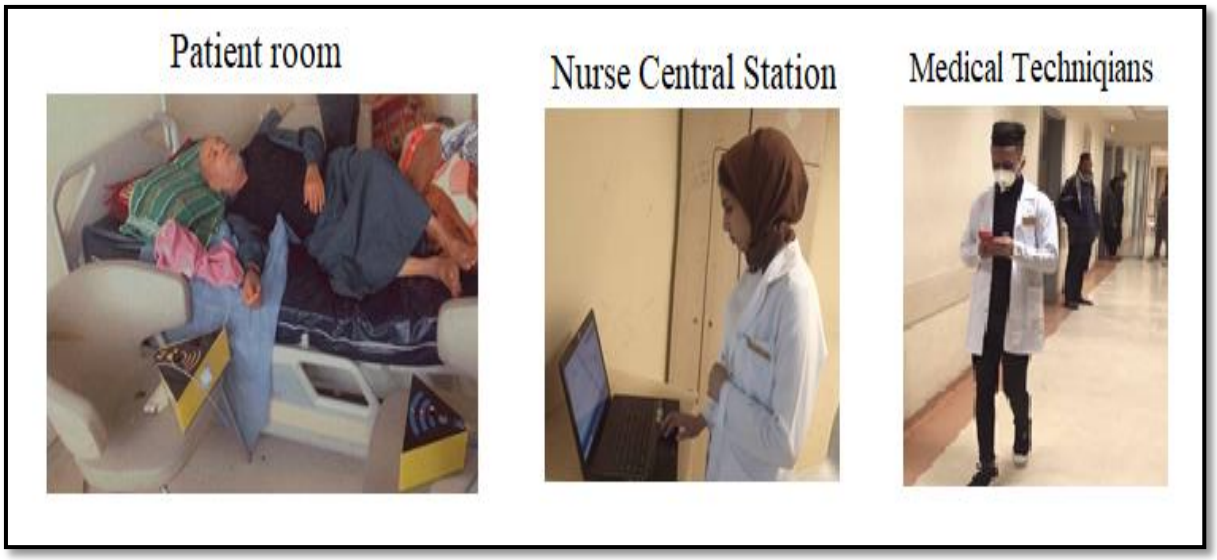

Figure (4-19): Intensive care of Al-Emam Al-Sadiq Hospital.

Data flow is checked as shown in figure(4-20). After that, searching the channel ID on the ThingSpeak website or ThingView mobile app, it is easy to access this channel, as shown in figure(4-21) and (4-22). Field1 and Field2 show the heart rate and temperature monitoring records, respectively. Graphs

depicting changes in heart rate or temperature over time are displayed every 16 seconds.

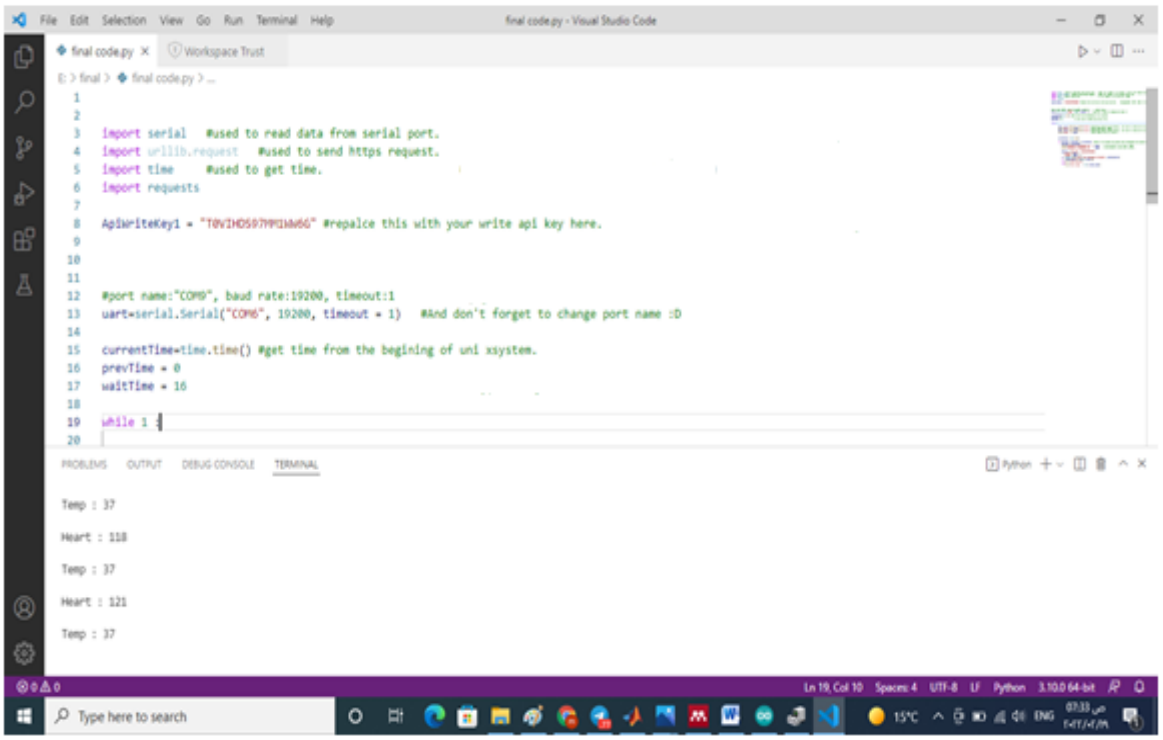

Figure (4-20): Data Flow in Python.

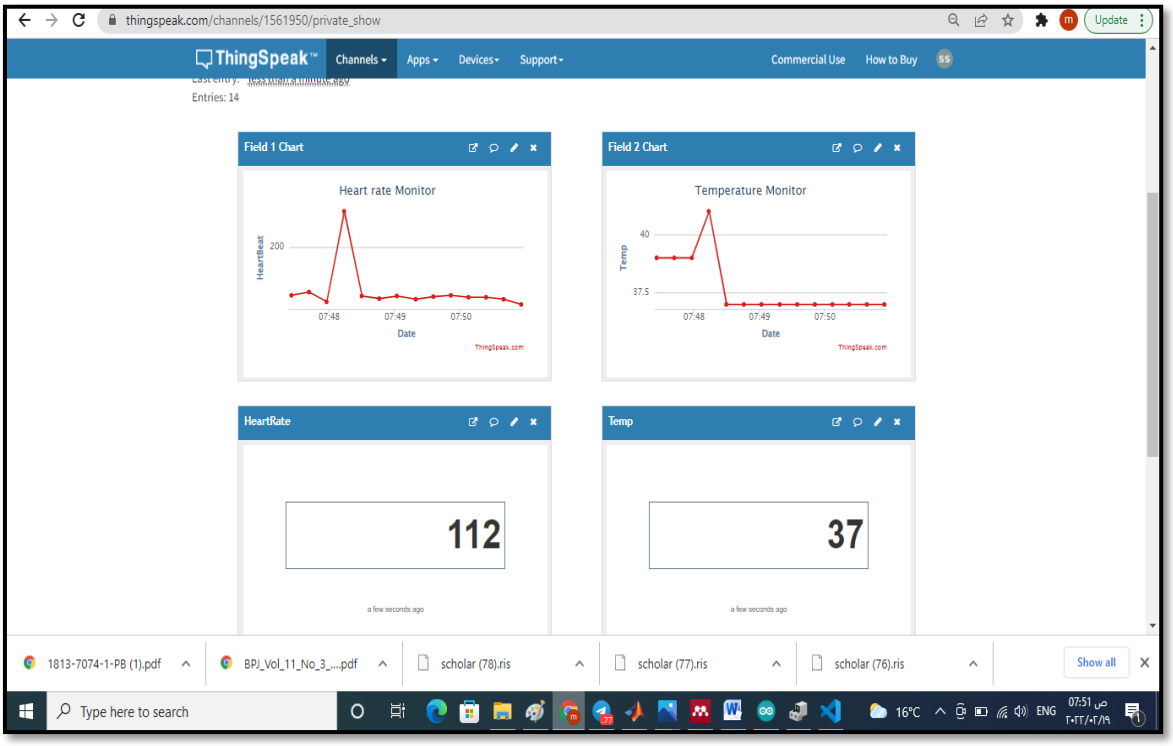

Figure (4-21): Channel view on ThingSpeak website.

Figure (4-22): Channel view in ThingView Mobile Application.

The IFFFT notifications was tested by varying the value around the sensor artificially. In this status the heart rate and body temperature values are out of the predefined values. So an email message is sent to the authorized devices with different cases as shown in figure(4-23).

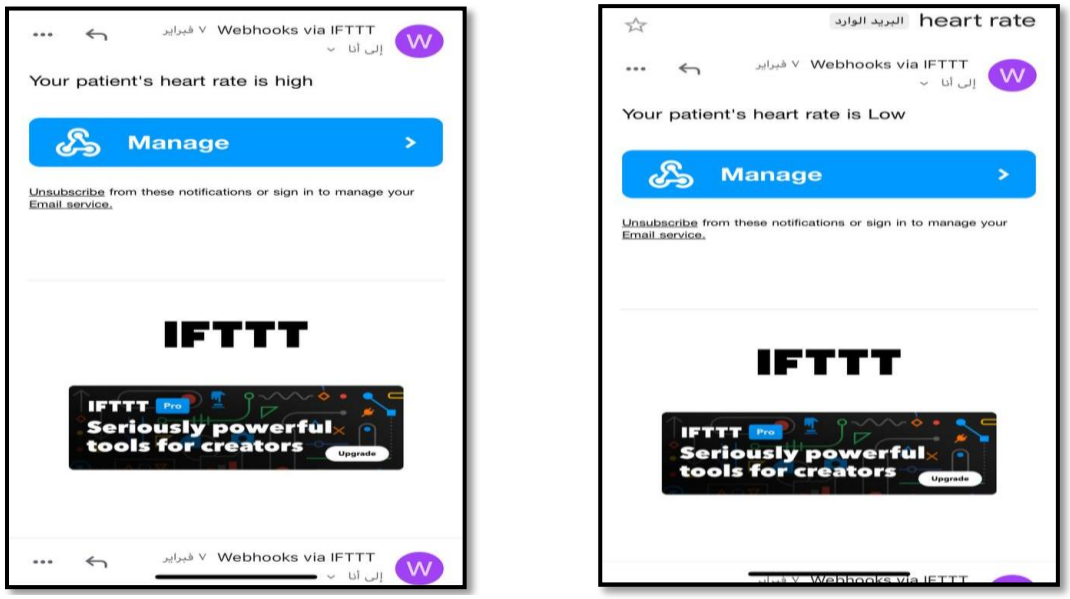

(a) (b)

(c) (d)

Figure (4-23): Alert Email with different cases (a) High Heart rate, (b)Low Heartrate, (c) High Temperature, and (d) Low Temperature.

Finally, this prototype is distinguished by low power consumption , low cost, and using light for illumination and data transfer. The cost of the implemented Li-Fi system was around 10$. Regarding the Internet of Things, ThingSpeak's cloud platform and IFTTT are all free. Except sensors are selected with a high-quality to obtain a high degree of accurate readings. Also, the experimental result shows a 100 % accuracy of the received data under all

test experiments circumstances. In addition, due to its design and IoT technology, it also makes measurements and monitoring simple and smart.

4.2 Performance of the Proposed IPS using VLC technology:

First, the steps in algorithm1 are applied to obtain the system's performance. The system is investigated when noise is taken into account. The residual noise is added to the received signal using the AWGN function from MATLAB® over the ESNR calculated based on Eq. (2-21). Based on our algorithm, as shown in table (4-7), only six LEDs is selected with more power. Then, the combination method was implemented to group the selected LEDs to create different groups when each group had 4 LEDs up to six. Each selected group is affected by different propagation channels (LOS and NLOS). The total number of groups is very large, so six groups are chosen randomly to present the result of the proposed algorithm. Then, the WLS method is used by each group to compute the target position.

Table (4-7): Types of propagation channels for every group of LEDs.

Group name	Number of LEDs	LOS channel	NLOS channel
G1	4	2 LED	2 LED
G2	4	1 LED	3 LED
G3	5	2 LED	3 LED
G4	5	1 LED	4 LED
G5	6	2 LED	4 LED
G6	6	1 LED	5 LED

For the evaluation stage, the target position is estimated by taking ten different points corresponding to his path inside the room and along the corridor. Then, the derived MSE is used to evaluate the estimated position for each group, as shown in tables (4-8) and (4-9). The highlighted red numbers are

the lowest value of MSE of each group of anchor nodes. The positioning accuracy will gradually improve when the target moves directly below the LEDs. This is because the NLOS power in the room center is lower than the corners. So, the best values of the MSE for the WLS approach are at ($x = 2.5, y = 2.5, z = 0.75$) and for scenarios 1 and 2. Also, it can be seen in table (4-8) and (4-9) that increasing the number of LEDs from 6 to 9 in room and from 18 to 24 in corridor will increase the accuracy of the system . For example, for G1 the average MSE is $0.83m^2$ with 6 LEDs and $0.57m^2$ with 9 LEDs. In general, the more LED lights that are installed on the ceiling, the higher the accuracy value.

Table (4-8): MSE for WLS method for different positions of the target in m^2 (Scenario1).

Point	Target position	MSE (WLS)					
		G1	G2	G3	G4	G5	G6
1	(0.25,2,0.85)	0.28	0.37	0.45	0.66	0.59	0.74
2	(1.5,2.5,0.85)	0.29	0.35	0.25	0.38	0.31	0.45
3	(4,0.25,0.75)	0.37	0.53	0.29	0.37	0.23	0.34
4	(2.5,2.5,0.75)	0.31	0.42	0.33	0.46	0.16	0.24
5	(4.75,4.75,0.8)	0.57	0.61	0.73	0.89	0.67	0.79
6	(5.25,2,0.8)	1.31	1.45	1.16	1.28	1.25	1.46
7	(9,2,0.7)	1.65	1.93	1.97	2.16	1.23	1.41
8	(17,3.5,0.7)	1.17	1.29	1.12	1.34	1.27	1.44
9	(21,1.5, 0.65)	0.56	0.67	0.73	0.81	0.59	0.78
10	(25,3.75,0.65)	1.73	2.05	1.84	2.14	1.93	2.33
Mean		0.83	0.96	0.88	1.04	0.81	0.99

Table(4-9): MSE for WLS method for different positions of the target in m^2 (Scenario2)

Point	Target position	MSE (WLS)					
		G1	G2	G3	G4	G5	G6
1	(0.25,2,0.85)	0.23	0.29	0.35	0.48	0.23	0.42
2	(1.5,2.5,0.85)	0.21	0.29	0.19	0.28	0.24	0.32
3	(4,0.25,0.75)	0.21	0.33	0.31	0.37	0.25	0.34
4	(2.5,2.5,0.75)	0.16	0.23	0.18	0.27	0.12	0.21
5	(4.75,4.75,0.8)	0.44	0.51	0.46	0.59	0.45	0.57
6	(5.25,2,0.8)	1.31	1.45	0.93	1.28	1.25	1.35
7	(9,2,0.7)	0.74	0.91	0.81	0.98	0.77	1.02
8	(17,3.5,0.7)	0.87	1.15	0.82	1.10	0.91	1.24
9	(21,1.5, 0.65)	0.34	0.47	0.43	0.61	0.33	0.48
10	(25,3.75,0.65)	1.18	1.32	1.24	1.43	1.03	1.27
Mean		0.57	0.69	0.57	0.74	0.55	0.72

Then, for each scenario, the group having the least MSE value was selected with its estimated position to be used as the initial point for the modified ML approach to calculate the final position of the target. The last step in this work is to evaluate and compare the proposed system with two related approaches, WLS conventional ML. In the conventional ML, a random fixed point was used as the initial point for iteration purpose [we chose ($x = 10, y = 5, z = 0.85$) for scenario 1 and 2], but, in the proposed algorithm, the initial point is made as a dynamic point that could be changed based on the best position obtained by AS approach as shown in tables(4-10) and (4-11). Also, it should be mentioned when the target position closes from the guess (initial) point of the conventional ML, the positioning accuracy of the ML will be enhanced and vice versa, as mentioned in points 6, 7, 8 in the tables. Then, the obtained points using the proposed approach and two different related approaches are evaluated using MSE MatLab function, as shown in the table.

Table (4-10) MSE for the proposed system compared to ML and WLS algorithms in m^2 (Scenario1)

Point	(target position)	WLS	ML	Proposed algorithm
1	(0.25,2,0.85)	0.59	0.29	0.17
2	(1.5,2.5,0.85)	0.31	0.19	0.18
3	(4,0.25,0.75)	0.23	0.29	0.19
4	(2.5,2.5,0.75)	0.16	0.14	0.10
5	(4.75,4.75,0.8)	0.67	0.23	0.24
6	(5.25,2,0.8)	1.25	0.10	0.11
7	(9,2,0.7)	1.23	0.11	0.12
8	(17,3.5,0.7)	1.27	0.13	0.15
9	(21,1.5, 0.65)	0.59	0.77	0.12
10	(25,3.75,0.65)	1.93	1.11	0.19
Mean		0.81	0.33	0.15

Table (4-11) MSE for the proposed system compared to ML and WLS algorithms in m^2 (Scenario2)

Point	(target position)	WLS	ML	Proposed algorithm
1	(0.25,2,0.85)	0.23	0.25	0.15
2	(1.5,2.5,0.85)	0.24	0.17	0.14
3	(4,0.25,0.75)	0.25	0.24	0.18
4	(2.5,2.5,0.75)	0.12	0.12	0.08
5	(4.75,4.75,0.8)	0.45	0.21	0.21
6	(5.25,2,0.8)	1.25	0.11	0.10
7	(9,2,0.7)	0.77	0.10	0.11
8	(17,3.5,0.7)	0.91	0.12	0.13
9	(21,1.5, 0.65)	0.33	0.69	0.11
10	(25,3.75,0.65)	1.03	0.93	0.17
Mean		0.55	0.29	0.13

It can be seen in both tables that the MSE of the proposed algorithm has an average of 0.15 m^2 for scenario 1 and 0.13 m^2 for scenario 2 in LOS and NLOS channels, compared with WLS and conventional ML that have an MSE for scenario1 about 0.81 m^2 ,0.33 m^2 and scenario 2 has 0.55 m^2 , 0.29 m^2 respectively. This indicates that the performance of the created system highly outperforms the other positioning approaches for the same environment.

The actual and estimated paths, including the proposed algorithm with two related approaches, WLS, and conventional ML, are shown in figure (4-24) for scenarios 1 and 2. As shown, the proposed system's position is more confined to actual position than other approaches.

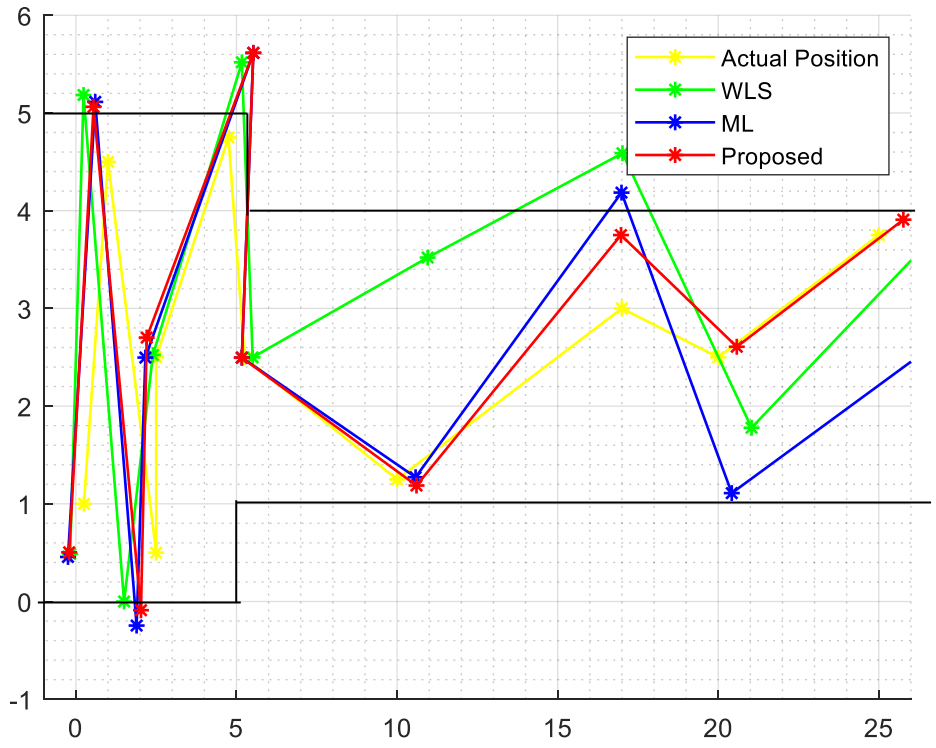

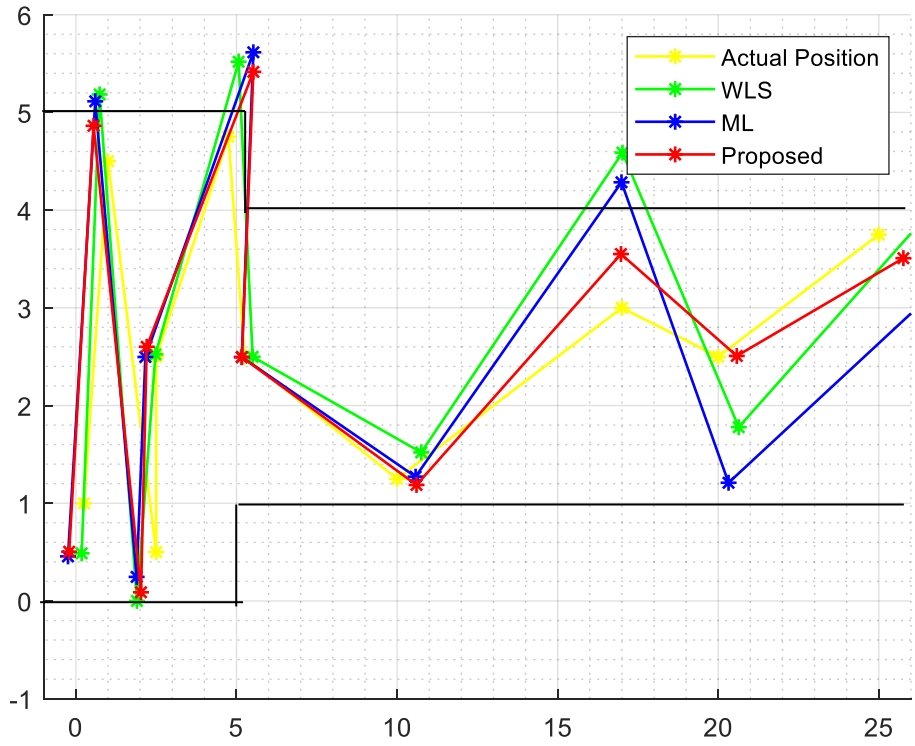

Figure (4-24): Real and estimated paths in m for scenarios 1 and 2, respectively.

Finally, the empirical cumulative distribution function (ECDF) of the MSE for every positioning algorithm is computed as shown in figure (4-25) for scenarios 1 and 2.

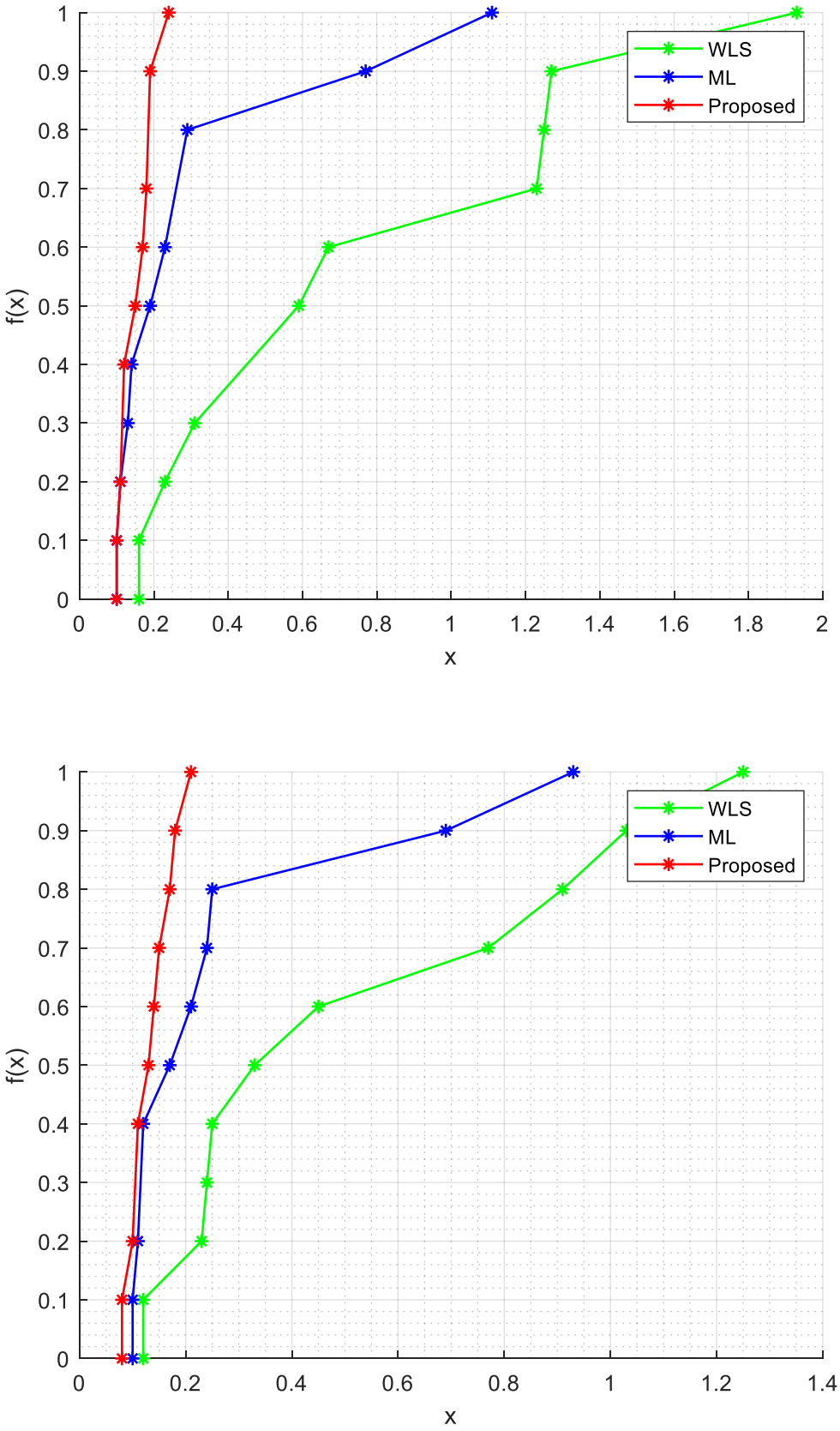

Figure (4-25): Empirical disrupted function of MSE for the proposed, WLS and ML indoor positioning approaches for scenarios 1 and 2, respectively.

4.3 Comparative Analysis of the Results

This chapter presents the first investigation of the performance of smart healthcare monitoring systems using the Li-Fi technology-based ThingSpeak IoT platform. The proposed system has been evaluated, validated, and compared, as shown in the table (4-12). The proposed system outperforms the other comparative systems.

When testing the proposed positioning system, which uses the RSS technique, it is necessary to compare the results to other positioning systems. Table (4-13) shows the characteristics of each previous piece of work. We are confident that the proposed algorithm has far more features than any other system that has been previously described.

Table (4-12): A comparison study related to Li-Fi's previous works.

parameter	[21]	[23]	[4]	[26]	**Proposed System**
Data rate(bps)	-	9600	4800	38400	38400
ESNR (dB)	-	-	6 to 12	-	6 to 22
LED power(W)	-	-	3	-	1
Distance (m)	-	-	1.5	-	5
Environment	-	-	-	-	7×5×3m under low and high ambient noise
Data	Sensors Data	Text	Text, Image, Video	Pulse, oxygen in the blood, airflow, body temperature, and ECG	Body temperature and Heart rate
Wavelength (nm)	-	-	375-780	375-780	375-780
Modulation	-	OOK	OOK	OOK	OOK
Microcontroller	PIC16F877A	Arduino-Uno	TTL		Arduino-Uno
Propagation link	-	LOS-Direct	LOS(Direct Non-direct)	-	LOS(Direct Non-direct) NLOS
Upload Data to Cloud	Microsoft Azure Cloud	-	-	-	ThingSpeak Cloud
Making Notifications	-	-	-	-	IFTTT to send Email

Table (4-13): A comparison study related to IPS's previous works.

parameter	[29]	[28]	[30]	[33]	**Proposed System**
Room size	$6 \times 6 \times 3.5m^3$	$6 \times 6 \times 3.5m^3$	$5 \times 5 \times 3m^3$	$8 \times 6 \times 3m^3$	$5 \times 5 \times 3m^3$ & $20 \times 3 \times 3m^3$
Number of LED	4	4	4	4	6 and 9
LED Power(w)	-	-	10	-	4
Positioning Type	3D	3D	3D	3D	3D
Link	LOS+NLOS	LOS+NLOS	LOS+NLOS	LOS	LOS+NLOS
Noise	Noiseless	Noiseless	Noisy	Noiseless	Noisy
Separation Received Signal	TDM	TDM	-	TDM	OCC
Positioning Method	LS	LS	LS	ML	WLS,ML and modified ML
Evaluation Performance	RMSE	Positioning Error	Positioning Error	RMSE	Modified MSE
Accuracy	0.806m	0.26m for OFDM 1.01m for OOK	0.5m with $\rho = 0.01$	0. 5m	0.15 m^2 and $0.13m^2$ for Scenario1 &2

Chapter Five

Conclusions and the Future Work

Chapter Five

Conclusions and the Future Work

5.1 Conclusions

Firstly, an indoor healthcare monitoring system based on Li-Fi technology is designed and implemented to transmit multiple medical data in a real-time. From the present work, the following conclusions can be drawn as follows:

1. This system allows the doctors to monitor the patient's health apart from the duty hours using IoT, where the patient's health is monitored remotely.
2. The system implementation uses very cheap components and license-free software, so it has the potential to be an incredibly cost-effective solution.
3. The proposed system has the following advantages: high accuracy and low power consumption. The lab result offers a 100 % accuracy of the received data under all test experiments circumstances with a LED of power 1w.
4. The system performance is affected by distance, link type transmitted half angle, and noise. For example, the OSNR is varied from 47.60 dB to 49.92dB for a distance of up to 5m under low ambient noise in the direct-LOS link and from 44.60 to50.54dB for a distance of up to 3m under low ambient noise. On the other hand, OSNR is changed from 44.60 to50.54dB for a distance of up to 2m under low noise, whereas OSNR is changed from 37.26 to42.07dB for a distance of up to 1.5m under high noise for the same link.
5. The noise and link type significantly affect the system, which requires increasing the transmitted power every time the above parameters are changed.

Secondly, a new algorithm for IPS based on VLC technology is designed and simulated using RSS –based trilateration method with the following conclusions:

1. Increasing the number of LEDs in the room from 6 to9 and corridor from 18 to 24 will boost the system accuracy; for example, for G1 the average MSE is $0.83m^2$ with 6 LEDs and $0.57m^2$ with 9 LEDs. In general, the more LED lights that are installed on the ceiling, the higher the accuracy value.
2. Simulation shows that the proposed algorithm has better performance in terms of MSE, which is about 0.15 m^2 for scenarios 1 and 0.13 m^2 for scenario 2, while WLS and conventional ML that have an MSE for scenario1 about 0.81 m^2 ,0.33 m^2 respectively and scenario 2 has 0.55 m^2 , 0.29 m^2 respectively.
3. The positioning accuracy will gradually improve when the target moves directly below the LEDs. This is because the NLOS power in the room center is lower than in the corners. So, the best values of the MSE for the WLS approach are at ($x = 2.5, y = 2.5, z = 0.75$) for scenarios 1 and 2.
4. When the given random initial position of the conventional ML closes from the actual position, the positioning accuracy of the ML will be enhanced and vice versa.

5.2 Future Work

The work in this thesis can be extended in the future to address the following Issues:

1. For the implemented Li-Fi system, employ some modulation format other than the OOK like the M-PPM, M-QAM, and OFDM and compare the performance of the new systems.

2. In IPS using VLC, new hybrid techniques such as RSS with AOA are introduced to increase distance measurement accuracy, thus increasing the accuracy of the overall system.
3. Studying the effect of receiver orientation on IPS performance.
4. Investigating the feasibility of implementing the IPS using VLC practically and employment it for IoT.

References

References

[1] Z. Ghassemlooy, W. Popoola, and S. Rajbhandari, "**Optical wireless communications: system and channel modelling with Matlab®**," CRC press, 2019.

[2] T. Adiono, S. Fuada, and S. Harimurti, "**Bandwidth Budget Analysis for Visible Light Communication Systems utilizing Available Components**," The 10th International Conference on Electrical and Electronics Engineering (ELECO 2017),IEEE, pp. 1375-1380, December, 2017.

[3] M. Kavehrad, M. I. S. Chowdhury, and Z. Zhou, " **Short-Range Optical Wireless: Theory and Applications**," John Wiley & Sons, 2016.

[4] H. J. Hasan, "**Design and Impelemintation of Short Range Optical Fiber-Wireless and Li-Fi for Indoor Communication System**, " PhD thesis, Mustansiriyah University,2020.

[5] D. Ramananda, A. Michael Sequeira, S. R. Raikar, and C. Kumar Shanbhag, "**Design and Implementation of LiFi Communication system**," IOP Conference Series: Materials Science and Engineering, vol. 594, no. 1, pp. 680-681, 2019.

[6] H. Haas, "**Wireless data from every light bulb**", In TEDex global conference, 2011.

[7] J. M. Ortman, V. a. Velkoff, and H. Hogan, "**An aging nation: The older population in the United States**," Population Estimates and Projections, May, pp. 1–28, 2014.

[8] C. Science, "**Protection of personal information used by IoT devices in health care**," MSc. Thesis, Flinders University, Australia, 2018.

[9] M. Yamada and K. Stober, "**Adoption of light-emitting diodes in common lighting applications,**" Energy and Efficieny and Renewable Energy , 2015.

[10] A. O. Korotkevich, Z. S. Galochkina, O. Lavrova, and E. A. Coutsias, "**On the comparison of energy sources: Feasibility of radio frequency and ambient light harvesting,**" Renewable Energy, vol. 81, pp. 804–807, 2015.

[11] J. S. Ramos, I. Demirkol, J. Paradells, D. Vossing, K. M. Gad, and M. Kasemann, "**Towards energy-autonomous wake-up receiver using Visible Light Communication**,"2016 13th IEEE Annual Consumer Communications & Networking Conference (CCNC),IEEE, pp. 544–549, 2016.

[12] P. K. Sharma, Y. S. Jeong, and J. H. Park, "**EH-HL: Effective communication model by integrated EH-WSN and hybrid LiFi/WiFi for IoT,**" IEEE Internet of Things Journal, vol. 5, no. 3, pp. 1719–1726, 2018.

[13] R. Prakash and P. Agarwal, "**The New Era of Transmission and Communication Technology : Li-Fi (Light Fidelity) LED & TED Based Approach**," International Journal of Advanced Research in Computer Engineering &Technology (IJARCET), vol. 3, no. 2, February, 2014.

[14] L. Wu, M. Q. H. Meng, H. Liang, and W. Gao, "**Accurate localization in combination with wireless sensor networks and laser localization,**" 2009 IEEE International Conference on Automation and Logistics, IEEE, pp. 146–151, 2009.

[15] S. Y. Jung, S. Hann, and C. S. Park, "**TDOA-based optical wireless indoor localization using LED ceiling lamps**," IEEE Transactions on Consumer Electronics,IEEE, vol. 57, no. 4, pp. 1592–1597, 2011.

[16] S. Kale and C. S. Khandelwal, "**Design and implementation of real time embedded tele-health monitoring system**," International Journal of computer Science and Network, IEEE, vol.2, issue.1, pp. 771–774, 2013.

[17] D. R. Dhatchayeny, A. Sewaiwar, S. V. Tiwari, and Y. H. Chung, "**Experimental Biomedical EEG Signal Transmission Using VLC**,"IEEE Sensors Journal, vol. 15, no. 10, pp. 5386–5387, 2015.

[18] S. Sudha, D. Indumathy, A. Lavanya, M. Nishanthi, D. M. Sheeba, and V. Anand, "**Patient monitoring in the hospital management using Li-Fi**,"2016 IEEE Technological Innovations in ICT for Agriculture and Rural Development (TIAR), IEEE, pp. 93–96, 2016.

[19] J. Patel, P. Trivedi, and D. Patel, "**A Performance Analysis of "Light Fidelity" and "Internet of Things" & It's Application**," 2017 International Conference on Transforming Engineering Education (ICTEE), IEEE, pp. 1–4, 2017.

[20] L. I. Albraheem, L. H. Alhudaithy, A. A. Aljaser, M. R. Aldhafian, and G. M. Bahliwah, "**Toward designing a li-fi-based hierarchical IoT architecture**," IEEE Access, vol. 6, no. c, pp. 40811–40825, 2018.

[21] J. D. Bokefode, S. A. Ubale and R.M. Gaikwad, "**Retrieving Real Time Data Through IOT Devices and Storing Securely on Cloud using Li-Fi**," 2018 3rd International Conference for Convergence in Technology (I2CT), IEEE**,** India, pp. 1–5, 2018.

[22] A. V. B, N. M, A. A, and G. P. B, "**Smart Health Care Monitoring System using Light Fidelity and Wireless Biomedical Sensor Network**," Proceedings of International Conference on Recent Trends in Computing, Communication & Networking Technologies (ICRTCCNT), IEEE, pp. 1–4, 2019.

[23] E. Ifada, N. T. Surajudeen-Bakinde, N. Faruk, A. Abubakar, O. O.

Mohammed, and A. O. Otuoze, "**Implementation of a Data Transmission System using Li-Fi Technology**," 2019 2nd International Conference of the IEEE Nigeria Computer , IEEE, pp. 1–7, 2019.

[24] J. Pradhan, V. K. Kappala, and S. K. Das, "**Performance Analysis of a Li-Fi System under Ambient Light Conditions,**" IEEE, 2020 National Conference on Communications (NCC), pp. 1–6, 2020.

[25] W. Hashmi, M. A. Arif, S. Shams, S. Wasi, and S. Nasim, "**Li-Fi : A Comparison Among Its Implementation Techniques**," International Journal of Scientific & Technology Research, vol. 10, no. 06, June,2021.

[26] Y. N. Mohammedtawfiq and A. N. Mohammedtawfeeq, "**Real-Time Monitoring System Based on Li-Fi Network Technology in Healthcare**," vol. 2021, pp. 193–200, 2021.

[27] V. M. Sangani, T. M. Patel, and D. A. Pandya, "Li-Fi Enabled Patient Monitoring System based on Embedded Low Power Module," vol. 13, no. 6, pp. 2–6, 2022.

[28] M. Aminikashani, W. Gu, and M. Kavehrad, **"Indoor Location Estimation with Optical-based OFDM Communications,**" 2016 13th IEEE Annual Consumer Communications & Networking Conference (CCNC), pp. 1–10, 2015.

[29] W. Gu, M. Aminikashani, and M. Kavehrad, "**Indoor visible light positioning system with multipath reflection analysis,**" 2016 IEEE International Conference on Consumer Electronics (ICCE). IEEE, pp. 89–92, 2016.

[30] F. I. K. Mousa, N. Almaadeed, K. Busawon, A. Bouridane, R. Binns and I. Elliot, **"Indoor visible light communication localization system utilizing received signal strength indication technique and trilateration method**," Optical Engineering, vol. 57, no. 1, p. 1, 2018.

[31] E. W. Lam and T. D. C. Little, "**Indoor 3D Localization with Low-Cost LiFi Components,**" 2019 Global LIFI Congress Conference,

IEEE, pp. 1–6, 2019.

[32] G. Shi, Y. Li, and W. Cheng, "**Accuracy analysis of indoor visible light communication localization system based on received signal strength in non-line-of-sight environments by using least squares method**," Optical Engineering , vol.58, no.5, 2019.

[33] S. Li, S. Shen, and H. Steendam, "**A positioning algorithm for VLP in the presence of orientation uncertainty**," Signal Processing, vol.160 , Elsevier, pp. 13–20, 2019.

[34] D. H. Mai, H. D. Le, T. V. Pham, and A. T. Pham, "**Design and Performance Evaluation of Large-Scale VLC-Based Indoor Positioning Systems under Impact of Receiver Orientation**," IEEE Access, vol. 8, pp. 61891–61904, 2020.

[35] M. S. P. do. S. Lima Junior, M. P. Halapi, and E. Udvary, "**Design of a real-time indoor positioning system based on visible light communication,**" Radioengineering, vol.29, no.3, pp. 445–451, 2020.

[36] B. Pamukti, M. M. Rahmawati, and N. M. Adriansyah, "**Impact of The Number of Light Emitting Diode Towards The Accuracy in Indoor Positioning System Based on Visible Light Communication**," vol. 20, no. 2, pp. 70–75, 2020.

[37] A. Chaabna, A. Babouri, and X. Zhang, "**Study of Ambient Light Impact on RSS-Based Indoor Positioning System Using Visible Light Communication**," pp. 1–11, 2021.

[38] X. Meng, C. Jia, C. Cai, F. He, and Q. Wang, "**Indoor High-Precision 3D Positioning System Based on Visible-Light Communication Using Improved Whale Optimization Algorithm**," 2022.

[39] K. Cui, G. Chen, Q. He, and Z. Xu, "**Indoor optical wireless communication by ultraviolet and visible light,**" Free-Space Laser Communications IX. Vol. 7464. International Society for Optics and

Photonics, 2009.

[40] Y. Tanakat, "**Wireless Optical Trasnsmissions with white colored LED for Wireless Home Links**," 11th IEEE International Symposium on Personal Indoor and Mobile Radio Communications, IEEE, 2000.

[41] F. Ibrahim, "**Secure Visible Light Communication Systems Based on the Position of the User**, " PhD thesis, Northumbria University of at Newcastle,September, 2017.

[42] F. Esteban, "**Robust localization system using Visible Light Communication technology for underground mines**, " PhD thesis, De Lorraine University, March, 2020.

[43] S. M. Sze, Y. Li, and K. K. Ng, "**Physics of semiconductor devices**, " John wiley & sons, 2021.

[44] M. Pattison, N. Bardsley, C. Elliot, M. Hansen, K. Lee. L. Pattison, J. Tsao and M. Yamada, "**2018 Solid-State Lighting R&D Opportunities**, " DOE BTO SSL Program, 2019.

[45] F. Mousa, T. Son, A., H. Le Minh, Z.Ghassemlooy, T.Q. Duong, A. C. Boucouvalas, J. Perez, X. Dai, "**Investigation of data encryption impact on broadcasting visible light communications**, " 2014 9th International Symposium on Communication Systems, Networks & Digital Sign (CSNDSP). IEEE, 2014.

[46] S. H. Lee, S.-Y. Jung, and J. K. Kwon, "**Modulation and coding for dimmable visible light communication**," IEEE Communication Magazine, vol. 53, no. 2, pp. 136–143, 2015.

[47] A. T. Hussein, "**Visible Light Communication System**," PhD thesis, University of Leeds, December, 2016.

[48] L. Wang, C. Wang, X. Chi, L. Zhao, and X. Dong, "**Optimizing SNR for indoor visible light communication via selecting communicating LEDs,**" Optics communications, vol. 387, pp. 174–181,

2017.

[49] L. A. H. Azizan, M. S. Ab-Rahman, and K. Jumiran, "**Analytical approach on SNR performance of visible light communication for modern lighting layout**," 2012 International Conference on Innovation Management and Technology Research. IEEE, pp. 332–336, 2012.

[50] P. Kuppusamy, S. Muthuraj, and S. Gopinath, "**Survey and challenges of Li-Fi with comparison of Wi-Fi,**" 2016 International Conference on Wireless Communications, Signal Processing and Networking (WiSPNET). IEEE, pp. 896–899, 2016.

[51] A. Shetty, "**A comparative study and analysis on Li-Fi and Wi-Fi**," International Journal of Computer Applications, vol. 150, no. 6, pp. 43–48, 2016.

[52] S. Dimitrov and H. Haas, "**Principles of LED light communications: towards networked Li-Fi**," Cambridge University Press, 2015.

[53] Y. Perwej, "**The next generation of wireless communication using Li-Fi (Light Fidelity) technology**," Journal of Computer Networks, vol. 4, no. 1, pp. 20–29, 2017.

[54] P. Bahl and V. N. Padmanabhan, "**RADAR: An in-building RF-based user location and tracking system**," Conference on computer communications. Nineteenth annual joint conference of the IEEE computer and communications societies,IEEE, pp. 775–784, 2000.

[55] M. Bilgi, M. Yuksel, and N. Pala, "**3-d optical wireless localization**," in 2010 IEEE Globecom Workshops, 2010, pp. 1062–1066.

[56] G. Roussos, "**Location sensing technologies and applications**," Sch. Comput. Sci. Inf. Syst. Birkbeck Coll. Univ. London, 2002.

[57] J. Armstrong, Y. A. Sekercioglu, and A. Neild, "**Visible light positioning: a roadmap for international standardization**," IEEE

Commun. Mag., vol. 51, no. 12, pp. 68–73, 2013.

[58] M. F. Keskin, A. D. Sezer, and S. Gezici, "**Localization via Visible Light Systems,**" Proceedings of the IEEE, vol.106, no.6, pp. 1–24, 2018.

[59] Y. B. Bai, "**Development of a Wi-Fi and RFID Based Indoor Location and Mobility Tracking System,**" PhD Thesis. RMIT University, February, 2016.

[60] J. Xiong and K. Jamieson, "**Arraytrack: A fine-grained indoor location system**," 0th USENIX Symposium on Networked Systems Design and Implementation (NSDI 13), pp. 71–84, 2013.

[61] T. Van Haute et al., "**D2. 2: Report on Experiments without Interference**." The EVARILOS Project, EVA-D22-iMinds-V2. 0, 2013.

[62] A. H. Azhar, T.-A. Tran, and D. O'Brien, "**A gigabit/s indoor wireless transmission using MIMO-OFDM visible-light communications**," IEEE photonics Technology Letters, vol. 25, no. 2, pp. 171–174, 2012.

[63] M. F. Keskin, O. Erdem, and S. Gezici, "**Cooperative localization in visible light networks: Theoretical limits and distributed algorithms**," arXiv Prepr. arXiv1804.00576, 2018.

[64] C., F. RK, J. A. Salehi, and V. K. Wei, "**Optical orthogonal codes: design, analysis and applications**," IEEE Transactions on Information theory, vol. 35, no.3, 1989.

[65] A. Küpper , "**Location-based services: fundamentals and operation,**" John Wiley & Sons, 2005.

[66] A. Kushki, K. N. Plataniotis, and A. N. Venetsanopoulos, "**WLAN positioning systems: principles and applications in location-based services,**" Cambridge University Press, 2012.

[67] P. Tarrío, A. M. Bernardos, and J. R. Casar, "**Weighted least squares techniques for improved received signal strength based**

localization," Sensors, vol. 11, no. 9, pp. 8569–8592, 2011.

[68] K. Tong, "**Location Estimation in Wireless Communication Systems,** " MSc. Thesis, University of Western Ontario, 2015.

[69] A. Albaidhani, A. Morell, and J. L. Vicario, "**Anchor selection for UWB indoor positioning**," Transactions on emerging telecommunications technologies, vol. 30, no. 6, pp. 1–17, 2019.

[70] A. Al baidhani, "**Modulated Mathematical Formulation of MSE for Assessment of a Positioning System in Live-status**," in Journal of Physics: Conference Series, vol. 1828, no. 1, 2021,.

[71] E. Borgia, "**The Internet of Things vision: Key features, applications and open issues**," Comput. Commun., vol. 54, pp. 1–31, 2014.

[72] K. Rose, S. Eldridge, and L. Chapin, "**The internet of things: An overview,**" The internet society (ISOC), vol. 80, pp. 1–50, 2015.

[73] A. Furness, "**A framework model for the internet of things**," GRIFS/CASAGRAS Hong Kong, China, 2008.

[74] N. Networks, "**ITU-T Y.2060**," 2012.

[75] D. Gil, A. Ferrández, H. Mora-Mora, and J. Peral, "**Internet of things: A review of surveys based on context aware intelligent services**," Sensors, vol. 16, no. 7, p. 1069, 2016.

[76] R. Khan, S. U. Khan, R. Zaheer, and S. Khan, "**Future internet: the internet of things architecture, possible applications and key challenges**," 2012 10th international conference on frontiers of information technology. IEEE, pp. 257–260, 2012.

[77] P. Sethi and S. R. Sarangi, "**Internet of things: architectures, protocols, and applications,**" Journal of Electrical and Computer Engineering, vol. 2017, 2017.

[78] R. Mahmoud, T. Yousuf, F. Aloul, and I. Zualkernan, "**Internet of things (IoT) security: Current status, challenges and prospective**

measures," 2015 10th international conference for internet technology and secured transactions (ICITST). IEEE, pp. 336–341, 2015.

[79] M. A. G. Maureira and L. Teernstra, "**ThingSpeak – an API and Web Service for the Internet of Things**," World Wide Web, 2011.

Appendices

Appendix A

Hardware Spesifications

A.1 Arduino-Uno

Overview

The Arduino Uno is a microcontroller board based on the ATmega328 (datasheet). It has 14 digital input/output pins (of which 6 can be used as PWM outputs), 6 analog inputs, a 16 MHz ceramic resonator, a USB connection, a power jack, an ICSP header, and a reset button. It contains everything needed to support the microcontroller; simply connect it to a computer with a USB cable or power it with a AC-to-DC adapter or battery to get started.
The Uno differs from all preceding boards in that it does not use the FTDI USB-to-serial driver chip. Instead, it features the Atmega16U2 (Atmega8U2 up to version R2) programmed as a USB-to-serial converter.
Revision 2 of the Uno board has a resistor pulling the 8U2 HWB line to ground, making it easier to put into DFU mode.
Revision 3 of the board has the following new features:

- 1.0 pinout: added SDA and SCL pins that are near to the AREF pin and two other new pins placed near to the RESET pin, the IOREF that allow the shields to adapt to the voltage provided from the board. In future, shields will be compatible both with the board that use the AVR, which operate with 5V and with the Arduino Due that operate with 3.3V. The second one is a not connected pin, that is reserved for future purposes.
- Stronger RESET circuit.
- Atmega 16U2 replace the 8U2.

"Uno" means one in Italian and is named to mark the upcoming release of Arduino 1.0. The Uno and version 1.0 will be the reference versions of Arduino, moving forward. The Uno is the latest in a series of USB Arduino boards, and the reference model for the Arduino platform; for a comparison with previous versions, see the index of Arduino boards.

Summary

Microcontroller	ATmega328
Operating Voltage	5V
Input Voltage (recommended)	7-12V

Input Voltage (limits)	6-20V
Digital I/O Pins	14 (of which 6 provide PWM output)
Analog Input Pins	6
DC Current per I/O Pin	40 mA
DC Current for 3.3V Pin	50 mA
Flash Memory	32 KB (ATmega328) of which 0.5 KB used by bootloader
SRAM	2 KB (ATmega328)
EEPROM	1 KB (ATmega328)
Clock Speed	16 MHz

Schematic & Reference Design

EAGLE files: arduino-uno-Rev3-reference-design.zip (NOTE: works with Eagle 6.0 and newer)
Schematic: arduino-uno-Rev3-schematic.pdf
Note: The Arduino reference design can use an Atmega8, 168, or 328, Current models use an ATmega328, but an Atmega8 is shown in the schematic for reference. The pin configuration is identical on all three processors.

Power

The Arduino Uno can be powered via the USB connection or with an external power supply. The power source is selected automatically.
External (non-USB) power can come either from an AC-to-DC adapter (wall-wart) or battery. The adapter can be connected by plugging a 2.1mm center-positive plug into the board's power jack. Leads from a battery can be inserted in the Gnd and Vin pin headers of the POWER connector.
The board can operate on an external supply of 6 to 20 volts. If supplied with less than 7V, however, the 5V pin may supply less than five volts and the board may be unstable. If using more than 12V, the voltage regulator may overheat and damage the board. The recommended range is 7 to 12 volts.
The power pins are as follows:

- **VIN.** The input voltage to the Arduino board when it's using an external power source (as opposed to 5 volts from the USB connection or other regulated power source). You can supply voltage through this pin, or, if supplying voltage via the power jack, access it through this pin.
- **5V.**This pin outputs a regulated 5V from the regulator on the board. The board can be supplied with power either from the DC power jack (7 - 12V), the USB connector (5V), or the VIN pin of the board (7-12V). Supplying voltage via the 5V or 3.3V pins bypasses the regulator, and can damage your board. We don't advise it.
- **3V3.** A 3.3 volt supply generated by the on-board regulator. Maximum current draw is 50 mA.
- **GND.** Ground pins.

Memory

The ATmega328 has 32 KB (with 0.5 KB used for the bootloader). It also has 2 KB of SRAM and 1 KB of EEPROM (which can be read and written with the EEPROM library).

Input and Output

Each of the 14 digital pins on the Uno can be used as an input or output, using pinMode(), digitalWrite(), and digitalRead() functions. They operate at 5 volts. Each pin can provide or receive a maximum of 40 mA and has an internal pull-up resistor (disconnected by default) of 20-50 kOhms. In addition, some pins have specialized functions:

- **Serial: 0 (RX) and 1 (TX).** Used to receive (RX) and transmit (TX) TTL serial data. These pins are connected to the corresponding pins of the ATmega8U2 USB-to-TTL Serial chip.
- **External Interrupts: 2 and 3.** These pins can be configured to trigger an interrupt on a low value, a rising or falling edge, or a change in value. See the attachInterrupt() function for details.
- **PWM: 3, 5, 6, 9, 10, and 11.** Provide 8-bit PWM output with the analogWrite() function.

- **SPI: 10 (SS), 11 (MOSI), 12 (MISO), 13 (SCK).** These pins support SPI communication using the SPI library.
- **LED: 13.** There is a built-in LED connected to digital pin 13. When the pin is HIGH value, the LED is on, when the pin is LOW, it's off.

The Uno has 6 analog inputs, labeled A0 through A5, each of which provide 10 bits of resolution (i.e. 1024 different values). By default they measure from ground to 5 volts, though is it possible to change the upper end of their range using the AREF pin and the analogReference() function. Additionally, some pins have specialized functionality:

- **TWI: A4 or SDA pin and A5 or SCL pin.** Support TWI communication using the Wire library.

There are a couple of other pins on the board:

- **AREF.** Reference voltage for the analog inputs. Used with analogReference().
- **Reset.** Bring this line LOW to reset the microcontroller. Typically used to add a reset button to shields which block the one on the board.

See also the mapping between Arduino pins and ATmega328 ports. The mapping for the Atmega8, 168, and 328 is identical.

Communication

The Arduino Uno has a number of facilities for communicating with a computer, another Arduino, or other microcontrollers. The ATmega328 provides UART TTL (5V) serial communication, which is available on digital pins 0 (RX) and 1 (TX). An ATmega16U2 on the board channels this serial communication over USB and appears as a virtual com port to software on the computer. The '16U2 firmware uses the standard USB COM drivers, and no external driver is needed. However, on Windows, a .inf file is required. The Arduino software includes a serial monitor which allows simple textual data to be sent to and from the Arduino board. The RX and TX LEDs on the board will flash when data is being transmitted via the USB-to-serial chip and USB connection to the computer (but not for serial communication on pins 0 and 1).
A SoftwareSerial library allows for serial communication on any of the Uno's digital pins.
The ATmega328 also supports I2C (TWI) and SPI communication. The Arduino software includes a Wire library to simplify use of the I2C bus; see the documentation for details. For SPI communication, use the SPI library.

A.2 PIN Photodiode

Silizium-PIN-Fotodiode mit sehr kurzer Schaltzeit
Silicon PIN Photodiode with Very Short Switching Time

SFH 203
SFH 203 FA

SFH 203

SFH 203 FA

Wesentliche Merkmale

- Speziell geeignet für Anwendungen im Bereich von 400 nm bis 1100 nm (SFH 203) und bei 880 nm (SFH 203 FA)
- Kurze Schaltzeit (typ. 5 ns)
- 5 mm-Plastikbauform im LED-Gehäuse
- Auch gegurtet lieferbar

Features

- Especially suitable for applications from 400 nm to 1100 nm (SFH 203) and of 880 nm (SFH 203 FA)
- Short switching time (typ. 5 ns)
- 5 mm LED plastic package
- Also available on tape and reel

Anwendungen

- Industrieelektronik
- „Messen/Steuern/Regeln"
- Schnelle Lichtschranken für Gleich- und Wechsellichtbetrieb
- LWL

Applications

- Industrial electronics
- For control and drive circuits
- Photointerrupters
- Fiber optic transmission systems

Typ Type	Bestellnummer Ordering Code
SFH 203	Q62702-P955
SFH 203 FA	Q62702-P956

SFH 203, SFH 203 FA

Grenzwerte
Maximum Ratings

Bezeichnung Parameter	Symbol Symbol	Wert Value	Einheit Unit
Betriebs- und Lagertemperatur Operating and storage temperature range	T_{op}; T_{stg}	– 40 ... + 100	°C
Löttemperatur (Lötstelle 2 mm vom Gehäuse entfernt bei Lötzeit $t \leq 3$ s) Soldering temperature in 2 mm distance from case bottom ($t \leq 3$ s)	T_S	230	°C
Sperrspannung Reverse voltage	V_R	50	V
Verlustleistung Total power dissipation	P_{tot}	100	mW

Kennwerte (T_A = 25 °C)
Characteristics

Bezeichnung Parameter	Symbol Symbol	Wert Value		Einheit Unit
		SFH 203	SFH 203 FA	
Fotostrom Photocurrent				
V_R = 5 V, Normlicht/standard light A, T = 2856 K, E_V = 1000 lx	I_P	80 (≥ 50)	–	µA
V_R = 5 V, λ = 950 nm, E_e = 1 mW/cm²	I_P	–	50 (≥ 30)	µA
Wellenlänge der max. Fotoempfindlichkeit Wavelength of max. sensitivity	$\lambda_{S\,max}$	850	900	nm
Spektraler Bereich der Fotoempfindlichkeit S = 10% von S_{max} Spectral range of sensitivity S = 10% of S_{max}	λ	400 ... 1100	800 ... 1100	nm
Bestrahlungsempfindliche Fläche Radiant sensitive area	A	1	1	mm²
Abmessung der bestrahlungsempfindlichen Fläche Dimensions of radiant sensitive area	$L \times B$ $L \times W$	1 × 1	1 × 1	mm × mm
Abstand Chipoberfläche zu Gehäuseoberfläche Distance chip front to case surface	H	4.0 ... 4.6	4.0 ... 4.6	mm
Halbwinkel Half angle	φ	± 20	± 20	Grad deg.

Kennwerte (T_A = 25 °C)
Characteristics (cont'd)

Bezeichnung Parameter	Symbol Symbol	Wert Value		Einheit Unit
		SFH 203	SFH 203 FA	
Dunkelstrom, V_R = 20 V Dark current	I_R	1 (≤ 5)	1 (≤ 5)	nA
Spektrale Fotoempfindlichkeit, λ = 850 nm Spectral sensitivity	S_λ	0.62	0.59	A/W
Quantenausbeute, λ = 850 nm Quantum yield	η	0.89	0.86	Electrons / Photon
Leerlaufspannung Open-circuit voltage E_v = 1000 lx, Normlicht/standard light A, T = 2856 K E_e = 0.5 mW/cm², λ = 950 nm	V_O V_O	420 (≥ 350) –	– 370 (≥ 300)	mV mV
Kurzschlußstrom Short-circuit current E_v = 1000 lx, Normlicht/standard light A, T = 2856 K E_e = 0.5 mW/cm², λ = 950 nm	I_{SC} I_{SC}	80 –	– 25	µA µA
Anstiegs- und Abfallzeit des Fotostromes Rise and fall time of the photocurrent R_L = 50 Ω; V_R = 20 V; λ = 850 nm; I_p = 800 µA	t_r, t_f	5	5	ns
Durchlaßspannung, I_F = 80 mA, E = 0 Forward voltage	V_F	1.3	1.3	V
Kapazität, V_R = 0 V, f = 1 MHz, E = 0 Capacitance	C_O	11	11	pF
Temperaturkoeffizient von V_O Temperature coefficient of V_O	TC_V	– 2.6	– 2.6	mV/K
Temperaturkoeffizient von I_{SC} Temperature coefficient of I_{SC} Normlicht/standard light A λ = 950 nm	TC_I	0.18 –	– 0.2	%/K
Rauschäquivalente Strahlungsleistung Noise equivalent power V_R = 20 V, λ = 850 nm	NEP	2.9×10^{-14}	2.9×10^{-14}	$\frac{W}{\sqrt{Hz}}$
Nachweisgrenze, V_R = 20 V, λ = 850 nm Detection limit	D*	3.5×10^{12}	3.5×10^{12}	$\frac{cm \times \sqrt{Hz}}{W}$

A.3 BC547 Transistor

BC546B, BC547A, B, C, BC548B, C

Amplifier Transistors

NPN Silicon

Features

- Pb−Free Packages are Available*

MAXIMUM RATINGS

Rating	Symbol	Value	Unit
Collector - Emitter Voltage BC546 BC547 BC548	V_{CEO}	 65 45 30	Vdc
Collector - Base Voltage BC546 BC547 BC548	V_{CBO}	 80 50 30	Vdc
Emitter - Base Voltage	V_{EBO}	6.0	Vdc
Collector Current − Continuous	I_C	100	mAdc
Total Device Dissipation @ T_A = 25°C Derate above 25°C	P_D	625 5.0	mW mW/°C
Total Device Dissipation @ T_C = 25°C Derate above 25°C	P_D	1.5 12	W mW/°C
Operating and Storage Junction Temperature Range	T_J, T_{stg}	−55 to +150	°C

THERMAL CHARACTERISTICS

Characteristic	Symbol	Max	Unit
Thermal Resistance, Junction−to−Ambient	$R_{\theta JA}$	200	°C/W
Thermal Resistance, Junction−to−Case	$R_{\theta JC}$	83.3	°C/W

Stresses exceeding Maximum Ratings may damage the device. Maximum Ratings are stress ratings only. Functional operation above the Recommended Operating Conditions is not implied. Extended exposure to stresses above the Recommended Operating Conditions may affect device reliability.

*For additional information on our Pb−Free strategy and soldering details, please download the ON Semiconductor Soldering and Mounting Techniques Reference Manual, SOLDERRM/D.

ON Semiconductor®

http://onsemi.com

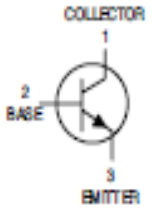

TO−92
CASE 29
STYLE 17

MARKING DIAGRAM

x = 6, 7, or 8
A = Assembly Location
Y = Year
WW = Work Week
• = Pb−Free Package
(Note: Microdot may be in either location)

ORDERING INFORMATION

See detailed ordering and shipping information in the package dimensions section on page 5 of this data sheet.

BC546B, BC547A, B, C, BC548B, C

ELECTRICAL CHARACTERISTICS (T_A = 25°C unless otherwise noted)

Characteristic		Symbol	Min	Typ	Max	Unit
OFF CHARACTERISTICS						
Collector – Emitter Breakdown Voltage (I_C = 1.0 mA, I_B = 0)	BC546	$V_{(BR)CEO}$	65	–	–	V
	BC547		45	–	–	
	BC548		30	–	–	
Collector – Base Breakdown Voltage (I_C = 100 μAdc)	BC546	$V_{(BR)CBO}$	80	–	–	V
	BC547		50	–	–	
	BC548		30	–	–	
Emitter – Base Breakdown Voltage (I_E = 10 μA, I_C = 0)	BC546	$V_{(BR)EBO}$	6.0	–	–	V
	BC547		6.0	–	–	
	BC548		6.0	–	–	
Collector Cutoff Current		I_{CES}				
(V_{CE} = 70 V, V_{BE} = 0)	BC546		–	0.2	15	nA
(V_{CE} = 50 V, V_{BE} = 0)	BC547		–	0.2	15	
(V_{CE} = 35 V, V_{BE} = 0)	BC548		–	0.2	15	
(V_{CE} = 30 V, T_A = 125°C)	BC546/547/548		–	–	4.0	μA
ON CHARACTERISTICS						
DC Current Gain		h_{FE}				–
(I_C = 10 μA, V_{CE} = 5.0 V)	BC547A		–	90	–	
	BC546B/547B/548B		–	150	–	
	BC548C		–	270	–	
(I_C = 2.0 mA, V_{CE} = 5.0 V)	BC546		110	–	450	
	BC547		110	–	800	
	BC548		110	–	800	
	BC547A		110	180	220	
	BC546B/547B/548B		200	290	450	
	BC547C/BC548C		420	520	800	
(I_C = 100 mA, V_{CE} = 5.0 V)	BC547A/548A		–	120	–	
	BC546B/547B/548B		–	180	–	
	BC548C		–	300	–	
Collector – Emitter Saturation Voltage		$V_{CE(sat)}$				V
(I_C = 10 mA, I_B = 0.5 mA)			–	0.09	0.25	
(I_C = 100 mA, I_B = 5.0 mA)			–	0.2	0.6	
(I_C = 10 mA, I_B = See Note 1)			–	0.3	0.6	
Base – Emitter Saturation Voltage (I_C = 10 mA, I_B = 0.5 mA)		$V_{BE(sat)}$	–	0.7	–	V
Base – Emitter On Voltage		$V_{BE(on)}$				V
(I_C = 2.0 mA, V_{CE} = 5.0 V)			0.55	–	0.7	
(I_C = 10 mA, V_{CE} = 5.0 V)			–	–	0.77	
SMALL–SIGNAL CHARACTERISTICS						
Current – Gain – Bandwidth Product		f_T				MHz
(I_C = 10 mA, V_{CE} = 5.0 V, f = 100 MHz)	BC546		150	300	–	
	BC547		150	300	–	
	BC548		150	300	–	
Output Capacitance (V_{CB} = 10 V, I_C = 0, f = 1.0 MHz)		C_{obo}	–	1.7	4.5	pF
Input Capacitance (V_{EB} = 0.5 V, I_C = 0, f = 1.0 MHz)		C_{ibo}	–	10	–	pF
Small – Signal Current Gain		h_{fe}				–
(I_C = 2.0 mA, V_{CE} = 5.0 V, f = 1.0 kHz)	BC546		125	–	500	
	BC547/548		125	–	900	
	BC547A		125	220	260	
	BC546B/547B/548B		240	330	500	
	BC547C/548C		450	600	900	
Noise Figure (I_C = 0.2 mA, V_{CE} = 5.0 V, R_S = 2 kΩ, f = 1.0 kHz, Δf = 200 Hz)		NF				dB
	BC546		–	2.0	10	
	BC547		–	2.0	10	
	BC548		–	2.0	10	

1. I_B is value for which I_C = 11 mA at V_{CE} = 1.0 V.

A. 4 LM358 Operational Amplifier

LM358

LINEAR INTEGRATED CIRCUIT

DUAL OPERATIONAL AMPLIFIER

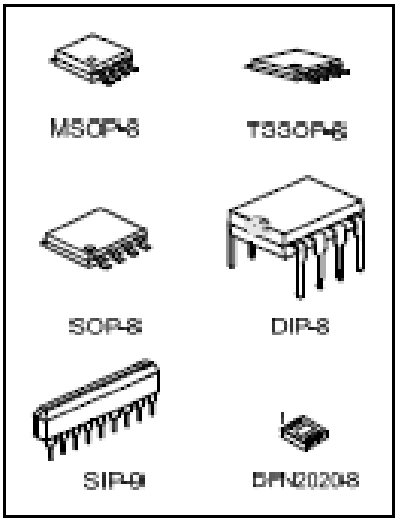

■ DESCRIPTION

The UTC LM358 consists of two independent high gain, internally frequency compensated operational amplifier. It can be operated from a single power supply and also split power supplies.

■ FEATURES

*Internally frequency compensated for unity gain.
*Wide power supply range 3V ~ 32V.
*Input common-mode voltage range include ground.
*Large DC voltage gain.

■ ORDERING INFORMATION

Ordering Number		Package	Packing
Lead Free	Halogen-Free		
LM358L-D08-T	LM358G-D08-T	DIP-8	Tube
LM358L-L09-T	LM358G-G09-T	SIP-9	Tube
LM358L-P08-R	LM358G-P08-R	TSSOP-8	Tape Reel
LM358L-S08-R	LM358G-S08-R	SOP-8	Tape Reel
LM358L-SM1-R	LM358G-SM1-R	MSOP-8	Tape Reel
LM358L-K08-2020-R	LM358G-K08-2020-R	DFN2020-8	Tape Reel

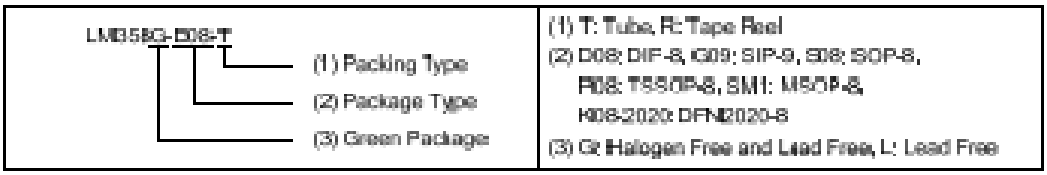

■ MARKING

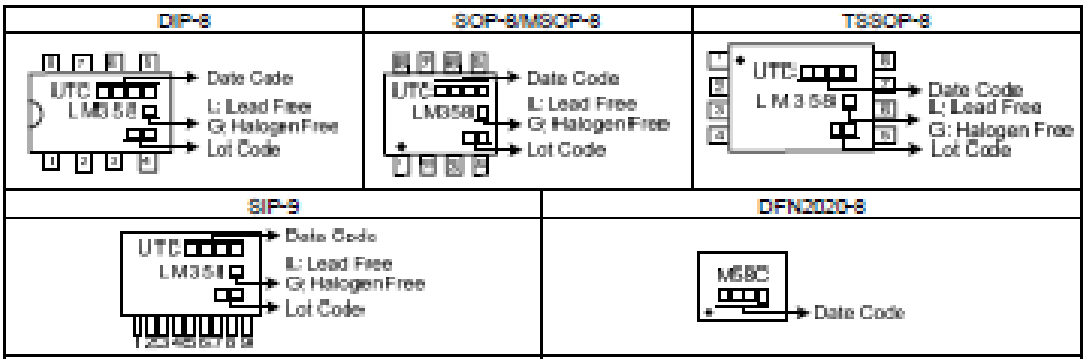

LM358 LINEAR INTEGRATED CIRCUIT

■ ABSOLUTE MAXIMUM RATINGS

PARAMETER		SYMBOL	RATINGS	UNIT
Supply Voltage		V_{CC}	±16 or 32	V
Differential Input Voltage		$V_{I(DIFF)}$	±32	V
Input Voltage		V_I	-0.3 ~ +32	V
Output Short to Ground			Continuous	
Power Dissipation	SIP-9	P_D	750	mW
	DIP-8		625	
	SOP-8		440	
	TSSOP-8		360	
	MSOP-8		300	
	DFN2020-8		830	
Junction Temperature		T_J	+150	°C
Operating Temperature (Note 2)		T_{OPR}	-40 ~ +125	°C
Storage Temperature		T_{STG}	-65 ~ +150	°C

Notes: 1. Absolute maximum ratings are those values beyond which the device could be permanently damaged. Absolute maximum ratings are stress ratings only and functional device operation is not implied.
2. It is guarantee by design, not 100% be tested.

■ ELECTRICAL CHARACTERISTICS (V_{CC}=5.0V, V_{EE}=GND, T_A=25°C, unless otherwise specified)

PARAMETER	SYMBOL	TEST CONDITIONS	MIN	TYP	MAX	UNIT
Input Offset Voltage	$V_{I(OFF)}$	V_{CM}=0V toV_{CC}-1.5V $V_{O(P)}$=1.4V, Rs=0Ω		2.0	5.0	mV
Input Common Mode Voltage	$V_{I(CM)}$	V_{CC}=30V	0		V_{CC}-1.5	V
Differential Input Voltage	$V_{I(DIF)}$				V_{CC}	V
Output Voltage Swing	V_{OH}	V_{CC}=30V, R_L=2KΩ	26			V
		V_{CC}=30V, R_L=10KΩ	27	28		V
	V_{OL}	V_{CC}=5V, R_L≥10KΩ		5	20	mV
Large Signal Voltage Gain	G_V	V_{CC}=15V, R_L≥2KΩ $V_{O(P)}$=1V ~ 11V	25	100		V/mV
Power Supply Current	I_{CC}	R_L=∞, V_{CC}=30V		0.8	2.0	mA
		R_L=∞, Full Temperature Range		0.5	1.2	mA
Input Offset Current	$I_{I(OFF)}$			5	50	nA
Input Bias Current	$I_{I(BIAS)}$			45	250	nA
Short Circuit Current to Ground	I_{SC}			40	70	mA
Output Current	I_{SOURCE}	V(+)=1V, V(-)=0V V_{CC}=15V, $V_{O(P)}$=2V	10	30		mA
	I_{SINK}	V(+)=0V, V(-)=1V V_{CC}=15V, $V_{O(P)}$=2V	10	15		mA
		V(+)=0V, V(-)=1V V_{CC}=15V, $V_{O(P)}$=200mV	12	100		μA
Common Mode Rejection Ratio	CMRR		65	80		dB
Power Supply Rejection Ratio	PSRR		65	100		dB
Channel Separation	CS	f=1KHZ ~ 20KHZ		120		dB

Appendix B

Creating IFTTT Notifications

Step1: First, create an IFTTT account. Then log in IFTTT.

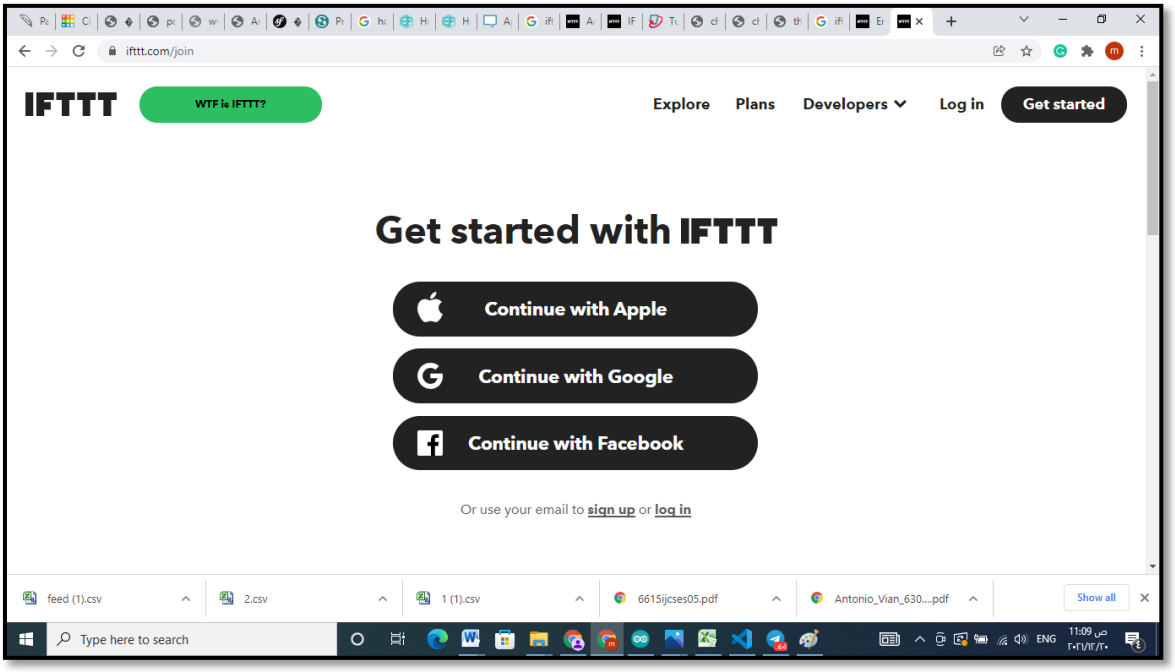

Figure(B-1): IFTTT.

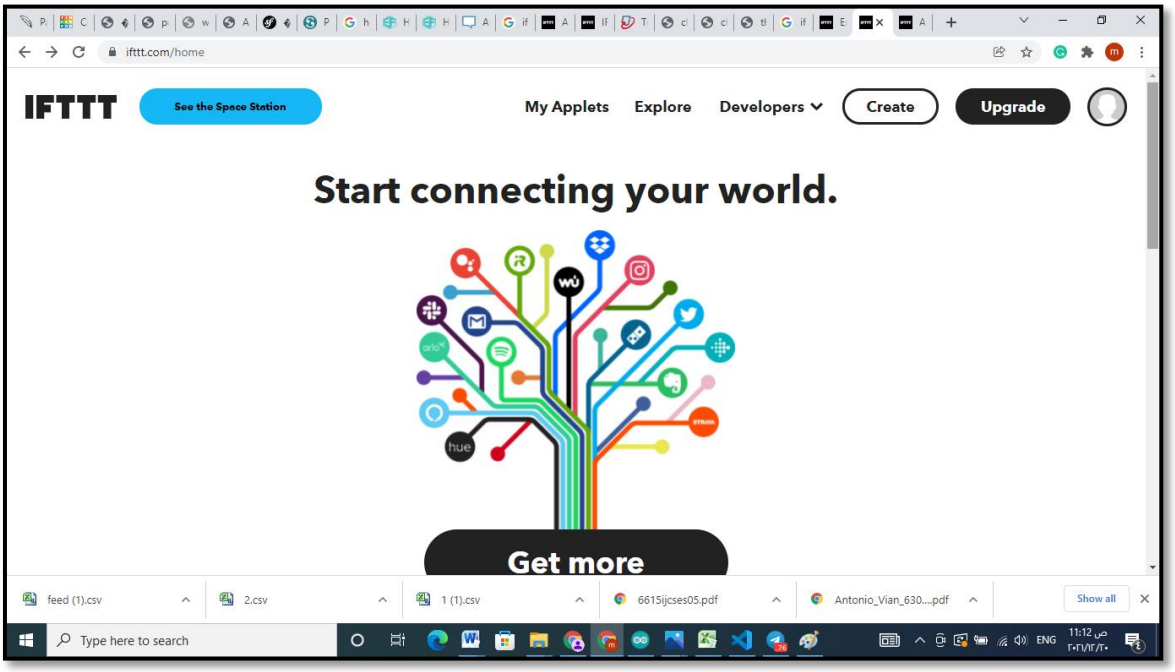

Figure(B-2): Log in IFTTT.

Step2: Create an applet

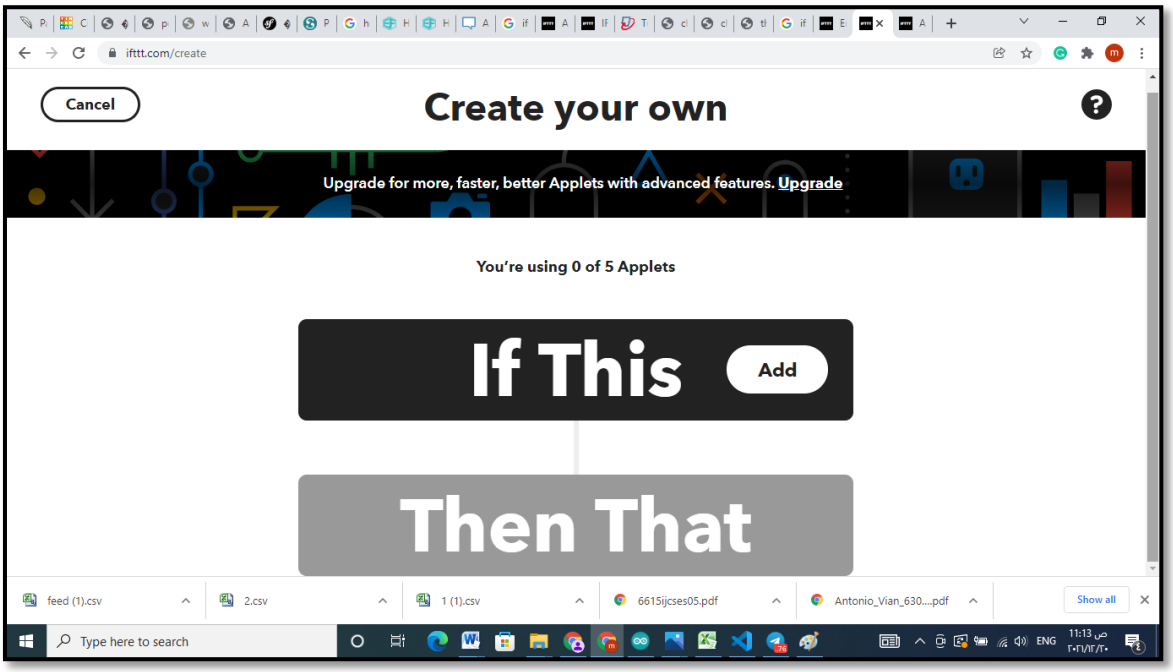

Figure(B -3):Creating Applet.

Step3: Create a Trigger

- Press "If This" to Choose a trigger. Then, Enter Webhooks in the search field.

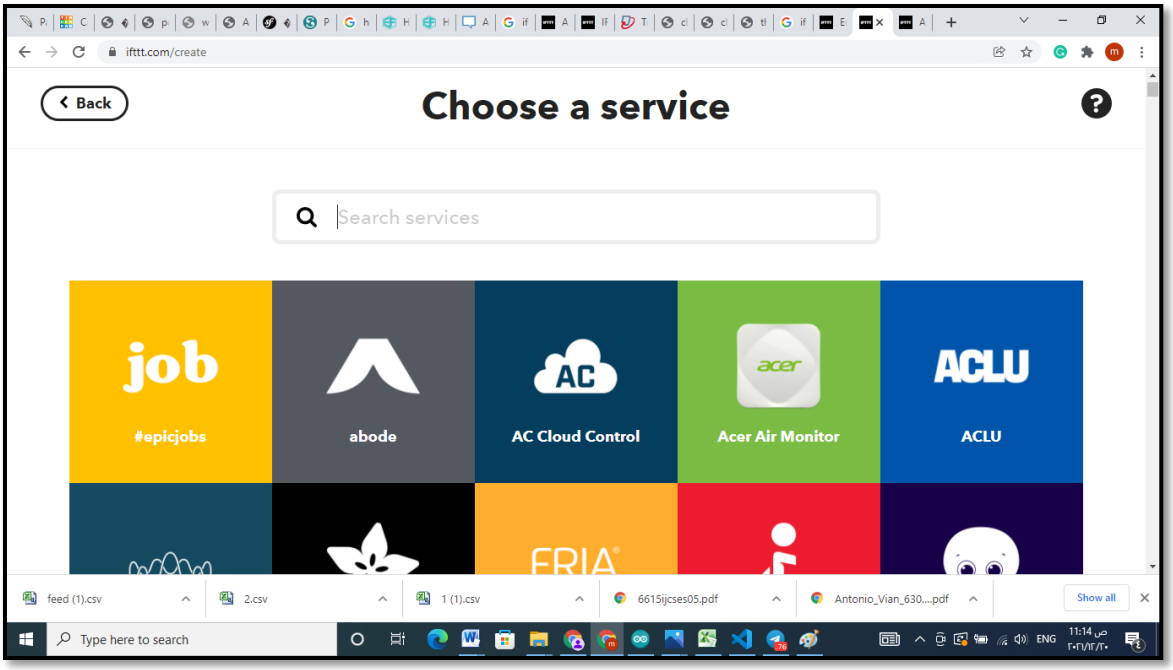

Figure(B-4):Applet Services .

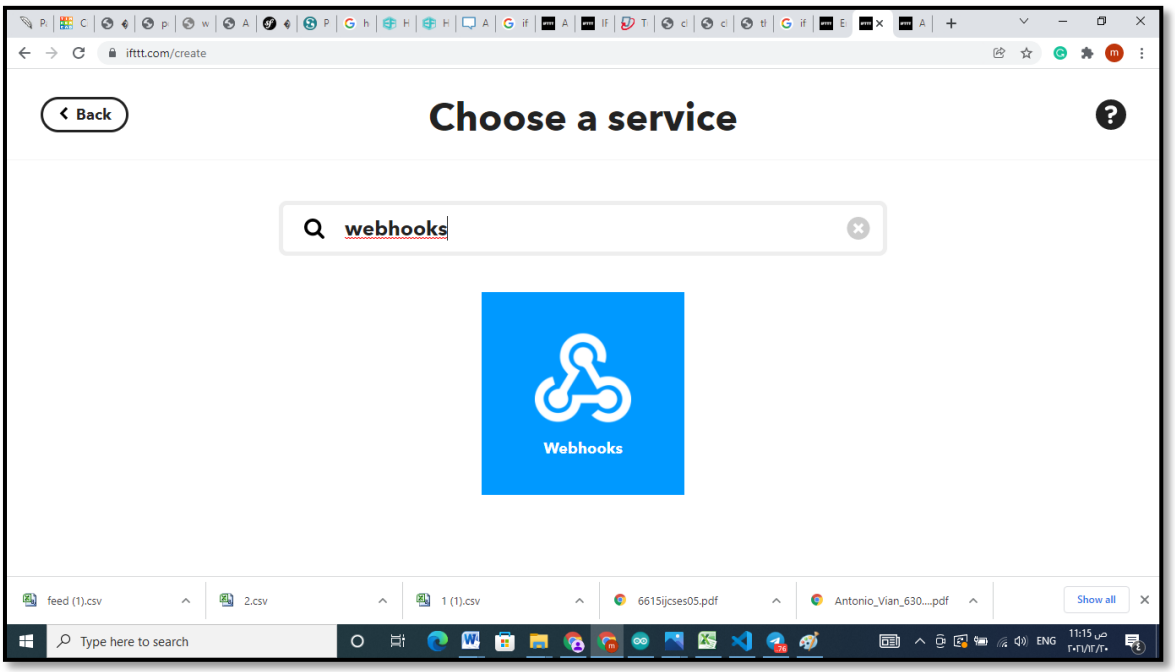

Figure(B-5): Choosing Webhoks service as a trigger.

- Press the Receive a web request box to continue. Then, Enter an event name (Health Monitoring in our project). Finally, Create trigger.

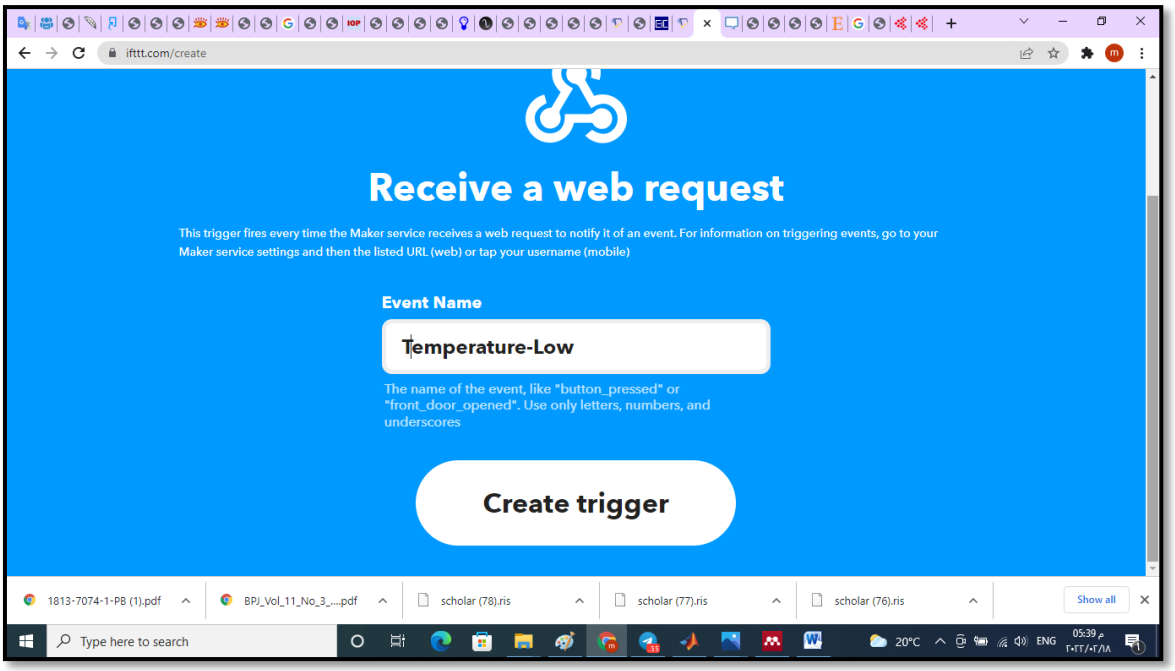

Figure(B-6):Inserting Event Name.

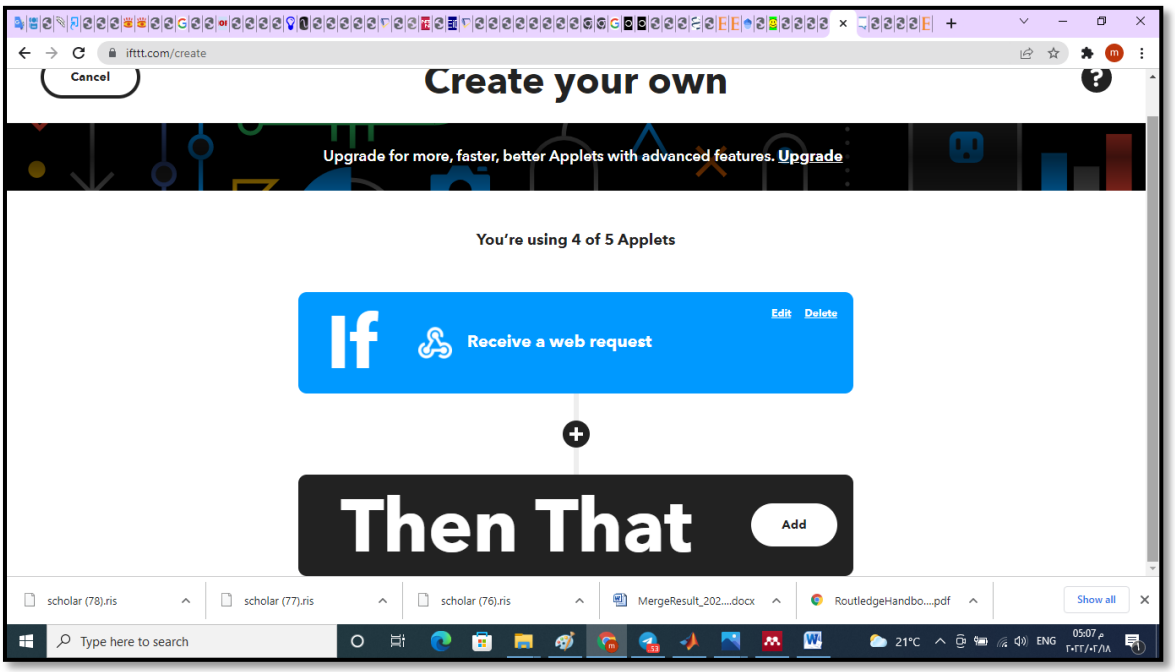

Figure(B-7): Finishing of creating the trigger.

Step4: Create an action

Now the trigger is created, for resulting action, click That.

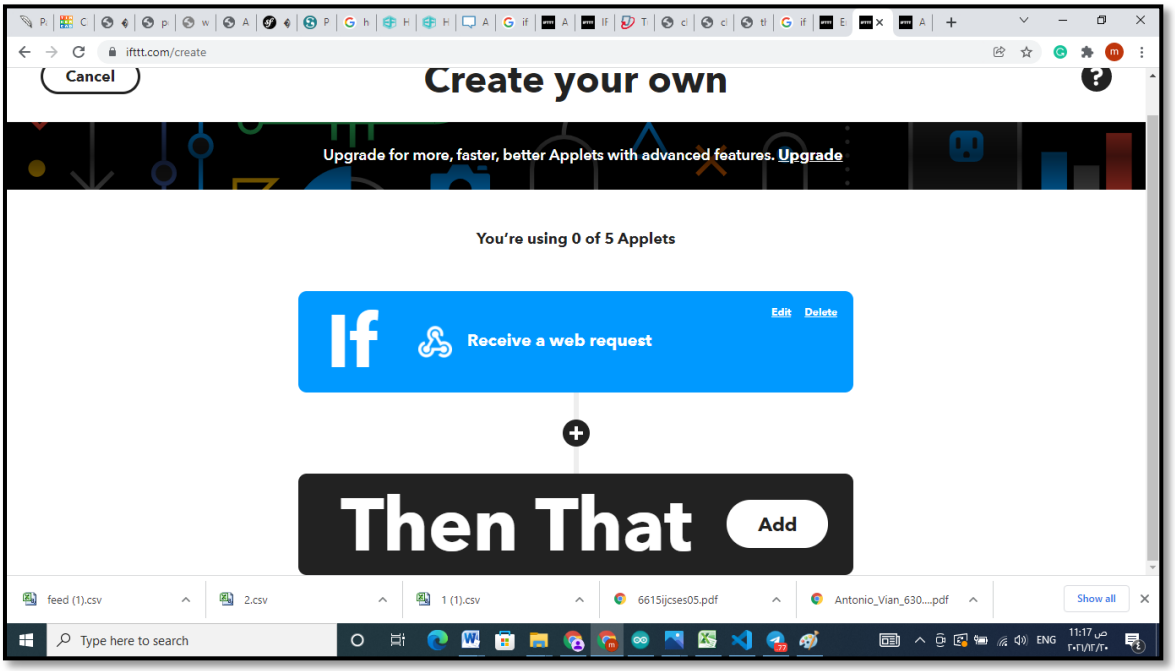

Figure(B-8): Adding an action.

- Enter "email" in search field, Then, complete the action fields.
- Press Continue
- Insert Email of the doctor (mayasah882016@gmail.com)

- Your applet should be created after you press the Finish.

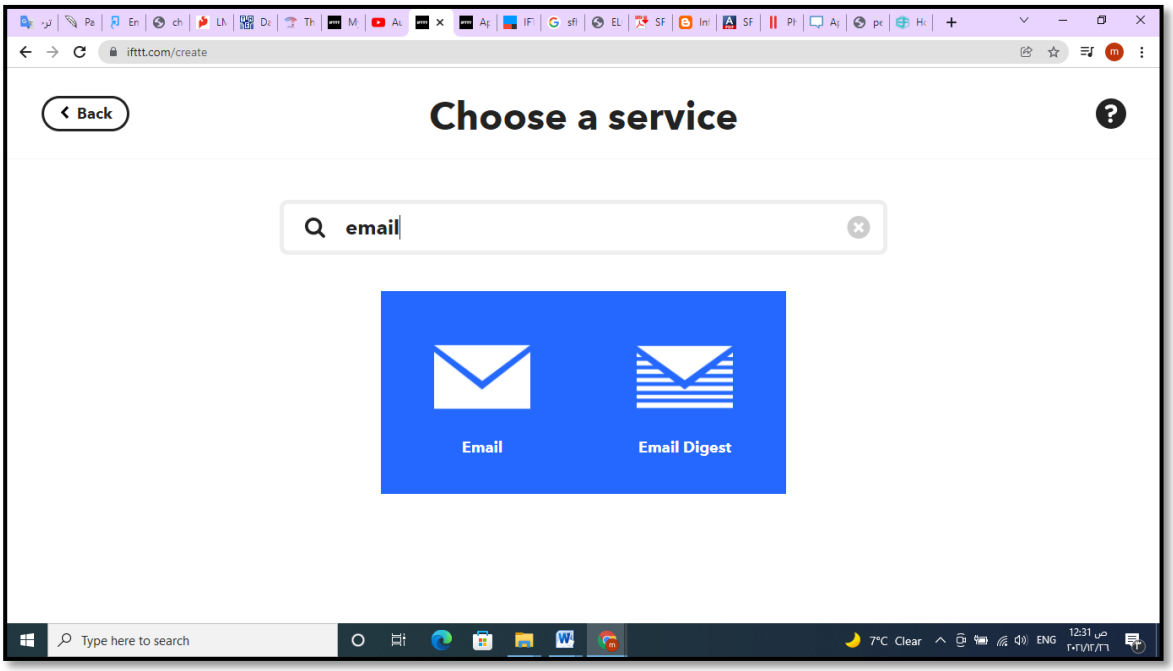

Figure(B-9): Choosing Emai service as an action.

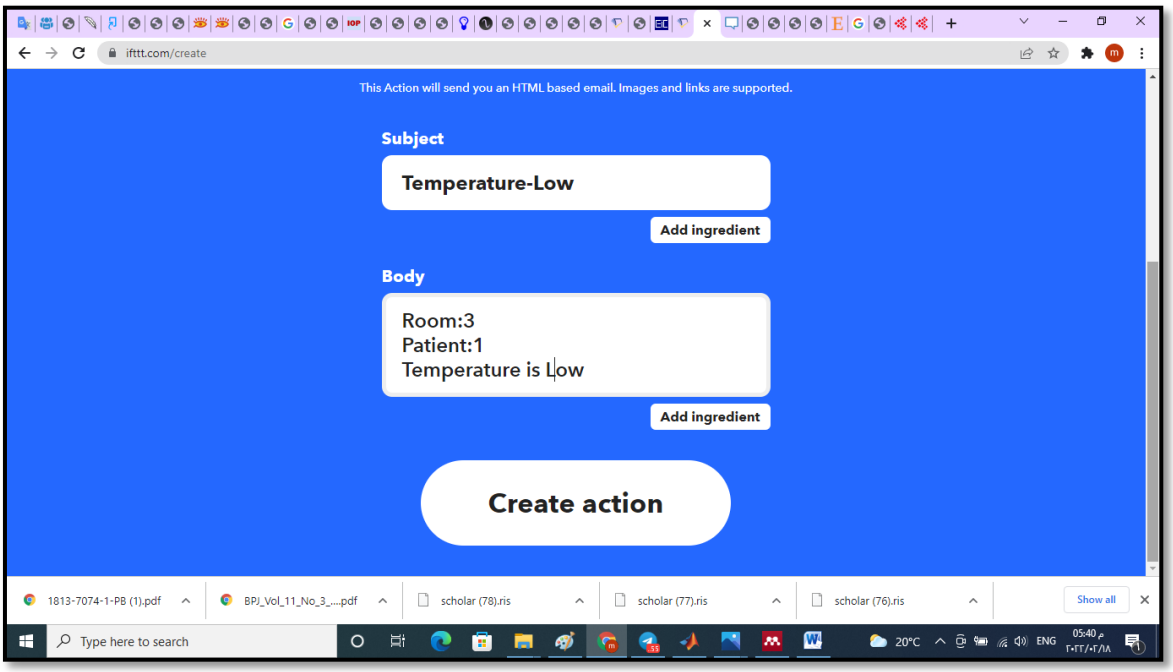

Figure(B-10): Completing an action Fields.

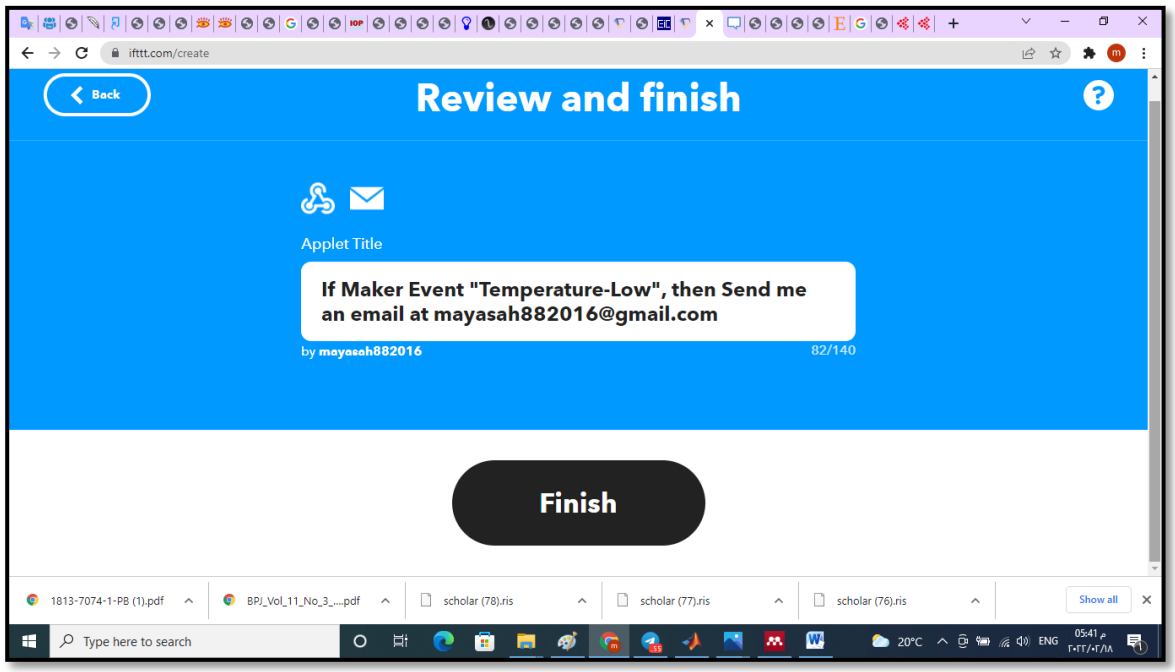

Figure(B-11): Adding Email and finishing the applet.

Step4: Get URL

- Click on **Webhooks** icon.
- After that click on **Documentation**.
- Below the heading **Make a POST or GET web request,** we shall find a URL. You would be able to remove the **{event}**-denoted part of this URL. Fill in the name of the case you just made (**Temperature-Low)**. Copy this URL.

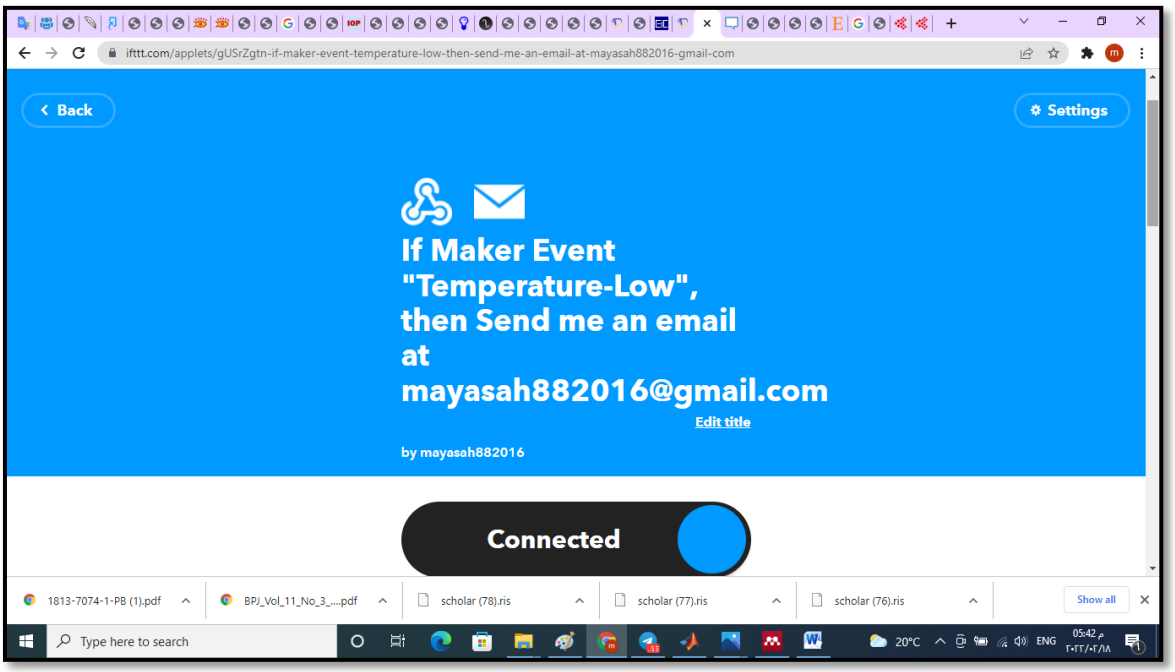

Figure(B-12):Pressing Connect.

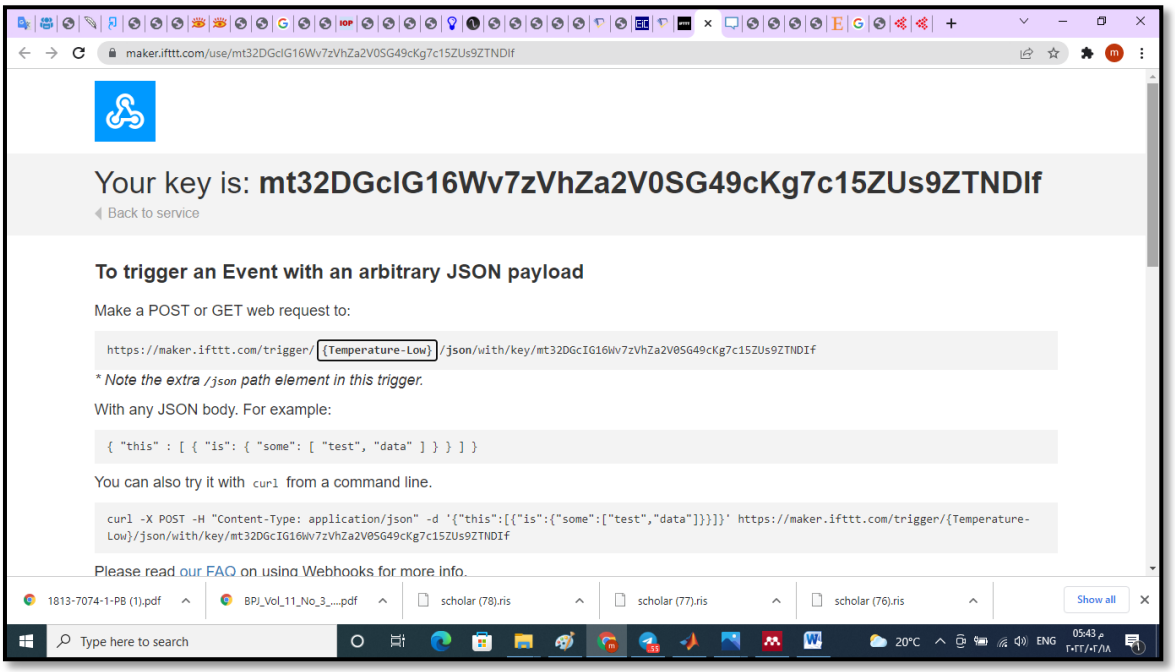

Figure(B-13):Getting URL.

Step5: To Configure ThingSpeak

Now configure a ThingHttp - action on thingspeak.com. We can find ThingHttp in the by pressing APPs in thingspeak Website.

- Give Name: Health Monitoring

- In URL, paste the URL you copied from the IFTTT Webhooks Documentation page.url
- method: POST
- HTTP Version: 1.1
- Then, Save ThingHttp.

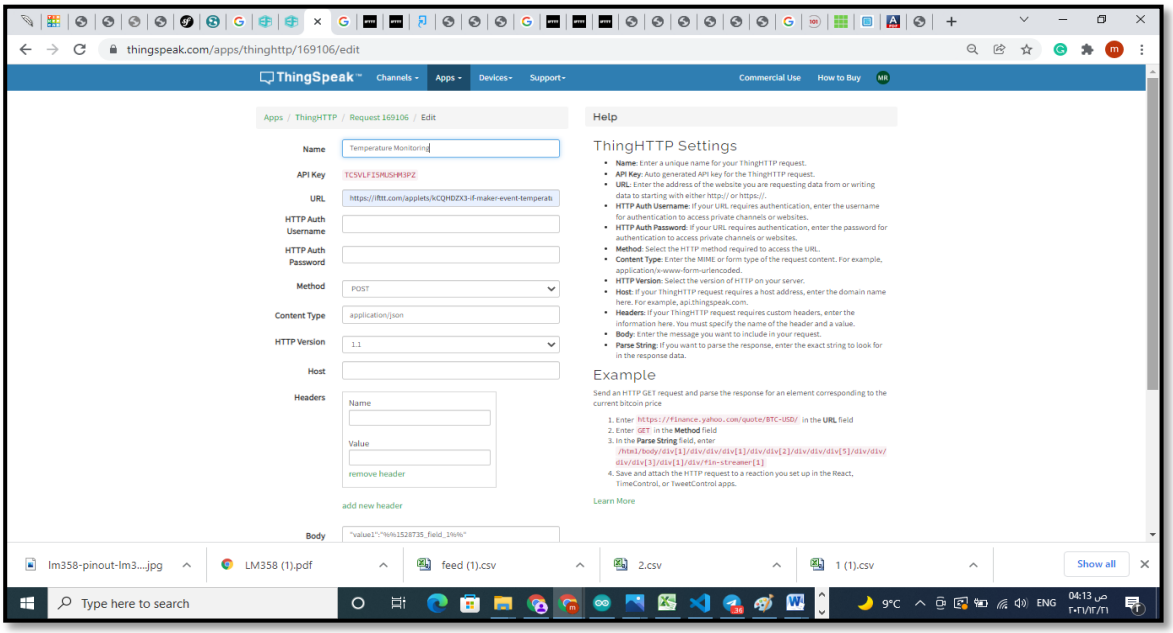

Figure (B-14): Configuration of ThingHttp.

Step6: To configure the Threshold values

Go to Thingspeak.com, press APPs press the REACT, open it and configure

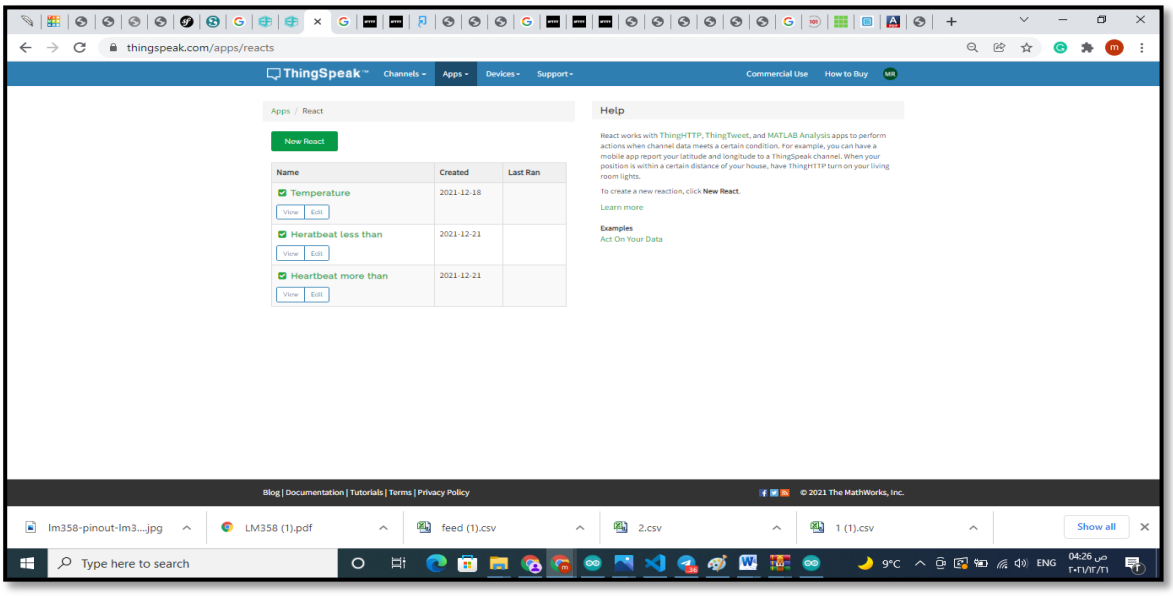

Figure (B-15): Creating React for Threshold values.

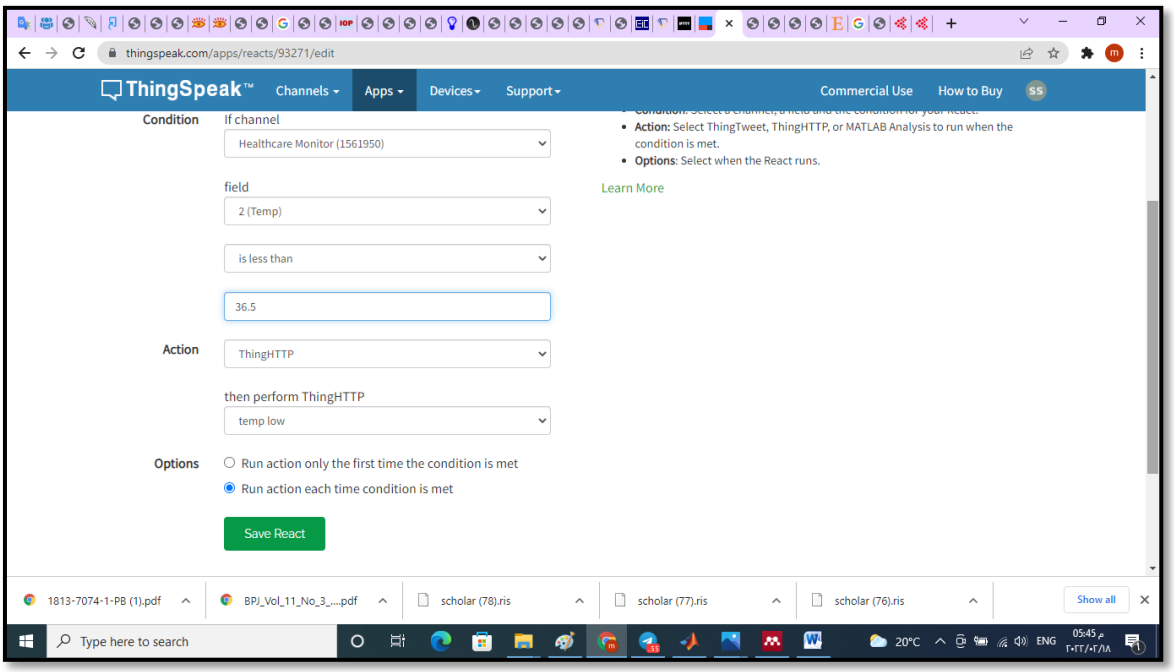

Figure (B-16):Setting Threshold value for Low Body Temperature.

All the above steps are repeated to get notifications for high body temperature, low and high heart rate cases.

الخلاصة

الاتصالات الضوئية المرئية (VLC) هي شكل من أشكال الاتصالات اللاسلكية الضوئية (OWC) التي نشأت في السنوات الأخيرة. بدلاً من استخدام الطيف الراديوي لنقل البيانات لاسلكيًا ، فإنه يستخدم طيف الضوء المرئي عبر إضاءة مصابيح الصمام الثنائي الباعث للضوء (LED). على الرغم من أن VLC يمكنه معالجة بعض مشكلات اتصالات الترددات الراديوية في مواقف معينة ، إلا أن قدراته على تطبيقات إنترنت الأشياء (IoT) لم تتحقق بعد.

تم أخذ الفوائد العديدة لـ VLC في أنظمة مراقبة الرعاية الصحية ، وخاصة شريحة كبار السن من الأشخاص في المستشفيات. فحصت الأطروحة تطبيقين لتقنية VLC: الأول هو نظام مراقبة الرعاية الصحية الذكي باستخدام تقنية Li-Fi (وهو تطبيق عملي لـ VLC) القائم على إنترنت الأشياء. والثاني هو نظام تحديد المواقع الداخلي (IPS) لمراقبة وضع المريض باستخدام تقنية VLC.

في النظام الأول ، يتم نقل درجة الحرارة ومعدل ضربات القلب للمريض عبر تقنية Li-Fi ، ثم إلى محطة التمريض المركزية. يتم تحميل هذه البيانات إلى سحابة منصة ThingSpeak عبر كود Python حتى يتمكن الطبيب من مشاهدتها في أي مكان. يتم توفير هذا النظام أيضًا من خلال إرسال إشعارات البريد الإلكتروني في الحالات غير الطبيعية. تم تصميم النظام وتنفيذه بجميع الخطوات ، بما في ذلك اختيار المكونات وبرمجة التشغيل. تضمنت البرامج والأنظمة الأساسية المستخدمة Arduino Integrated Development Environment (IDE) للحصول على بيانات المستشعر ، ومنصة Thingspeak IoT كواجهة مستخدم رسومية للطبيب ، ولغة Python لتحميل هذه البيانات إلى Thingspeak ، وتطبيق If-this-then-that (IFTTT) لغرض التنبيه. تم تقسيم النتائج إلى جزأين. الجزء الأول يتعلق بتقنية Li-Fi. اختبر النظام مسافات متعددة ، وحالة قناة مختلفة، والضوضاء

المحيطة. الجزء الثاني كان نتائج إنترنت الأشياء ، حيث تم تقديم النتائج على منصة ThinkSpeak والإخطار عبر البريد الإلكتروني في الحالات الحرجة. تم اختبار النظام بنجاح على مرضى مستشفى الامام الصادق – مدينة بابل. النتائج التي تم الحصول عليها تمت الموافقة عليها ومرضية.

أما النظام الثاني فيعتمد على تحديد مكان المريض داخل المستشفى باستخدام تقنية VLC. يعتمد النظام المصمم على خوارزمية هجينة جديدة. لها خطوات مختلفة. أولاً ، تقسم طريقة الدمج العقد الثابتة بأكملها إلى مجموعات مختلفة. ثانيًا ، يتم استخدام نهج تحديد موقع المربعات الصغرى الموزونة (WLS) لحساب موضع المريض من قبل كل مجموعة. بعد ذلك ، يتم استخدام اختيار العقدة الثابتة (AS) لتحديد المجموعة التي تتمتع بأفضل دقة لتحديد المواقع باستخدام مقياس الخطأ المتوسط التربيعي المشتق (MSE). أخيرًا ، يتم اختيار المجموعة المحددة لنقل المريض باستخدام موضعها المقدر كنقطة أولية لنهج تحديد المواقع بأقصى احتمالية (ML). تظهر نتائج المحاكاة أن الخوارزمية المقترحة تتفوق على WLS ونهج ML التقليدي. وجد أيضًا أن زيادة عدد مصابيح (LEDs) في السقف يؤدي إلى تحسين دقة النظام .تمت المحاكاة بمساعدة MATLAB 2019A.

جمهورية العراق
وزارة التعليم العالي والبحث العلمي
جامعة بابل

تصميم وتحليل منظومة مراقبة الرعاية الصحية بالاعتماد على اتصالات الضوء المرئي (VLC)

أطروحة

مقدمة إلى قسم الهندسة الكهربائية / كلية الهندسة في جامعة بابل
وهي جزء من متطلبات نيل درجة الدكتوراه فلسفة في الهندسة / الهندسة الكهربائية / الكترونيك و اتصالات

من قبل

مياسة رزاق عبدعلي محمد

بإشراف

أ. د. إبراهيم عبدالله مرداس

آب ٢٠٢٢